Université de Montréal

The influence of cell size on cytokinesis *in situ* and genomic interrogation of human cell size regulation

par Karine Gauvin Bourdages

Programme de biologie moléculaire
Faculté de médecine

Thèse présentée
en vue de l'obtention du grade de doctorat
en biologie moléculaire
option biologie des systèmes

Décembre, 2017

Résumé

La cellule est l'élément fondamental de la vie. Plus d'une vingtaine de trillions de cellules forment les organes et tissus de notre corps. Ces cellules sont de taille spécifique puisqu'elles ont des fonctions précises au sein de leur tissu respectif. Dans la plupart des cas, les cellules doivent proliférer en se divisant pour se renouveler et ainsi assurer le bon fonctionnement d'un organisme. La dernière étape de la division cellulaire, la cytokinèse, est exécutée par la contraction d'un anneau contractile d'actomyosine, nécessaire pour effectuer la séparation physique de la cellule en deux cellules filles. La première partie des travaux décrits dans cet ouvrage portent sur la caractérisation de la cytokinèse en utilisant, comme modèle *in vivo*, les cellules précurseur de la vulve (VPCs) du nématode *C. elegans*. Notre étude révèle que plusieurs aspects de l'anneau d'actomyosine s'ajustent en fonction de la taille de la cellule. Entre autres, la largeur de l'anneau contractile, juste avant sa constriction, s'ajuste en fonction de la longueur des VPCs. De plus, la rapidité avec laquelle l'anneau se contracte dépend de la circonférence de la cellule. Ces découvertes nous ont amené à nous demander comment la cellule régule sa taille? Les cellules en prolifération maintiennent leur taille en homéostasie en équilibrant leur taux de croissance et de division cellulaire. Afin d'interroger les gènes impliqués dans le maintien de la taille cellulaire du mammifère, nous avons utilisé la technologie CRISPR/Cas9, afin d'éliminer par délétion tous les gènes humains, à raison d'un par cellule, pour identifier ceux qui causent une augmentation ou une diminution de la taille cellulaire. Cette étude nous a permis d'identifier plusieurs gènes déjà connus régulant la croissance cellulaire. De plus, nous avons identifié un groupe de gènes, incluant TLE4 un corépresseur de la transcription que nous avons caractérisé, n'ayant jamais été associé avec une fonction de contrôle de la taille cellulaire chez les mammifères. En somme, nos travaux ont contribué à l'approfondissement des connaissances sur la division cellulaire, plus précisément la cytokinèse, et des gènes impliqués dans le maintien de la taille cellulaire. Une meilleure connaissance du fonctionnement de ces deux évènements cellulaires est essentielle puisque leur dérégulation peut entrainer plusieurs pathologies, incluant le cancer.

Mots-clés: Cytokinèse, taille cellulaire, *C. elegans*, VPCs, CRISPR/Cas9, criblage, mTORC1, TLE4

Abstract

Cells are the fundamental building blocks of life. The human body contains over twenty trillion cells that make up the different tissues and organs of our bodies. Cells within organs are of specific sizes to perform their specialized functions. In most cases, these cells must divide to proliferate and replenish the population of cells essential for proper organism function. The final stage of cellular division, termed cytokinesis, entails the assembly and constriction of a contractile ring that drives the dramatic cell shape changes required to physically partition the cell into two daughter cells. The first part of the work presented in this thesis addresses the characterization of cytokinesis in the epithelial vulval precursor cells (VPCs) of the nematode worm *C. elegans*. This study principally revealed that several aspects of cytokinesis scale with cell size. For instance, I observed that the breadth of the actomyosin ring scaled with VPC length. In addition, the speed of contractile ring constriction scaled with the circumference of VPCs. These scaling events raised the more general question as to how cells regulate their size. Proliferating cells attain cell size homeostasis by balancing cell growth and cell division. In order to define the molecular regulators of size in human cells a genome-wide approach was taken. Recently developed CRISPR/Cas9 technology was used to perform the first pooled knockout screens for human cell size regulators in the NALM-6 pre-B lymphocytic cell line. These screens revealed many genes that affect the size of NALM-6 cells, a number of which were previously known to be involved in growth regulation. In addition, these screens revealed the identity of many genes with no previously established functions associated with cell size regulation. Amongst the previously unknown regulators, I characterized the function of a co-repressor of transcription, TLE4, which I showed functions as a regulator of the B-cell lineage. This work contributes to the knowledge of the mechanics of cytokinesis in *C. elegans* epithelial cells and of the genes that coordinate cell size in humans. These results provide insights into cell growth and division in normal cells and how these processes may be perturbed in cancer and other diseases.

Keywords: Cytokinesis, cell size, *C. elegans*, VPCs, CRISPR/Cas9, screen, mTORC1, TLE4

Table of Contents

List of Figures and Table

List of Abbreviations

4E-BP1: Eukaryotic translation initiation factor 4E-binding protein 1

AC: Anchor cell

AH: Anillin Homology

AJM-1: Apical junction molecule 1

AJs: Adherens junctions

ALL: Acute lymphoblastic leukemia

C. elegans: Caenorhabditis elegans

CD: Cluster of differentiation

Cdc: Cell division cycle

CDKs: Cyclin-dependent kinases

CeAJs: *C. elegans* apical junctions

Chip-Seq: Chromatin immunoprecipitation sequencing

CPC: Chromosomal passenger complex

CRISPR: Clustered regularly interspaced short palindromic repeats

CRISPRi: CRISPR interference

crRNA: CRISPR RNA

CyanRing: Cytokinesis analysis of the contractile ring

DIC: Differential interference contrast

DLG-1: Discs Large 1

E. coli: *Escherichia coli*

Egl: Egg-laying defective

eIF4E: Eukaryotic translation initiation factor 4E

EKO: Extended knockout

F-actin: Filamentous actin

FACS: Fluorescence-activated cell sorting

GeCKO: Genome-scale CRISPR/Cas9 KO

GFP: Green fluorescent protein

GSCs: Glioblastoma stem-like cells

HDR: Homology-directed repair

HMP: Humpback

HMR: Hammerhead

HR: Homologous recombination

Hyp7: hypodermis

IgM: Immunoglobulin M

INCENP: Inner centromere protein

Indels: Insertions or deletions

L1-4: Larval stage 1 through -4

LAM-1: Laminin-1

MKLP1: Mammalian kinase-like protein 1

MKLP2: Mammalian kinase-like protein 2

mTOR: Mechanistic target of rapamycin

mTORC1: Mechanistic target of rapamycin complex 1

mTORC2: Mechanistic target of rapamycin complex 2

Muv: Multiple vulvae

NHEJ: Non-homologous end joining

NMY-II: Non-muscle myosin II

NSCs: Neuronal stem cells

PAM: Protospacer adjacent motif

PLC: Phospholipase C

PLK1: Polo-like kinase 1

PRC1: Protein regulating cytokinesis 1

Pre-BCR: Pre-B cell receptor

Pvl: Protruding vulva

RANKS: Robust analytics and normalization for knockout screens

Rb: Retinoblastoma

rMLC: Regulatory myosin light chain

RNA-Seq: RNA sequencing

RNAi: RNA interference

ROCK: Rho-dependent kinase

S6K1: S6 kinase 1

sgRNA: Single guide or synthetic guide RNA

shRNA: short hairpin RNA

siRNA: Small interfering RNA

SJs: Septate junctions

TALENS: Transcription activator-like effector nucleases

TJs; Tight junctions

TKO: Toronto knockout

TLE4: Transducin like enhancer of split 4

TOR: Target of rapamycin

tracrRNA: Trans-activating CRISPR RNA

TSC: Tuberous sclerosis complex

VPCs: Vulval precursor cells

Vul: Vulvaless

ZFNs: Zinc fingers nucleases

Je dédie cet ouvrage à mes parents, qui m'ont transmis leur amour pour les sciences, particulièrement à ma mère là-haut.

Acknowledgements

I want to begin by expressing how thankful I am to everyone I had the pleasure of working with over the course of my graduate studies. First and foremost, I want to thank both of my supervisors, Dr. Amy Maddox and Dr. Mike Tyers, who gave me the opportunity to work on exciting projects. Thank you, Amy, for teaching me to be rigorous and detailed oriented in science. You were a great mentor and always believed in me. Mike, I want to thank you for sharing your passion and exciting ideas about science and for the warm welcome to your lab. You were an excellent mentor, who allowed me to bring my own ideas and be more independent. I also want to thank Dr. Paul Maddox and Dr. Lea Harrington, with whom I shared insightful scientific discussions. Thank you for making this journey even more enjoyable by bringing labs together for scientific exchanges. I also want to thank the members of my thesis committee, Dr. Sébastien Carréno, Dr. Brian Wilhelm and Dr. Christian Rocheleau for their support and helpful comments throughout the years.

I want to thank all members of both Maddox labs. It was an immense pleasure to work with you all. I will always remember the fun we had on our ASCB trips to San Francisco and New Orleans! Benjamin, you were an incredible mentor who taught me everything I needed to know when I arrived in the Maddox lab. You were always there to encourage me and support my work in the lab. I also want to thank Carlos and Jonas for their contribution to the scientific publication we brought to completion with Ben and Amy. It was a great pleasure to work with such incredible colleagues. I also want to say thank you to my colleagues of the Labbé lab. It was great to talk about *C. elegans* and share numerous moments of laughter. Eugénie, I thank you for being such an exceptional friend. A special thank you to Valérie, it was a pleasure to work with you during the Maddox times and to renew our friendship when you came back to IRIC. I thank you for all the great advice you gave me over the years.

I want to thank all members of the Tyers lab. You kindly welcomed me and made the transition to your lab easy for me. I am grateful to have had the chance to work with such knowledgeable colleagues. Thierry, I thank you for your incredible mentorship. You taught me everything I needed to know and shared your passion for research. Thank you for all the tips you gave me and for our insightful conversations. A special thank you to Luisa, you were

always there to help me. Your guidance was key to the realization of this work. You taught me so such much about science and life in general and for that I am very grateful. Jasmin, thanks for your contribution to the project, without you this work wouldn't have been feasible. Almer, Susan and Andrew, I thank you all for the animated scientific discussions we had over the years. I also thank you for all the great moments we shared over lunch and during office chats. I also want to thank Sylvain for his help with thesis-related work. I thank Samuel, Jing, Lily, Ghada, Linnea, Daniel, Corinne, Yahya, Manon, Caroline and Roger for being incredible colleagues.

I thank the members of IRIC platforms for their technical help on experiments. Thank you, Christian Charbonneau, for your help with microscopes and for training with the Illustrator software. I want to say thank you to Gaël Dulude and Danièle Gagné for technical assistance with FACS experiments. I also want to thank all members of the high-throughput screening facility and genomics platform at IRIC. Also, thank you to Dr. Mader and members of her lab with whom I did my master's degree rotation. I want to say thanks to everyone at the academic affairs of IRIC for their help over all these years. A special thank to Julie for answering all my questions and for your help in preparation of the next chapter.

Finally, I would not have been able to make it through my doctoral studies without the support from my family. I want to thank my dad and sister for having been there when I needed encouragement and advice. You were always there for me so thank you. I want to thank my grandparents, Gérald and Marie-Claire, who gave me the inspiration to write this thesis at their lake house. As well, I thank my grandmother Marie-Berthe for her encouragements. I thank my aunt Diane and my uncle Tom, who supported me during my doctoral studies and especially while writing my thesis. I also thank all other members of my family. Finally, I want to say thanks to my significant other, Jean-Mathieu, for his ongoing support and his patience during the past four years. Thank you for believing in me.

Introduction

1 General concepts

1.1 The intriguing question of size

Cells are the fundamental structures of life in all living organisms. Across species, cell shape and size variations are remarkable (Maniloff and Morowitz, 1972; Smith et al., 1992). However, within an organism, cells of the same tissue type show very little variation in size, including cells that make up the different organs in our body (Ginzberg et al., 2015). How cells achieve this uniformity in size despite experiencing changing environmental conditions and physiological stress represents a fundamental question in biology. This question of how cells precisely regulate their size has remained an enigma from the early days on modern cell biology. Haldane stated: "The most obvious differences between different animals are differences of size, but for some reason the zoologists have paid singularly little attention to them" (Haldane, 1985). Even though most differences of size are attributed to differences in cell number, cell size variations are important in body size determination (Conlon et al., 2001). Nonetheless, it is fascinating how such a striking observation in nature has remained underappreciated and little studied over nearly one hundred years. In recent decades, studies on cell size regulation began to emerge (Amodeo and Skotheim, 2016; Cook and Tyers, 2007; Ginzberg et al., 2015; Jorgensen and Tyers, 2004; Turner et al., 2012). New molecular genetic approaches developed in the post-genomic era have enabled the long-standing question of how cells regulate their size to be addressed. In the following sections, the progress made in identifying the molecular regulators of cell size will be summarized for unicellular organisms to mammals, including humans.

1.1.1 Enormous size scale

The astonishing range in size of living organisms is perhaps the most obvious feature of life on earth (Bonner, 2011). The smallest bacteria, such as *Pelagibacter ubique* and mycoplasma species are only 0.2 μm and 0.3 to 1 μm in diameter, respectively (Maniloff and Morowitz, 1972; Rappe et al., 2002). At the other end of the spectrum lies the largest mammal on earth, the blue whale that can reach 100 feet in length and weigh 200 tons (Marshall et al.,

2012). The diversity in species size is further underscored by the incredibly small size of nano-organisms, approximately 6 aL in volume, compared to the clonal *Armillaria* fungi that can span thousands of acres (Smith et al., 1992; Uwins et al., 1998). This remarkable range in organism size is largely attributed to variations in cell number and to a lesser extent to differences in cell size. For instance, the large difference in body size between a human adult and a mouse is the result of a 3000-fold difference in cell number (Conlon and Raff, 1999). Even though cell number variations are predominant, differences in cell size are also important to consider. For instance, cells of tetraploid salamanders are twice the size of that of diploid animals whilst body sizes are the same (Fankhauser, 1945).

Cell size also spans a vast range. Small unicellular eukaryotes, such as yeast cells of only 3 μm in length, are dwarfed when compared to the largest unicellular eukaryote, the giant *Caulerpa taxifolia* alga that can span several meters in length (Ranjan et al., 2015). Within the human body cells span a substantial range of sizes, from small blood cells of only 10 to 30 μm in diameter to meter-long motor neurons to large oocytes of 100 μm in diameter (Figure 1.1.1) (Guertin and Sabatini, 2006). In contrast, cells of the same type, such as pancreatic cells or columnar cells of the epidermis show hardly any variation in size (Ginzberg et al., 2015). Evolution has shaped this diversity in cell size to accomplish specialized functions (Guertin and Sabatini, 2006).

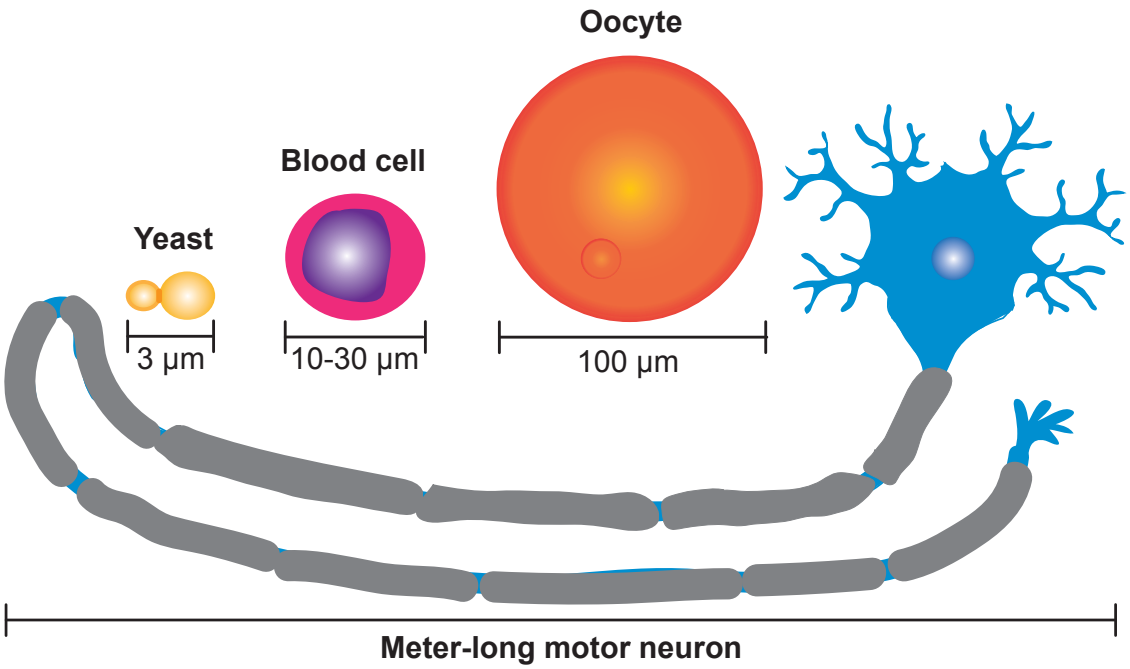

Figure 1.1.1 Examples of the cell size diversity observed in nature

Schematic representing a meter-long motor neuron (blue) compared to a budding yeast *S. cerevisiae* (yellow) approximately 3 µm in length (yellow), a blood cell (pink) 10 to 30 µm in diameter and compared to a human oocyte (orange) 100 µm in diameter. Adapted from (Guertin and Sabatini, 2006).

1.1.2 Cell size de-regulation associated with human diseases

Even though there is a broad diversity in cell size observed in nature, cell-type specific homogeneity in size is achieved within a cell population. Cell size homeostasis, an equilibrium state between cell growth and cell division, needs to be attained for proper cell function. Diseases can arise when cells fail to achieve size homeostasis. For instance, cardiac hypertrophy results when cardiac myocytes enlarge to compensate for anomalies of the heart (Heineke and Molkentin, 2006). Individuals with gigantism, due to growth hormone over-secretion, present severe organ overgrowth and are usually of abnormally large heights due to increased cell size and cell numbers (Melmed, 2009). In tuberous sclerosis (TSC), where affected patients develop benign tumors mainly in the brain, kidney, lungs and skin, giant cells are characteristic of brain tumors (Goto et al., 2011). These giant cells are the result of uncontrolled cell growth caused by loss-of-function mutations in either TSC1 or TSC2 genes, which negatively regulate the mTOR growth control network (Goto et al., 2011). In another

example, abnormally large cancer cells can arise upon entosis (cell engulfment) or aberrant cell division, including cytokinesis failure, which will be discussed in the following sections (Lacroix and Maddox, 2012).

Other examples of cell size plasticity include the active modulation of pathogen cell size to avoid immune detection by the host. For instance, the pathogenic yeast *C. neoformans* increase in size and become "titan" cells to escape immune surveillance (Zaragoza and Nielsen, 2013). Cell size de-regulation has also been observed in metabolic and mitochondrial disorders, aging and Parkinson's Disease (Herrera et al., 2015; Maciak et al., 2014). Thus, cell size de-regulation is associated with various diseases reflecting the importance of understanding how cells achieve cell size homeostasis.

1.2 Cytokinesis

Individual proliferating cells achieve size homeostasis by balancing cell growth and cell division. The size of a cell is dictated by the size of the precursor (mother) cell it originates from and the amount of growth it accomplishes. Cell size uniformity for a particular cell type depends on a tight coordination between cell growth and cell division for each individual cell in the population. Therefore, it is important to understand how both cell growth and cell division are governed. In part, my studies have focused on the final step of cell division termed cytokinesis.

Cytokinesis is the final stage of cellular division that physically partitions the cytoplasm of a cell into two daughter cells. Cytokinesis is intricately coordinated in space and time. Cytokinesis begins in anaphase, following chromosome segregation to opposite spindle poles. Cytokinesis is robust to physical perturbations and drives cell shape changes in the form of membrane curves that ingress to bisect the cell. In the early events of cytokinesis, the spindle midzone specifies the site of division. At this precise location, a contractile ring is assembled beneath the plasma membrane and constricts to drive cell shape changes (Figure 1.2). Membrane ingression driven by the contractile ring proceeds until only a structure called the midbody remains (Figure 1.2). The midbody is resolved during abscission, involving membrane scission to render the newly formed daughter cells topologically distinct (Figure

1.2). The proper coordination of these events is essential, as cytokinesis failure can lead to diseases including cancer (Lacroix and Maddox, 2012).

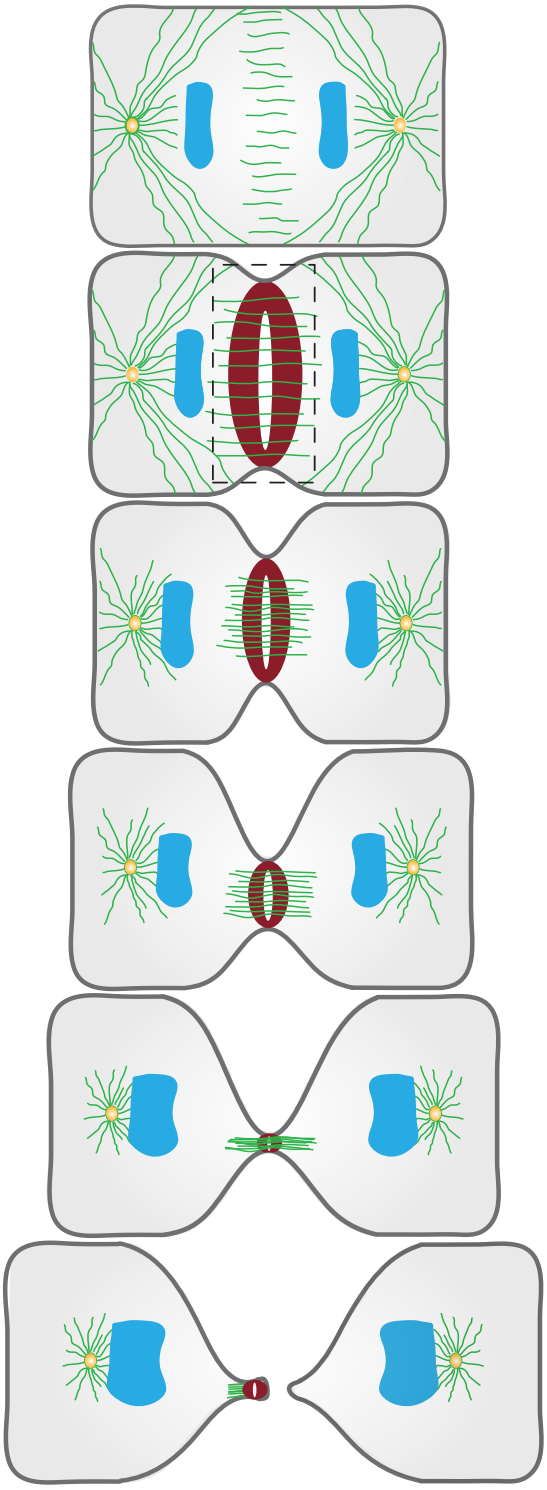

Figure 1.2 An overview of cytokinesis

Schematic representation of a cell undergoing cytokinesis. A contractile ring (red) assembles between segregated chromosome masses (blue). The contractile ring constricts and drives membrane ingression (dark grey). Contractile ring closure progresses until the midbody remains, a structure cleaved during abscission. This process marks the physical separation of a cell into two newly formed daughter cells. Adapted from (Green et al., 2012).

1.2.1 Cytokinesis and cancer

In the event of cytokinesis failure, cells become tetraploid, containing four copies of the genome. In most cases, tetraploidy results in activation of the p53 tumor suppressor gene and thus cell cycle arrest in G1 that can lead to cell death (Ganem and Pellman, 2007). However, under certain conditions including loss of p53, tetraploid cells can further proliferate. Upon division, these cells can fail to assemble a bipolar spindle due to their supernumerary microtubules organizing centers (Fujiwara et al., 2005). This can lead to merotelic chromosome attachments and chromosome segregation errors resulting in genetic instability (Ganem et al., 2009; Silkworth et al., 2009). Chromosome instability is manifested in several ways including mutations, deletions, chromosomal rearrangements and fusion, gene amplification and aneuploidy, an important hallmark of cancer (Lacroix and Maddox, 2012; Williams and Amon, 2009). Experiments in mice showed that cells that fail a round of cytokinesis are more prone to tumorigenesis (Fujiwara et al., 2005). However, it is important to mention that while cytokinesis failure may lead to cancer, it can also cause cell death upon p53 activation (Ganem and Pellman, 2007). How the decision between these two outcomes is made remains unknown. Thus, it is important to establish a deep understanding of the mechanisms ensuring the proper execution of cytokinesis.

Cytokinesis failure can be viewed as a double-edged sword. For certain cells, cytokinesis failure can cause genetic instability leading to diseases, as previously described. However, other cell types purposely fail cytokinesis to perform specialized functions (Lacroix and Maddox, 2012). For these cells, the completion cytokinesis can lead to pathological states (Lacroix and Maddox, 2012). These specialized cell types include hepatocytes, megakaryocytes and cardiomyocytes that reach high levels of ploidy by either failing cytokinesis or an earlier step in mitosis (Lacroix and Maddox, 2012). This re-enforces the importance of understanding the fundamental principles governing cytokinesis.

1.3 Scaling unifies cytokinesis and cell size

"Everywhere Nature works true to scale and everything has its proper size accordingly." This citation by D'Arcy Wentworth Thompson nicely illustrates the fundamental biological principle of scaling according to size (D'Arcy Wentworth, 1945). In biology, scaling describes the ability of an organelle or any cellular component to adjust according to changes in cell size (Reber and Goehring, 2015). Adequate scaling events are essential for proper cell, organ and consequently organism function (Levy and Heald, 2012). This important question of how molecular structures scale with cell size for proper function rapidly generated interests in the biological science community. However, the lack of tools to precisely measure small structures in the micrometer range of most cells and organelles prevented progress in the early days of the scaling field. High-resolution microscopy and other imaging techniques, have allowed intracellular scaling to be examined at unprecedented resolution (Levy and Heald, 2012; Reber and Goehring, 2015). The following sections describe scaling events important for cell division.

1.3.1 Cell size influences cell division processes including cytokinesis

Cell size and cytokinesis are intimately related. Several examples illustrate the impact of cell size on intracellular structures governing cell division processes. Early observations by Schroeder demonstrated scaling of contractile rings filaments in cells of different sizes (Schroeder, 1972). Larger amphibian eggs possessed filaments of increased dimensions compared to smaller somatic cells (Schroeder, 1972). In addition, other subcellular structures are scaled to cell size as it reduces during early embryonic development, as the embryo undergoes several rounds of rapid cleavage in the near absence of growth. In both *C. elegans* and *Xenopus* embryos, the size of the cell influences mitotic spindle length. As cells get smaller during rapid cleavages so does the length of the mitotic spindle (Brown et al., 2007; Hara and Kimura, 2009; Loughlin et al., 2011). Experiments performed in *C. elegans* embryos showed that both spindle length and the speed of spindle elongation scaled with cell size (Hara and Kimura, 2009; Marshall et al., 2012). Elegant work in *C. elegans* embryos also showed that chromosome length scaled with cell size (Ladouceur et al., 2015). Altogether, these findings demonstrate that cell size influences the molecular architecture of the cell.

Several other examples illustrate the influence cell size has on the proper orchestration of cytokinesis events. For instance, my work demonstrated that several aspects of cytokinesis scale with cell size (Chapter 3). Using high-resolution microscopy, I characterized cytokinesis occurring in the vulval precursor cells (VPCs) of the nematode *Caenorhabditis elegans* (*C. elegans*). As the VPCs decrease in length from one round of division to the next, we observed that the breadth of the contractile ring scaled with cell length (Chapter 3). Quantitative assessments of the speed of contractile ring closure in the *C. elegans* VPCs revealed that it scaled with cell circumference and thus cell dimensions (Chapter 3). This observation supported previous findings in the *C. elegans* embryo and filamentous fungi *Neurospora crassa* that illustrated the conserved nature of this property (Calvert et al., 2011; Carvalho et al., 2009). This work is described in detail in Chapter 3. An understanding of how both cytokinesis and cell size are coordinated and influence each other should reveal general principles of scaling in biology.

2 The events of cytokinesis

Cytokinesis proceeds by a series of sequential events, each described in the following sections. The beginning of cytokinesis is marked by re-organization of the mitotic spindle to specify the site of contractile ring assembly. Molecular signals emanating from microtubules of the spindle midzone reach the above cortex to promote the recruitment of contractile ring components. This event triggers the assembly of a contractile ring beneath the plasma membrane and primarily composed of actin filaments, the motor non-muscle myosin II and scaffolding proteins including septins and anillin. Molecular motors of the contractile ring drive cell shape changes. Membrane ingression proceeds until the midbody remains. The final event of cytokinesis is termed abscission and involves midbody severing to physically separate the two daughter cells.

2.1 Division site specification

The initial event in cytokinesis is the establishment of the division plane. The maintenance of genome integrity requires that cell partitioning occurs at a precise location that is between segregated chromosome masses. Pioneering work in the cytokinesis field provided insights on the molecular structures implicated in this early event of cytokinesis. Later studies provided a detailed map of the molecular players involved in the specification of the division plane. Lastly, distinct cues provide different contributions to division site establishment depending on the organism.

2.1.1 Cues from the mitotic apparatus

More than 50 years ago, Ray Rappaport performed several elegant micromanipulation experiments that led to the identification of the mitotic spindle as the general structure responsible for positioning the cleavage furrow. In a first experiment, Ray pressed a glass rod into the middle of a sand dollar egg, such that the first cleavage did not completely divide the egg but generated a binucleate doughnut-shaped cell (Rappaport, 1961). During the next division, two mitotic spindles juxtaposed to the rod were formed and each induced a cleavage furrow (Rappaport, 1961). Surprisingly, an additional furrow appeared between astral

microtubules emanating from the two opposing spindles (Rappaport, 1961). This demonstrated that the mitotic spindle and its emanating astral microtubules could specify the division plane, independently of intervening chromosomes.

In another experiment, Rappaport deformed echinoderm eggs in a capillary tube. Sideways movements of the tube provoked displacement of the mitotic spindle along the tubular cell. Cleavage furrow initiation occurred to bisect the spindle (Rappaport, 1985). Upon displacement of the spindle, the cleavage furrow regressed from its initial location and reformed to bisect the spindle at this new site (Rappaport, 1985). Altogether, Rappaport's observations suggested that the mitotic spindle signals the overlying cortex to specify the division plane. The first experiment suggested that the anaphase spindle and not the metaphase plate dictated the location of the cleavage furrow. Rappaport's later experiment illustrated the dynamicity of the signal sent by the mitotic spindle.

Subsequent studies supported Rappaport's early findings. In another micromanipulation experiment, a microneedle was used to create small perforations in adherent epithelial cells in culture (Cao and Wang, 1996). When the perforation was made adjacent to chromosome masses before anaphase onset, the cell failed to induce a cleavage furrow next to the perforation (Cao and Wang, 1996). This result further supports the role of the mitotic spindle in specifying the division plane.

Another group imaged cytokinesis in sea urchin embryos placed in chambers with adjustable atmospheric pressure. Increased pressure disrupted the structure of cortical cytoskeletal components and prevented astral microtubule elongation resulting in failure of cleavage furrow induction (Salmon and Wolniak, 1990). Restoring normal pressure in the chamber prior to the second round of division allowed the cell to proceed with the assembly of two mitotic spindles and induce four cleavage sites during cytokinesis (Salmon and Wolniak, 1990). This experiment indicates that astral microtubules play a role in determining the site of division.

Eckley and colleagues performed a similar experiment to that of Salmon and Wolniak but in somatic cells. In their experiment, they fused two cells together generating a v-shaped cell (Eckley et al., 1997). When dividing, the two mitotic spindles were oriented in a diagonal

(v-shape). In most cases, they observed induction of two cleavage furrows adjacent to both mitotic spindles (Eckley et al., 1997). However, in rare instances they saw a third furrow between microtubule asters of the opposing spindles (Eckley et al., 1997). Thus, in somatic cells, the mitotic spindle seems to play a more prominent role in division plane specification. These results also support the contribution from astral microtubules in determining the site of division. Altogether, these elegant micromanipulation experiments by Rappaport and others well illustrate the participation of the mitotic spindle and astral microtubules in establishing the site of division.

2.1.2 Formation of the spindle midzone

The mitotic spindle elongates during anaphase to pull apart sister chromatids towards opposing poles of the cell. Following faithful genome partitioning, re-organization of the mitotic spindle occurs. During this critical step, microtubules accumulate between chromosome masses to form a cellular structure known as the spindle midzone (Figure 2.1.2). The spindle midzone is composed of a bundle of overlapping antiparallel microtubules with their plus-ends oriented towards the cell center (Mastronarde et al., 1993). This specific region presents a small overlap of microtubules (Hu et al., 2011). The kinesin motor protein KIF4 is essential to restrict the microtubule overlap to delimit the division plane (Hu et al., 2011). In addition, microtubules of the midzone are much more stable than microtubules emanating from the spindle poles (Canman et al., 2003). These stable microtubules deliver signaling molecules to the equatorial cortex and membrane via plus-end directed molecular motors localized along these microtubules (Foe and von Dassow, 2008; Odell and Foe, 2008). The more dynamic astral microtubules near the cell poles act negatively to prevent accumulation of signaling molecules that promote contractile ring assembly (Foe and von Dassow, 2008; Odell and Foe, 2008). The identification of this specialized structure and its characteristics was key to the understanding of the mechanisms governing division site specification.

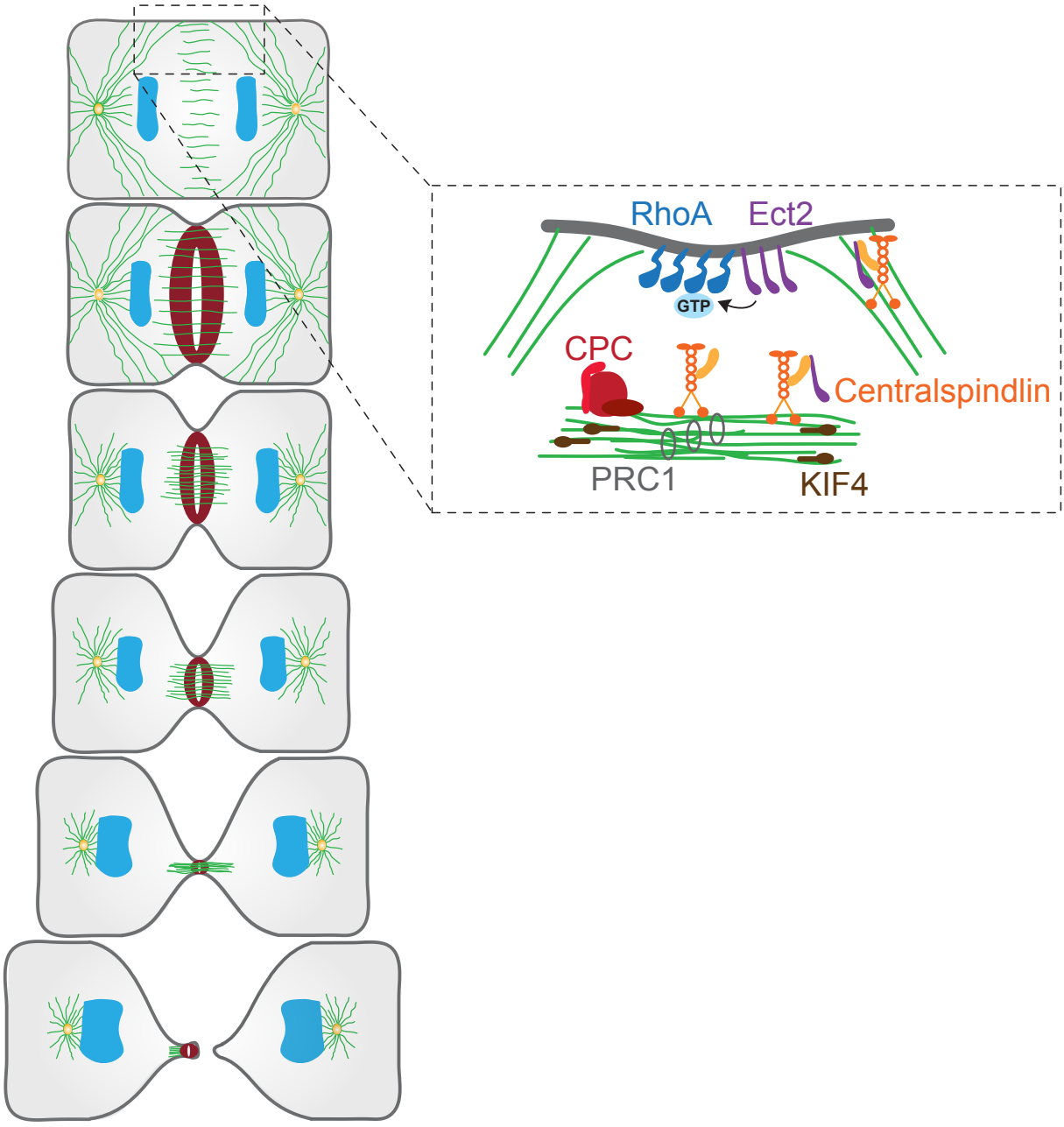

Figure 2.1.2 Molecular constituents of the spindle midzone

The CPC (red), centralspindlin complex (orange), PRC1 (light grey) and KIF4 (brown) are recruited on microtubules of the midzone. The centralspindlin complex recruits Ect2 (purple) at the equatorial membrane for activation of RhoA (blue). Adapted from (Green et al., 2012).

The active participation of the spindle midzone in determining the site of division is well established (Cao and Wang, 1996; Foe and von Dassow, 2008; Odell and Foe, 2008; Rappaport, 1961; Rappaport, 1985). Several elegant imaging and inhibitory experiments performed in different organisms identified the conserved molecules required for spindle midzone assembly. Establishment of the spindle midzone requires three major components; protein regulating cytokinesis 1 (PRC1), the chromosomal passenger complex (CPC) and the centralspindlin complex. Described below are the molecular constituents of each complex that form an intricate signaling network that contributes to proper positioning of the cleavage furrow.

PRC1 directly interacts with microtubules of the midzone and promotes their bundling (Figure 2.1.2) (Jiang et al., 1998; Mollinari et al., 2002; Neef et al., 2003). PRC1 also recruits the kinesin motor protein KIF4 to the overlapping bundles of microtubules (Bieling et al., 2010). KIF4 in turn binds to the plus-end of microtubules and inhibits their elongation once proper overlap has been achieved (Figure 2.1.2) (Bieling et al., 2010; Hu et al., 2011). Upon KIF4 depletion, the spindle midzone over elongates resulting in a broadened zone of division place specification (Hu et al., 2011). Thus, PRC1 acts as a cross-linker of midzone microtubules, while KIF4 provides negative feedback to inhibit this process upon completion.

Spindle midzone formation also requires the presence of the Chromosomal Passenger Complex. The CPC includes inner centromere protein (INCENP), Aurora B kinase, Survivin and Borealin (Earnshaw and Bernat, 1991; Earnshaw and Cooke, 1991). The CPC forms a communication bridge between chromosomes and microtubules of the midzone. At anaphase onset, the CPC translocates from mitotic chromosomes to microtubules of the spindle (Figure 2.1.2) (Gruneberg et al., 2004). During animal cytokinesis, the mammalian kinase-like protein 2 (MKLP2) mediates this process (Gruneberg et al., 2004). Conversely, in *C. elegans* embryos, the localization of the Aurora B orthologue AIR-2 at the spindle midzone is dependent on INCENP (ceICP-1) (Kaitna et al., 2000).

The presence of Aurora B at the spindle midzone is required for proper cytokinesis (Terada et al., 1998). Early studies in mammalian cells revealed high levels of multinucleation due to cytokinesis failure upon Aurora B overexpression (Terada et al., 1998). *C. elegans*

embryos depleted of Aurora B (ceAIR-2) initiate furrow ingression but the furrow rapidly regresses to form a binucleated cell (Kaitna et al., 2000). Similar cytokinesis defects were observed following the depletion of INCENP (ceICP-1) (Kaitna et al., 2000).

Aurora B and INCENP of the CPC participate in signal transmission to the cell cortex for division plane establishment (Lewellyn et al., 2011). Early work revealed the presence of INCENP and Aurora B at both the spindle midzone and cell cortex at the future site of division (Earnshaw and Cooke, 1991). At the spindle midzone, Aurora B promotes the recruitment of the centralspindlin complex (Kaitna et al., 2000; Severson et al., 2000).

The centralspindlin complex is composed of a heterotetramer of two molecules of the kinesin-6 motor MKLP1 and two MgcRacGAP/CYK-4 molecules (Figure 2.1.2) (Mishima et al., 2002; Pavicic-Kaltenbrunner et al., 2007; Somers and Saint, 2003). Work in *C. elegans* embryos supported the role of Aurora B (ceAIR-2) in recruiting the centralspindlin complex to the midzone. Experiments led by Severson showed that AIR-2 interacts with MKLP1 (ceZEN-4) to promote ZEN-4 localization at the spindle mizdone (Severson et al., 2000).

The centralspindlin complex is required for proper cytokinesis and contributes to midzone microtubule bundling. The activity of the centralspindlin complex is regulated in a precise temporal fashion. The master cell cycle regulator, Cdk1-cyclin B, phosphorylates MKLP1 (ceZEN-4) and MgcRacGAP/CYK-4 (ceCYK-4) during mitosis (Mishima et al., 2004). After anaphase onset, MKLP1 (ceZEN-4) dephosphorylation by CDC-14 promotes its localization to the spindle midzone and motor activities (Gruneberg et al., 2002; Mishima et al., 2004). In addition, work in *C. elegans* embryos and mammalian cultured cells, has demonstrated that MKLP1 (ceZEN-4) alone or together with MgcRacGAP/CYK-4 (CYK-4) function to bundle microtubules *in vitro* (Jantsch-Plunger et al., 2000; Mishima et al., 2002; Mishima et al., 2004). Furthermore, *C. elegans* embryos depleted of both components independently exhibited similar cytokinesis defects. During the first cleavage, embryos showed furrow initiation and ingression but failed to complete membrane ingression (Powers et al., 1998; Raich et al., 1998). Work in mammalian cells also demonstrated the essential role of this complex during cytokinesis. HeLa cells overexpressing MgcRacGAP/CYK-4 were for the most part multinucleated (Hirose et al., 2001).

Another important function of the centralspindlin complex is to recruit the RhoGEF Ect2 to the spindle midzone (Figure 2.1.2). Experiments in HeLa cells showed that both MKLP1 and CYK-4 are necessary for Ect2 localization at the spindle midzone and equatorial cortex (Nishimura and Yonemura, 2006; Yuce et al., 2005). Direct interaction between CYK-4 and Ect2 was demonstrated in a yeast two-hybrid assay performed in *Drosophila* S2 cells (Somers and Saint, 2003). This interaction was later reported in HeLa cells by co-immunoprecipitation (Yuce et al., 2005). The interaction between CYK-4 and Ect2 at the spindle midzone is cell-cycle dependent requiring Ect2 dephosphorylation after anaphase onset (Yuce et al., 2005). This ensures spatiotemporal coordination of division plane specification following faithful chromosome segregation. Altogether, these elegant studies in various organisms illustrate the importance of the centralspindlin complex in the early events of cytokinesis.

An additional molecular component of the spindle midzone and required for cytokinesis is polo-like kinase 1 (PLK1). In *Drosophila*, polo kinase (plk) associates with the MKLP1 fly orthologue Pavarotti (pav) (Adams et al., 1998). This interaction is required for the establishment of the cleavage furrow and membrane ingression (Adams et al., 1998). Conversely, during mammalian cytokinesis MKLP2 recruits PLK1 to the spindle midzone (Neef et al., 2003). The presence of PLK1 at the midzone further enhances the activity of MKLP2 (Neef et al., 2003). Thus, the synergistic relationship between PLK1 and MKLP2 is important for cytokinesis in mammalian cells.

In addition to spindle midzone assembly, PLK1 is required for furrowing formation (Brennan et al., 2007). The development of PLK1 chemical inhibitors allowed for functional characterization of PLK1 during cytokinesis. In mammalian cultured cells, PLK1 inhibition resulted in the absence of furrow ingression and prevented anaphase spindle elongation (Brennan et al., 2007). Cells treated with PLK1 inhibitors failed to recruit RhoA and its GEF Ect2 at the cell equator (Brennan et al., 2007). Furthermore, PLK1 mediates the interaction between the centralspindlin complex and Ect2 required for subsequent targeting of Ect2 at the cell equator for contractile ring assembly (Kim et al., 2014). These results demonstrate that PLK1 coordinates different aspects of cytokinesis.

2.1.3 Cell-type specific requirements for division plane establishment

Even though the molecular machinery operating at the spindle midzone is conserved, these components provide different contributions depending on the organism. For instance, *Drosophila* cytokinesis is highly sensitive to the localization of Pavarotti (*pav*; MKLP1) at the spindle midzone. *Pav* mutant fly embryos showed abnormal spindle midzones and failed to establish a cleavage furrow (Adams et al., 1998). Conversely, mammalian cell cytokinesis is strongly dependent on MKLP2 function, only found in mammals. MKLP2 depletion leads, in most cases, to cytokinesis failure due to a failure in recruitment of Aurora B and PLK1 to the spindle midzone (Neef et al., 2003). Altogether, these findings suggest that components of the spindle midzone play a prominent role in establishing the site of division in both mammals and *Drosophila*.

The contribution from molecular players at the spindle midzone differs during *C. elegans* embryonic cleavage. In *C. elegans* zygotes depleted of the centralspindlin components CYK-4 and ZEN-4 independently, the site of cleavage is properly defined and membrane ingression proceeds (Jantsch-Plunger et al., 2000; Powers et al., 1998; Raich et al., 1998). Micromanipulation experiments showed that ablating part of the spindle midzone did not prevent furrowing (Bringmann and Hyman, 2005). In another study, PRC1 (ceSPD-1) depletion prevented formation of the spindle midzone but cytokinesis proceeded to completion (Verbrugghe and White, 2004). Thus, in *C. elegans* embryos the spindle midzone is dispensable for cleavage plane specification.

In *C. elegans* embryos, signals from astral microtubules play a prominent role in determining the site of cleavage. In an experiment, Lewellyn and colleagues restricted spindle elongation by genetic manipulations and observed an increase in cortical contractility leading to the apparition of multiple furrows (Lewellyn et al., 2010). The shorter astral microtubules failed to reach the cell cortex to restrict the site of division between segregated chromosome masses (Lewellyn et al., 2010). In another study, Zanin and colleagues also demonstrated the importance of astral microtubules in restricting signals to the equatorial cortex for division plane establishment. Upon nocodazole treatment, HeLa cells showed hypercontractility at the poles of the cell and a broadening of RhoA accumulation at the equatorial cortex (Zanin et al.,

2013). In sum, these results support the role of astral microtubules in restricting molecular components required for furrowing at the equatorial cortex.

A different scenario was observed in *Drosophila* neuroblasts depleted of centrioles, where astral microtubules emanate. In most cases, cells without centrioles were able to assemble a functional contractile ring and complete cytokinesis (Basto et al., 2006). This indicates that in flies, astral microtubules are dispensable for establishing the division site and for proper execution of cytokinesis (Basto et al., 2006). Altogether, these findings demonstrate that astral microtubules and the spindle midzone make different contributions to specify the site of furrowing, depending on the organism.

2.1.4 Ect2-dependent RhoA activation at the equatorial cortex

Once the site of division has been determined, the information is relayed to the equatorial cortex. A central player during cytokinesis and enriched at the equatorial cortex is the GTPase RhoA (Figure 2.1.2). Yüce and colleagues used florescent imaging to show that RhoA localizes at the equatorial cortex and is enriched throughout furrow ingression (Yuce et al., 2005). RhoA enrichment at the cell equator is essential for the cell to proceed with later events of cytokinesis in all systems studied. For instance, RhoA inhibition by either the C3 enzyme or its inhibitory protein RhoGDI prevented furrow formation in *Xenopus* embryos (Kishi et al., 1993). *C. elegans* embryos depleted of RhoA also failed to assemble a contractile ring (Jantsch-Plunger et al., 2000). In human cells, RhoA depletion by RNA interference (RNAi) prevented furrow ingression (Yuce et al., 2005). These studies illustrate the conserved nature of RhoA and its crucial role in cytokinetic furrow formation.

RhoA is activated by the exchange of GDP to GTP mediated by the RhoGEF Ect2 (Figure 2.1.2) (Prokopenko et al., 1999; Tatsumoto et al., 1999; Yuce et al., 2005). The first evidence that Ect2 promoted RhoA activity came from work in *Drosophila*, where it was demonstrated that Rho1 (RhoA) interacts with Pebble (*Drosophila* Ect2) *in vivo* (Prokopenko et al., 1999). The Rho1 and Pebble interaction was observed in a yeast two-hybrid experiment (Prokopenko et al., 1999). In addition, both proteins localized at the ingressing furrow and Rho1 mutant flies presented binucleated cells resulting from cytokinesis failure (Prokopenko et al., 1999). In mammalian cells, expression of a dominant negative form of Ect2 resulted in

cytokinesis failure (Tatsumoto et al., 1999). HeLa cells depleted of Ect2 failed to present RhoA enrichment at the equatorial cortex (Yuce et al., 2005). These studies supported the role of Ect2 in promoting local RhoA activation.

Other studies were directed at the identification of the GAP protein responsible for RhoA inactivation. Minoshima and colleagues first demonstrated that MgcRacGAP/CYK-4 processed a GAP activity towards RhoA (Minoshima et al., 2003). This group showed that Aurora B phosphorylated MgcRacGAP/CYK-4 *in vitro* and this event stimulated the inactivating GAP activity of MgcRacGAP/CYK-4 towards RhoA (Minoshima et al., 2003). In a later study, Miller and coworkers demonstrated the importance of the GAP activity of MgcRacGAP/CYK-4 for RhoA enrichment during cytokinesis. *Xenopus laevis* embryos injected with MgcRacGAP/CYK-4 harboring defective GAP domains showed a broadening of RhoA enrichment at the equatorial cortex (Miller and Bement, 2009). Completely removing the GAP domain of MgcRacGAP/CYK-4 led to broader RhoA enrichment accompanied by furrow oscillation causing cytokinesis failure (Miller and Bement, 2009). These results supported the Rho GTPase flux model. This model proposes that a constant flux of RhoA activation by its GEF Ect2 and inactivation by the GAP domain of MgcRacGAP/CYK-4 is required for proper enrichment of RhoA at the equatorial cortex and the subsequent stages of cytokinesis (Miller and Bement, 2009).

Work in *C. elegans* zygotes and human cells illustrated variations to this model. The identification of MP-GAP (ceRGA-3 and ceRGA-4) as a GAP acting to inactivate RhoA included a new molecular regulator of RhoA activity (Zanin et al., 2013). Unlike MgcRacGAP/CYK-4, MP-GAP depletion caused cortical hypercontractility but did not lead to a broadening of the RhoA zone at the equatorial cortex (Zanin et al., 2013). Only when astral microtubule function was abolished by nocodazole treatment did MP-GAP participate in restricting RhoA enrichment at the cell equator (Zanin et al., 2013). Therefore, MP-GAP also contributes to the RhoA GTPase flux model and acts as a fail-safe mechanism for proper RhoA enrichment at the equatorial cortex.

Molecular regulators at the spindle midzone also contribute to local RhoA enrichment. MKLP1, member of the centralspindlin complex, participates in restricting RhoA enrichment at the cell equator (Yuce et al., 2005). In HeLa cells, MKLP1 depletion results in broadening

of the RhoA zone at the cell equator. This group also showed that depleting MgcRacGAP/CYK-4 prevented RhoA enrichment at the cell equator altogether (Yuce et al., 2005). In addition, Aurora B was recently implicated in RhoA recruitment at the furrowing site, since it promotes centralspindlin localization at the equatorial membrane, a requirement for the activation of RhoA (Basant et al., 2015). Aurora B and the centralspindlin complex contribute to RhoA enrichment at the site of contractile ring assembly.

Bement and colleagues showed that the breadth of the RhoA zone at the cell equator scaled with diameter of both urchin and frog embryos (Bement et al., 2005). They also showed that local RhoA enrichment preceded the recruitment of contractile ring components (Bement et al., 2005). Later work revealed the important role of RhoA in targeting several downstream effectors required for contractile ring assembly (Su et al., 2011). Thus, the breadth of RhoA enrichment at the equatorial cortex is important for subsequent assembly of a contractile ring scaling with cell size. The work presented in Chapter 3 will address this property of the contractile ring (Bourdages et al., 2014).

2.2 Contractile ring assembly

In the next stage of cytokinesis, structural components are recruited to the equatorial cortex and assemble to form a contractile ring (Figure 2.2.1A). In the following section, principal constituents of the contractile ring are described along with their requirements for contractile ring assembly. The contractile ring is a robust yet dynamic structure that constricts to mechanically separate a cell into two. How this is achieved will be addressed in a later section. Finally, high-temporal resolution of contractile rings revealed an interesting property of contractile ring closure. Across metazoans, the contractile ring closes asymmetrically as will be discussed in the ending section.

2.2.1 Structural components of the contractile ring

Structural analysis of contractile rings began with the advent of electron and fluorescence microscopy techniques. Early observations uncovered the invariable nature of the basic architecture of contractile rings (Schroeder, 1970; Schroeder, 1972). The contractile ring assembles beneath the plasma membrane as a very thin layer (0.1-0.2 μm) as measured by

electron microscopy (Schroeder, 1972). In general, contractile rings are 5-10 μm wide once assembled and when viewed in two dimensions (Schroeder, 1972).

Actin filaments (F-actin) and non-muscle myosin II are the major constituents of contractile rings (Figure 2.2.1B). F-actin and non-muscle myosin II present in contractile rings assemble as mini-filaments (Figure 2.2.1B) (Cao and Wang, 1990; Otto and Schroeder, 1990; Sanger and Sanger, 1980; Zhou and Wang, 2008). Upon contractile ring assembly, F-actin and non-muscle myosin II overlap at the equatorial cortex where they assemble into a ring and remain enriched throughout constriction (Cao and Wang, 1990; Otto and Schroeder, 1990; Zhou and Wang, 2008). Actin microfilaments of different orientations form bundles arranged circumferentially beneath the plasma membrane (Kamasaki et al., 2007; Mabuchi et al., 1988). Imaging adherent cells beneath the surface revealed the presence of myosin II mini-filaments accompanying F-actin (Zhou and Wang, 2008).

Actin filaments and non-muscle myosin II are the molecular drivers of contractile ring ingression, further described in a later section. When cells are treated with actin or myosin inhibitors, such as cytochalasin B or blebbistatin, contractile ring constriction is completely blocked (Mabuchi et al., 1988). Thus, actin and non-muscle myosin II mini-filaments assemble into a ring around the cell equator that constricts to physically partition the mother cell into two daughter cells.

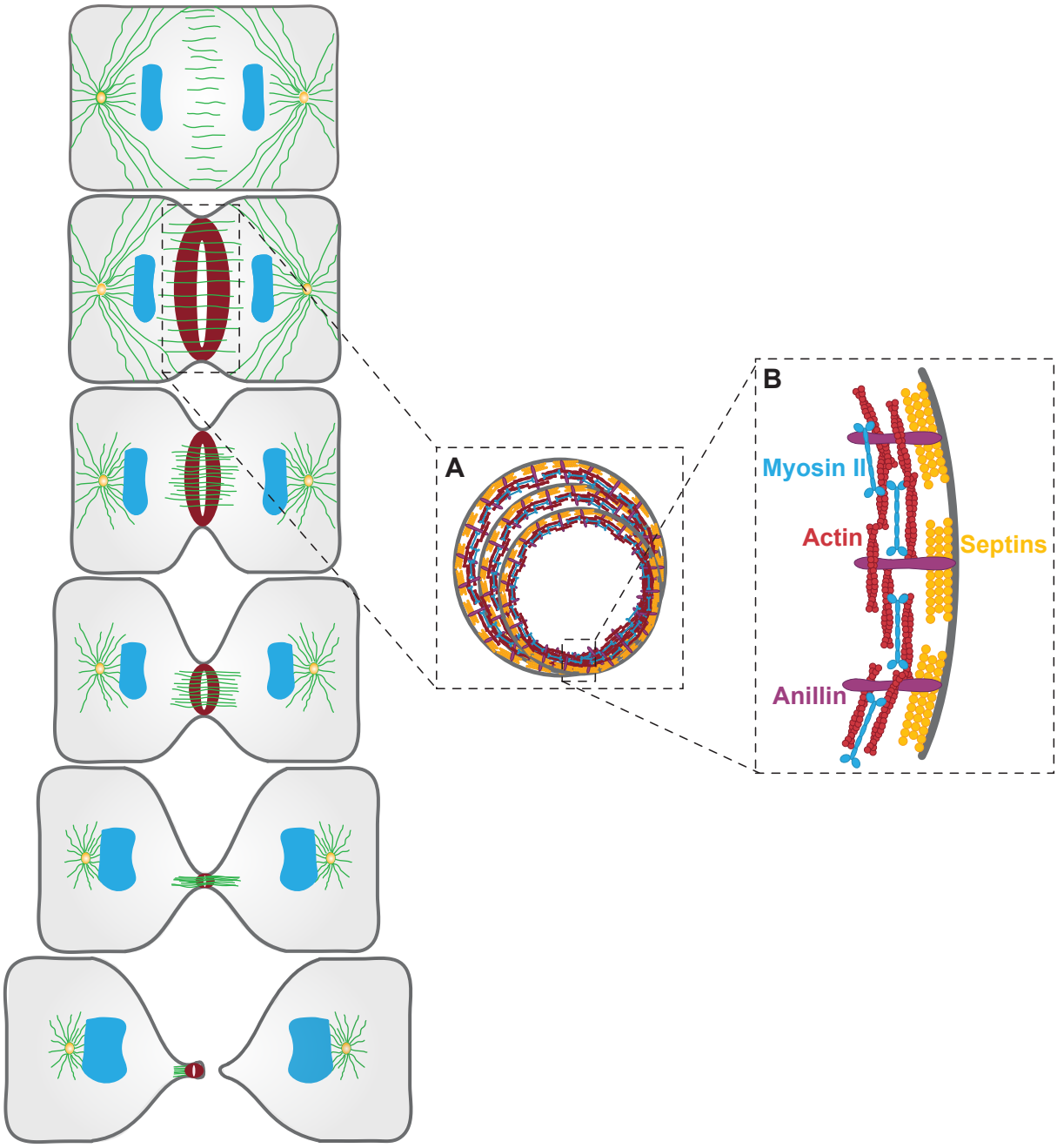

Figure 2.2.1 Structural components of the contractile ring

(A) Schematic representing contractile ring constriction over time. (B) Magnified view on the contractile ring in A, depicting the principal structural components, non-muscle myosin II (blue), actin filaments (red), septins (yellow) and Anillin (purple). Adapted from (Green et al., 2012).

2.2.2 Molecular constituents required for contractile ring assembly

Additional components have been implicated in contractile ring assembly and ensure proper spatiotemporal coordination of contractile ring closure. As previously mentioned, activated RhoA at the equatorial cortex targets several effectors necessary for contractile ring assembly (Su et al., 2011). This includes formins that bind to GTP-bound RhoA and promote the assembly of actin filaments (Piekny et al., 2005). Formins drive actin nucleation and polymerization to generate actin filaments (Piekny et al., 2005). This process is also mediated by profilin, that binds to G-actin monomers and facilitates nucleation and polymerization by formins (Piekny et al., 2005).

Contractile ring assembly also requires the activation of the motor protein non-muscle myosin II. The RhoA effector Rho-dependent kinase (ROCK) is the primary kinase responsible for myosin II activation. ROCK phosphorylates the regulatory light chain (rMLC) of myosin II and promotes the assembly of myosin filaments (Kosako et al., 2000). ROCK also stimulates the inhibition of myosin phosphatases to prevent myosin II inactivation (Piekny et al., 2005). Upon ROCK inhibition cleavage furrow ingression is delayed (Kosako et al., 2000). This illustrates the importance of ROCK-dependent myosin II activation in the temporal control of cytokinesis. Other kinases, including Citron-kinase, are known to be implicated in myosin II activation (Yamashiro et al., 2003), but their contributions to cytokinesis are less well defined.

Another molecular constituent of the contractile ring is septin (Figure 2.2.1B). Mammalian septin complexes were found to co-localize with actin filaments and contribute to their bundling *in vitro* (Kinoshita et al., 2002). A later study confirmed the bundling activity of septins towards F-actin in *Drosophila* embryo furrow canals (Mavrakis et al., 2014). In addition, *Drosophila* septin (Peanut) was able to induce curvature of actin filament bundles (Mavrakis et al., 2014). Septin also interacts with lipids of the plasma membrane, suggesting that it plays a role in linking the underlying actin cytoskeleton to the membrane during cytokinesis (Tanaka-Takiguchi et al., 2009). A further role for septin and specific to *C. elegans* embryos is to promote asymmetric ingression of the contractile ring together with Anillin, as further described in a later section (Maddox et al., 2007). In sum, the recruitment of septins is required for proper contractile ring assembly.

2.2.3 The scaffolding protein Anillin

Anillin is a key structural component of the contractile ring. It functions as a scaffolding protein of contractile rings assembled during cytokinesis. Anillin is a multi-domain protein that binds several structural components of the cortical cytoskeleton, including actin filaments, myosin II and septin amongst others (Figure 2.2.1B) (Piekny and Maddox, 2010; Zhang and Maddox, 2010). Thus, Anillin serves diverse functions required for the proper spatiotemporal coordination of contractile ring closure. Characterization studies of Anillin across eukaryotes revealed its conserved nature (Field and Alberts, 1995; Field et al., 2005; Maddox et al., 2007; Oegema et al., 2000; Straight et al., 2005; Sun et al., 2015). In the following section, the numerous activities of Anillin during cytokinesis are addressed in detail.

Anillin was first isolated from *Drosophila* embryo extracts (Field and Alberts, 1995). Early work with *Drosophila* provided important insights into the function of Anillin during cytokinesis. *In vitro*, Anillin was identified as an actin filament binding protein and a minimal domain of it was subsequently shown to be sufficient to bundle F-actin (Field and Alberts, 1995). *In vivo* studies showed that Anillin localized to contractile structures, including the contractile ring of *Drosophila* cultured cells and furrow canals (Field and Alberts, 1995; Field et al., 2005). Anillin co-localized with actin, myosin II and septin of *Drosophila* contractile furrow canals (Field et al., 2005). This work with *Drosophila* laid the foundation for functional characterization studies of Anillin.

Later work in mammalian cells supported the idea of a conserved role for Anillin during cytokinesis. Oegema and colleagues observed translocation of human Anillin from the nucleus in interphase to the contractile ring of dividing HeLa cells (Oegema et al., 2000). Functional analysis of the Anillin protein revealed its large multi-domain identity. The C-terminal region of Anillin comprises an Anillin Homology (AH) domain and a PH domain (Piekny and Maddox, 2010). Anillin recruits septins to the contractile ring via its PH domain (D'Avino et al., 2008; Hickson and O'Farrell, 2008; Oegema et al., 2000). Additional studies showed that Anillin interacted with PIP2 component of the plasma membrane via its PH domain (Liu et al., 2012; Sun et al., 2015). In mammalian cells, this interaction is required for the recruitment of Anillin to the contractile ring (Liu et al., 2012). This was previously demonstrated by introducing mutations in the PH domain of Anillin that resulted in failure to

recruit Anillin to the contractile ring (Oegema et al., 2000). These studies also suggested that Anillin provided a link between the plasma membrane and the underlying furrow (Liu et al., 2012).

Mechanistic insights regarding the recruitment of Anillin to the division plane were obtained via the expression of tagged truncations in mammalian cultured cells (Piekny and Glotzer, 2008). In this elegant study in mammalian cells, Anillin was depleted by RNAi and various Anillin constructs harboring different domain truncations and tagged with the green fluorescent protein (GFP) were re-introduced in the cell (Piekny and Glotzer, 2008). Truncation of the PH domain prevented Anillin enrichment at the contractile ring as previously demonstrated. Cytokinesis failure was observed upon truncation of both the actin and myosin II binding domains located at the N-terminal region of the protein. Finally, removal of the AH domain caused defects during furrow ingression, as Anillin translocated at the cell poles leading to furrow oscillation (Piekny and Glotzer, 2008). Furthermore, the authors observed the co-localization of Anillin and RhoA at the cytokinetic furrow (Piekny and Glotzer, 2008). These proteins interacted *in vitro* via Anillin's AH domain. Cells depleted of either RhoA or its GEF activator Ect2 failed to accumulate Anillin at the equatorial cortex (Hickson and O'Farrell, 2008; Piekny and Glotzer, 2008). Thus, RhoA is responsible for recruiting Anillin to the equatorial cortex and the PH domain of Anillin is essential for its enrichment at the contractile ring (Hickson and O'Farrell, 2008; Piekny and Glotzer, 2008).

Anillin possesses additional interacting partners during cytokinesis suggesting that it serves other activities. However, it is important to note that these interactions are not as well characterized. Anilin interacts with the F-actin polymerization protein formin (Watanabe et al., 2010). Anillin participates in the recruitment of formin to the equatorial cortex required for actin nucleation and polymerization (Watanabe et al., 2010). In *Drosophila* Anillin directly interacts with the centralspindlin complex component CYK-4 (*Drosophila* RacGAP50C) suggesting a role for Anillin in division plane establishment (D'Avino et al., 2008; Hickson and O'Farrell, 2008). Thus, Anillin performs numerous activities during cytokinesis.

Anillin is an essential structural component of the contractile ring ensuring proper contractile ring closure. As previously mentioned, truncations of either the myosin II or the actin-binding domain of Anillin results in furrow oscillation and contractility at the poles,

causing cytokinesis failure in most cases (Kechad et al., 2012; Piekny and Glotzer, 2008). The phenotype of lateral furrow oscillation was also reported in *Drosophila* and human cultured cells depleted of Anillin (Hickson and O'Farrell, 2008; Kechad et al., 2012; Straight et al., 2005). In mammalian cells, Anillin inhibition following injection with an anti-anillin antibody leads to slower contractile ring closure (Oegema et al., 2000). Subsequent studies in *Drosophila* epithelial cells also reported slower constriction upon Anillin and septin depletion (Guillot and Lecuit, 2013). Altogether, these studies illustrate the crucial role of Anillin during cytokinesis.

Anillin remains enriched at the contractile ring during the late stage of ring constriction. At this stage, the contractile ring transition into the midbody ring (Kechad et al., 2012). Anillin provides structural stability of the midbody ring for subsequent abscission (Kechad et al., 2012). Anillin also localizes at contractile rings assembled during polar body cytokinesis occurring during meiotic division (Dorn et al., 2010). Anillin contributes to the maintenance of the structural architecture of polar body cytokinetic rings by linking cytoskeletal components to the plasma membrane (Dorn et al., 2010). Thus, Anillin act as a scaffold for all cytokinetic rings.

2.3 The mechanics of contractile ring closure

The actomyosin ring assembled at the cell equator generates enough force to drive membrane ingression. How this occurs mechanistically generated a lot of interest in both the biology and physics field. While several groups investigated the general mechanism of ring constriction, others focused their work on the physical and mechanical properties of contractile ring components. Even though the mechanism driving contractile ring closure is not fully understood, several important features of constriction were identified. Interestingly, several studies revealed that several aspects of the actomyosin ring scaled with cell size. These findings are the major focus of this section.

A study combining biological experiments in budding yeasts and theoretical modeling revealed the importance of F-actin depolymerization during constriction (Mendes Pinto et al., 2012). Blocking actin depolymerization by either a small molecule (jasplakinolid) or mutation of cofilin (actin severing and depolymerizing component) slowed constriction (Mendes Pinto

et al., 2012). Yeast cells expressing myosin II deleted of its motor domain also exhibited slower constriction rates, suggesting that the motor activity of myosin II contributes to F-actin polymerization (Mendes Pinto et al., 2012). In addition, their model proposed that constriction driven by actin filaments depolymerization involved cross-linking of components of the contractile ring, such as Anillin and septins (Mendes Pinto et al., 2012).

Additional studies provided evidences of the occurrence of cytoskeleton components cross-linking promoting actomyosin filaments sliding during constriction. The mathematical model of Carlsson included cross-linking of actin filaments for the generation of contractile ring contractions (Carlsson, 2006). The contribution from cross-linking of the structural components of contractile rings was demonstrated in a recent study with *C. elegans* zygotes (Descovich et al., 2016). This study revealed that the level of cross-linking in the contractile ring is finely tuned. RNAi-based depletions at intermediate levels of either the Anillin protein (ANI-1 in *C. elegans*) or NMY-II (non-muscle myosin II) led to an increase in furrowing speed compared to control embryos (Descovich et al., 2016). These results suggested that intermediate levels of cytoskeletal components cross-linking were needed for optimal furrowing (Descovich et al., 2016). In addition, they showed that the motor, non-muscle myosin II, and cross-linkers, including septins and Anillin, both drove constriction but also acted as brakes ensuring proper kinetics of contractile ring closure (Descovich et al., 2016). Thus, Descovich et al, demonstrated that a balance between motor activity and cross-linking of contractile ring components was required for optimal contractile ring dynamics (Descovich et al., 2016).

Actomyosin filament sliding has been proposed to drive contractile ring closure (Dorn et al., 2016; Mendes Pinto et al., 2012). Dorn and colleagues developed a mathematical model that accurately recapitulated F-actin sliding powered by non-muscle myosin II motor activity (Dorn et al., 2016). In addition, this model described the positive feedback occurring between the initial membrane curvature, actin filaments alignment in the contractile ring and the contractile force generated to drive constriction over time (Dorn et al., 2016). This study provided important insights onto the mechanics of contractile ring closure.

Work with *C. elegans* embryos revealed an interesting property of contractile ring closure. Carvalho and colleagues first illustrated the scalable nature of the rate of contractile

ring closure (Carvalho et al., 2009)). They observed that contractile rings of different initial diameters during rapid embryonic cleavages took the same total amount of time to bring about contractile ring closure (Carvalho et al., 2009). This led the authors to propose a model whereby a series of contractile units are incorporated into the ring at the time of contractile ring assembly. These units are of fixed size, which means that larger cells are composed of more of these units compared to smaller cells. During constriction, these units shorten causing larger rings to constrict at a faster but constant rate since they possess more units. Conversely, smaller cells possess fewer units and thus constrict at a slower rate making the duration of ring closure independent of initial cell size (Carvalho et al., 2009). The nature of these units corresponded to contractile ring components, primarily actin and myosin II filaments. However, the mechanism of contractile unit shortening was not addressed per se. This study provided the first evidence that the mechanics of contractile ring closure were influenced by cell size.

Different scaling properties of the contractile ring were observed in the filamentous fungi *Neurospora crassa*. This study proposed that contractile rings generated sufficient force by rapid actin and myosin II turnover (Calvert et al., 2011). Interestingly, this work presented evidences of a size-dependent force that drives cell shape changes in hyphae of different diameters, supporting previous observations by Carvalho and colleagues (Calvert et al., 2011). Altogether, these findings suggested that contractile rings possessed a conserved property that rendered the time required for ring closure independent of initial size with differences in the mechanics of contractile ring ingression depending on the organism.

2.3.1 Asymmetric cytokinesis

There is an important distinction to be made between asymmetric cellular division and asymmetric cytokinesis. Asymmetric cell division refers to cells that divide to produce daughter cells of unequal fates and/or sizes, such as the first mitotic division of *C. elegans* embryos, the extrusion of small polar bodies from large oocytes, and stem cell divisions. Conversely, asymmetric cytokinesis refers to the geometry of the contractile ring within the division plane, specifically that contractile ring ingression is dominant in one direction resulting in off-center placement of the midbody. Careful monitoring of contractile ring

ingression over time revealed the conserved nature of this property across metazoans (Dorn et al., 2016).

Mammalian MDCK epithelial cells in culture undergo asymmetric furrowing (Reinsch and Karsenti, 1994). Reinsch and Karsenti observed contractile ring ingression biased towards the apical junctions of these epithelial cells (Reinsch and Karsenti, 1994). Nonconcentric (asymmetric) furrowing was also observed in several other epithelial tissues including mouse intestinal epithelial cells (Fleming et al., 2007), neural progenitor cells of the retina in *zebrafish* (Das et al., 2003), and in the chick neuroepithelium (Dubreuil et al., 2007).

The mechanism underlying this property of contractile rings has been very little studied. Insights were gained from elegant work with *C. elegans* embryos (Maddox et al., 2007). As previously mentioned, contractile ring closure is asymmetric during embryonic cleavage of *C. elegans* zygotes (Dorn et al., 2016; Maddox et al., 2007). Anillin and septins were found to be required for nonconcentric contractile ring closure of the zygote (Maddox et al., 2007). Embryos depleted of either Anillin or septins underwent symmetric contractile ring closure (Maddox et al., 2007). Imaging of fluorescently labeled Anillin (ANI-1) and septins (UNC-59 and UNC-61) confirmed their localization at the leading edge of the ingressing furrow (Maddox et al., 2007). In addition, structural components of the contractile ring, including non-muscle myosin II, Anillin and septins, were asymmetrically distributed in the closing ring (Maddox et al., 2007). The authors observed increased expression of these components on the side of the contractile ring with the greatest impression, consistent with asymmetric contraction of the ring (Maddox et al., 2007). These results led the authors to propose that in isolated systems asymmetric furrowing confers robustness to the contractile ring confronted with mechanical challenges (Maddox et al., 2007). Maddox and colleagues forced symmetric contractile ring closure by depleting septins and reduced ring contraction by depletion of Rho-kinase, an activator of non-muscle myosin II (Maddox et al., 2007). This resulted in approximately 60% cytokinesis failure supporting the idea of reduced robustness of the contractile ring under these conditions (Maddox et al., 2007). The theoretical model proposed by Dorn et al, supported the idea that asymmetric cytokinesis makes contractile ring closure more robust (Dorn et al., 2016).

Contractile ring closure in epithelial cells is polarized, occurring towards the apical domain of the epithelium (Dubreuil et al., 2007; Fleming et al., 2007; Reinsch and Karsenti, 1994). Work with *Drosophila* epithelial cells demonstrated that asymmetric contractile ring closure is dictated by the mechanical properties of apical junctions, further discussed in the following section (Guillot and Lecuit, 2013).

2.4 Mechanistic insights into cytokinesis in epithelial cells

Most of the current knowledge of the different events of cytokinesis comes from studies in isolated cells, including zygotes, yeasts, and mammalian cultured cells. For years, a large void remained in the cytokinesis field regarding the mechanics of cytokinesis occurring in multicellular tissues. Epithelial cells present different characteristics since they are interconnected to one-another and confined in a tissue. Epithelial cells must maintain tissue integrity during the dramatic cell shape changes of cytokinesis. In the following sections, the progress made in characterizing the mechanisms governing cytokinesis in epithelial cells within intact tissues will be reviewed.

2.4.1 Molecular composition of intercellular junctions

Animal tissues are composed of epithelial cells that perform specialized functions. These cells act as a barrier against the surrounding environment and delimit distinct tissues. Epithelial cells are mechanically coupled with one another and are polarized. Cell polarity is reflected by differences in cell shape, asymmetric distribution of molecular constituents and by the orientation and alignment of the underlying cytoskeleton (Knust and Bossinger, 2002). The plasma membrane comprises an apical surface facing the outside environment or a lumen and a basolateral domain in contact with neighboring cells or the basal substratum (Knust and Bossinger, 2002).

The mechanical and biochemical barrier functions of epithelia require that the cells are connected by intercellular adhesions. A high degree of similarity in the structural constituents of intercellular junctions is observed between species (Knust and Bossinger, 2002; Takeichi, 2011). Across metazoans, epithelial cells are interconnected via adherens junctions, composed of apically localized protein complexes (Takeichi, 2011). Adherens junctions establish

adhesion via the core transmembrane protein E-cadherin, cytoplasmic components beta-catenin and alpha-catenin, and the actomyosin cytoskeleton (Baum and Georgiou, 2011; Takeichi, 2011).

Even though the basic architecture of apical junctions is conserved, additional domains have evolved. Vertebrate epithelial cells possess tight junctions (TJs), a specialized domain located apical to adherens junctions (Knust and Bossinger, 2002). Similarly, *Drosophila* epithelial cells have septate junctions (SJs) located on the basolateral membrane (Knust and Bossinger, 2002). Both TJs and SJs function as barriers between adjacent cells and mediate cellular exchanges ensuring tissue homeostasis (Knust and Bossinger, 2002).

2.4.2 The *C. elegans* apical junctions

The structural organization of the different components of intercellular junctions differs in *C. elegans*. Apical junctions are present as a single electron dense structure composed of three different domains (Lynch and Hardin, 2009). This structure is referred to as the *C. elegans* apical junctions (CeAJs). In *C. elegans* epithelial cells, adherens junctions are located at the apical most part of the CeAJs. Adherens junctions include the conserved components E-cadherin (HMR-1), beta-catenin (HMP-2) and alpha-catenin (HMP-1). These components were identified in a genetic screen for *C. elegans* embryos with morphological defects (Costa et al., 1998). These mutants were described based on their phenotype from the screens, namely Hammerhead (hmr) for defects in worm elongation and failure of the epidermis to enclose the entire body of the developing worm, shaped as a hammer in the eggshell (Costa et al., 1998). Humpback (hmp) describes body elongation defects resulting in large bulges on the newly hatched worm (Costa et al., 1998). Unlike in vertebrates and *Drosophila*, adherens junctions are dispensable for intercellular adhesions in the worm (Costa et al., 1998). Interestingly, a null mutation either in *hmr-1*, *hmp-2* or *hmp-1* alone resulted in mild intercellular adhesion defects (Costa et al., 1998).

Thus, CeAJs of the worm include other constituents that redundantly contribute to the maintenance of intercellular adhesion. Located basal to the cadherin and catenins are the Apical Junction Molecule (AJM-1) and Discs Large (DLG-1) proteins, together referred to as the DLG-1/AJM-1 complex (Koppen et al., 2001). Altogether, both the cadherin-catenin and

DLG-1/AJM-1 complexes contribute to intercellular adhesion in *C. elegans* epithelial cells of the developing worm (Costa et al., 1998; Koppen et al., 2001).

2.4.3 The mechanics of cytokinesis in *Drosophila* epithelia

As previously mentioned, the stability and persistence of adherens junctions is required for the maintenance of epithelial integrity (Baum and Georgiou, 2011). Importantly, adherens junctions are remodeled during tissue morphogenesis and cell division (Cavey and Lecuit, 2009). This poses a challenge for dividing cells that must concomitantly preserve intercellular integrity while they undergo dramatic cell shape changes. Recent studies in *Drosophila* epithelial tissues addressed the mechanism cells employ to face this challenge. Elegant work by several groups provided the first mechanistic insights of cytokinesis occurring in living epithelial cells of *Drosophila*. Findings from the groups of Bellaiche, Le Borgne, and Lecuit were summarized in a short preview of my own published work in collaboration with my supervisor (Bourdages and Maddox, 2013).

The authors used the dorsal thorax epithelium and the embryonic epithelium of *Drosophila* as models to elucidate the requirements for cytokinesis in epithelial cells (Founounou et al., 2013; Guillot and Lecuit, 2013; Herszterg et al., 2013a). They first noticed that as cells divided in the plane of these epithelia, the contractile ring closed asymmetrically towards the apical membrane of the cell, as previously observed in other epithelia (Dubreuil et al., 2007; Fleming et al., 2007; Founounou et al., 2013; Guillot and Lecuit, 2013; Herszterg et al., 2013a; Reinsch and Karsenti, 1994). A little after these studies were published, asymmetric contractile ring closure towards apical junctions was also reported in *Drosophila* follicular cells (Morais-de-Sa and Sunkel, 2013).

As previously mentioned, during embryonic *C. elegans* cytokinesis, Anillin and the septins dictate the asymmetry of contractile ring closure in this cell-autonomous context (Maddox et al., 2007). Thus, the authors investigated the roles of these conserved structural components of the contractile ring in the *Drosophila* epithelia (Founounou et al., 2013; Guillot and Lecuit, 2013; Morais-de-Sa and Sunkel, 2013a). Interestingly, they found that these proteins were not required for asymmetric furrowing in epithelial cells (Founounou et al., 2013; Guillot and Lecuit, 2013; Morais-de-Sa and Sunkel, 2013a). Instead, Anillin and septins

are required for the normal rate of ring closure in the embryonic and pupal epithelia (Founounou et al., 2013; Guillot and Lecuit, 2013).

Next, these groups investigated the contribution from adherens junctions to cytokinesis in *Drosophila* epithelia (Founounou et al., 2013; Guillot and Lecuit, 2013; Herszterg et al., 2013a; Morais-de-Sa and Sunkel, 2013a). Prior to their work, Baker and Garrod presented evidence that adherens junctions were maintained throughout cell division (Baker and Garrod, 1993). However, the recent *Drosophila* studies showed that this was not always the case. Imaging of fluorescently-labeled components of adherens junctions revealed that apical junctions disengaged from the contractile ring in embryonic epithelial cells (Guillot and Lecuit, 2013). In the dorsal thorax epithelium, adherens junctions were significantly reduced during furrow ingression (Founounou et al., 2013; Guillot and Lecuit, 2013; Herszterg et al., 2013a). Electron microscopy revealed that adherens junctions in follicular epithelial cells only disengaged from the contractile ring on of side of the cell in most cases (Morais-de-Sa and Sunkel, 2013a). These findings suggested that adherens junctions play a prominent role during cytokinesis in epithelial cells.

Following these observations, the authors proposed that "adhesion disengagement" was required to reduce tension at intercellular junctions allowing increased tension in the contractile ring for proper constriction (Founounou et al., 2013; Guillot and Lecuit, 2013). Indeed, E-cadherin overexpression caused strengthening of apical junctions and delayed junction detachment from the ring in *Drosophila* embryonic cells (Guillot and Lecuit, 2013). In addition, reducing tension on the dividing cell by laser ablation of neighbor cell junctions prevented the occurrence of adhesion disengagement (Guillot and Lecuit, 2013). On the contrary, weakening of the contractile ring by removal of septins or Anillin extended the time required for junction detachment to occur (Founounou et al., 2013; Guillot and Lecuit, 2013). These studies led to the conclusion that cytokinesis in epithelial is achieved by tension in the contractile ring exceeding that at apical junctions. For this to occur, tension at adherens junctions is reduced by either disengagement from the contractile ring on both sides or on a single side of the dividing cell or reduced expression of adherens junction components (Founounou et al., 2013; Guillot and Lecuit, 2013; Herszterg et al., 2013a; Morais-de-Sa and Sunkel, 2013a).

Interestingly, a recent study with *Xenopus* epithelial cells reported the occurrence of different mechanics at intercellular junctions of dividing cells. Higashi and colleagues observed that in *Xenopus* epithelial cells the architecture of intercellular junctions remained intact throughout cytokinesis (Higashi et al., 2016). A fluorescent dye injected into dividing epithelial did not permeate the leading edge of adherens junctions as they were remodeled during cytokinesis suggesting that intercellular junctions were maintained throughout division (Higashi et al., 2016). In addition, the authors observed that adherens junctions juxtaposed to the contractile ring were more stable, illustrated by the reduced recovery of fluorescence following FRAP at this location (Higashi et al., 2016). This result suggested that the dividing cell increased tension at adherens junctions, instead of reducing it as in *Drosophila* epithelial cells (Higashi et al., 2016). The mechanical requirements for cytokinesis in epithelial cells thus appear to vary between organisms.

The work of several independent groups has elegantly shown that intercellular junctions are remodeled during cytokinesis (Founounou et al., 2013; Guillot and Lecuit, 2013; Herszterg et al., 2013a; Higashi et al., 2016; Morais-de-Sa and Sunkel, 2013a). Regardless of the status of adherens junctions juxtaposed to the contractile ring, forces are balanced during cytokinesis to maintain tissue integrity (Founounou et al., 2013; Guillot and Lecuit, 2013; Herszterg et al., 2013a; Higashi et al., 2016; Morais-de-Sa and Sunkel, 2013a). These studies provided important insights into the mechanics of contractile ring closure in epithelial cells of tissues compared to isolated cells. Whether these properties of cytokinesis in epithelial cells are conserved across metazoans remains to be addressed.

2.5 The *C. elegans* vulva as a model epithelium to study cytokinesis

Epithelial cells of the *C. elegans* vulva present an interesting model to further characterize cytokinesis occurring in the context of a living epithelium. In this section, I describe the *C. elegans* model, the advantages it confers and the seminal discoveries made using this organism.

2.5.1 The model organism *C. elegans*

The establishment of *C. elegans* as a mainstay model organism by Sydney Brenner occurred over fifty years ago (Brenner, 1973). Brenner originally selected *C. elegans* for biological research mainly for its ease of manipulation to study developmental processes and neuronal biology (Brenner, 1973). Over the years, *C. elegans* has been established as a powerful model organism and led to many groundbreaking discoveries in various fields.

C. elegans is a free-living worm found worldwide mostly in compost, rotten fruits and plants stems (Blaxter and Denver, 2012; Felix and Duveau, 2012). *C. elegans* grown in laboratory settings feed on the bacteria *Escherichia coli* (*E. coli*) (Bourdages et al., 2014). Worms can be maintained at temperatures ranging from 12 to 25°C (Corsi et al., 2015). *C. elegans* nematodes are small, reaching 1 mm in length at adulthood (Corsi et al., 2015). Thus, worm visualization and manipulation requires a dissecting scope or higher resolution microscopes. *C. elegans* populations are almost entirely composed of self-fertilizing hermaphrodites (XX genotype) that can lay up to 300 eggs in a single life cycle. Males (XO genotype) are also present in populations but at low incidence (0.2%) due to the rare event of X chromosome non-disjunction in meiosis (Corsi et al., 2015). The ability of *C. elegans* to self-reproduce makes it a powerful genetic system.

C. elegans have a very short life cycle of approximately 3 days at 25°C (Altun, 2017). Their life cycle begins by embryonic development, where rapid rounds of cell cleavages within the eggshell occur over the course of approximately six hours. This is followed by several stages of embryonic morphogenesis. After 16 hours of embryonic development, the newly hatched worm goes through four larval stages (L1-L4) (Altun, 2017). Molting of the outer cuticle precedes each larval stage. L2 worms experiencing starvation can enter an alternative stage as L3 larvae, called the *dauer* stage (Altun, 2017). These worms can survive without food supply for weeks. Upon nutrient restoration worms re-enter the life cycle and continue to grow to adulthood.

In addition to its small size, short life cycle and ease of manipulation, *C. elegans* provides several other advantages. *C. elegans* worms are transparent, thus easily amenable for imaging using simple differential interference contrast (DIC) microscopy and more complex

imaging techniques using fluorescent proteins. This nematode has a simple genome of approximately 20,000 genes and retains approximately 60% homology to human protein coding genes (Corsi et al., 2015). The genome of *C. elegans* was the first to be sequenced amongst multicellular eukaryotic organisms (Consortium, 1998) and has served as a benchmark for functional characterization of the human genome.

C. elegans also possesses a simple anatomy based on largely tubular organ structures (Figure 2.5.1) (Altun, 2017). A thick cuticle surrounds the entire surface of the animal providing protection against the outside environment. Juxtaposed to the cuticle is the worm's ventral hypodermis lined by a layer of muscles required for body movement (Figure 2.5.1). The animal has a pharynx for feeding, an intestine, a two-armed gonad, a vulva and a nervous system (Figure 2.5.1). These distinct tissues can be easily followed throughout development under the microscope due to the worm's transparency. Relatively simple imaging-based experiments and genetic screens have led to important discoveries in the field of developmental biology.

Figure 2.5.1 Anatomy of an adult *C. elegans* worm

Schematic depicting the tubular organs including the pharynx (green), the intestinal lumen (pink), the two-armed gonad (dark purple) including oocytes (light purple) in the uterus and a ventral slit (turquoise) representing the vulva.

2.5.2 Seminal discoveries using *C. elegans*

One of the most remarkable achievements in modern cell biology occurred early in worm history. A group of scientists in the late 1970's took advantage of the worm's transparency to trace the fate of every single cell from the embryo all the way to the adult hermaphrodite and male (Kimble and Hirsh, 1979; Sulston and Horvitz, 1977; Sulston et al., 1983). These intensive observations led to the important discovery that *C. elegans* possess an invariant lineage, including 959 somatic cells and led to the discovery of the phenomena of programmed cell death (Kimble and Hirsh, 1979; Sulston and Horvitz, 1977; Sulston et al.,

1983). These findings laid the foundation for future work in cell lineage characterization, tissue morphogenesis and neurological systems studies.

Another key discovery made in the *C. elegans* system was the ability of a small double-stranded RNA to induce mRNA-directed silencing of a specific target gene (Fire et al., 1998; Montgomery and Fire, 1998; Montgomery et al., 1998). This method earned Craig Mello and Andy Fire a Nobel Prize in 2006. This facile RNAi method can be carried out at low cost since RNAi can be introduced into the worm by simple feeding of *E. coli* bearing appropriate recombinant expression plasmids. Importantly, systematic collections of RNAi constructs that covered all protein coding genes allowed rapid genome-wide functional characterization of *C. elegans* genes acting early in embryo development (Sonnichsen et al., 2005).

2.5.3 The *C. elegans* vulva

The vulva of the worm is the organ responsible for egg-laying and mating. It forms a tubular organ at adulthood making the connection with the outside environment. The *C. elegans* vuvla has been referred to as a "paradigm of morphogenesis" (Sharma-Kishore et al., 1999). The vuvla is a simple organ system comprised of only 22 cells that divide over the course of approximately six hours (Bourdages et al., 2014; Schindler and Sherwood, 2013). The signaling pathways and morphogenetic events governing vulva formation are well characterized (Felix and Barkoulas, 2012). This organ also provides an ideal system for genetic screens since egg-laying can be perturbed but viable progeny produced (Lacroix et al., 2014). Genetic mutations or protein depletion by RNAi can cause defects in the egg-laying apparatus, including vulva less worms (Vul), worms with multiple vulvae (Muv), a protruding vulva (Pvl) and embryos retained in the uterus (Egl), all of which are easily scored under a stereomicroscope (Lacroix et al., 2014; Schindler and Sherwood, 2013). The *C. elegans* vulva starts to develop at the third larval stage (L3). The following section describes the well-defined stages of vulva formation from a single row of cells into a mature egg-laying apparatus.

2.5.4 The *C. elegans* vulval precursor cells (VPCs)

The *C. elegans* vulval precursor cells (VPCs) originate from the P ectoblast lineage (Kimble and Hirsh, 1979; Sulston and Horvitz, 1977; Sulston et al., 1983). During the first larval stage of worm development, twelve epidermal cells (P1.p-P12.p) are born and located at the ventral midline of the worm. The P1.p-P2.p and P9.p-P12.p cells rapidly fuse with the ventral hypodermis (hyp7) of the worm (Schindler and Sherwood, 2013). The remaining six VPCs, namely P3.p, P4.p, P5.p, P6.p, P7.p and P8.p, stay quiescent until the third larval stage (L3) (Schindler and Sherwood, 2013). The P3.p to P8.p cells receive developmental cues at the L3 stage and all become competent to form the vulva (Schindler and Sherwood, 2013). All six VPCs are competent to form the vulva. The neighboring cell compensates laser cell ablation of any of these cells. For instance, the P5.p cell replaces the P6.p cell when it is ablated (Sternberg and Horvitz, 1986; Sulston and White, 1980).

The VPCs are comprised in an epithelium and exhibit apico-basal polarity. Cells are comprised between an apical membrane juxtaposed to the ventral cuticle of the worm and a basal membrane facing the uterus (Gupta et al., 2012). A specialized cell called the anchor cell (AC) is located in the uterus, just above the VPCs (Ihara et al., 2011). This cell sends an EGF signal mediated by the LIN-3 gene to the P5.p, P6.p and P7.p cells (Horvitz and Sternberg, 1991; Ririe et al., 2008; Saffer et al., 2011; Skorobogata et al., 2014). The AC directly sends signals to the P6.p cell below for it to adopt primary VPC fate. The neighboring P5.p and P7.p cells receive a weaker signal from the AC and consequently adopt the secondary VPC fate (Horvitz and Sternberg, 1991; Ririe et al., 2008; Saffer et al., 2011; Skorobogata et al., 2014). Lateral signals are also sent for VPC cell fate patterning. Notch signals provide lateral cues to the VPCs via the gene LIN-12 (Hoyos et al., 2011; Ririe et al., 2008). This lateral LIN-12/Notch signal contributes to the specification of the secondary fate for the P5.p and P7.p cells (Hoyos et al., 2011). Finally, the remaining P3.p, P4.p and P8.p cells adopt tertiary VPC fate, dividing only once before fusing with the ventral hypoderm of the worm (Horvitz and Sternberg, 1991; Hoyos et al., 2011; Ririe et al., 2008; Skorobogata et al., 2014).

The P5.p, P6.p and P7.p cells undergo three rounds of division to generate a total of twenty-two cells (Figure 3.5.1A) (Bourdages et al., 2014; Schindler and Sherwood, 2013). The middle primary fate VPC (P6.p) gives rise to eight daughter cells, while the secondary fate

VPCs (P5.p and P7.p) generate seven daughter cells each (Bourdages et al., 2014; Schindler and Sherwood, 2013). The 22 cells generated are of different types referred to as VulA, VulB1, VulB2, VulC, VulD, VulE and VulF, from the anterior to posterior of the worm and display mirror image symmetry making two half vulvae (Schindler and Sherwood, 2013). The first two rounds of VPC division occur in the longitudinal axis (anterior to posterior) of the worm (Figure 3.5.1A). During the final round of division, both longitudinal (VulA and VulB) and transverse (ventral to dorsal), for VulC, VulE and VulF cell types, orientations are observed (Figure 3.5.1A) (Bourdages et al., 2014). The cells of VulD origin do not undergo a third and final round of division (Bourdages et al., 2014).

Following all three rounds of division, the VPCs undergo well-characterized morphogenetic changes. Inward VPC migration causes tissue invagination towards the worm's midline and is initiated during the final round of VPC division (Schindler and Sherwood, 2013; Sharma-Kishore et al., 1999). At the L4 stage, invagination progresses and is accompanied by cell fusion events (Sharma-Kishore et al., 1999). Cells on the same half of the vulva and of the same type first fuse together. This is followed by fusion of cells of the same type but from the other half of the vulva (i.e. anterior with posterior VulA) (Schindler and Sherwood, 2013; Sharma-Kishore et al., 1999). This event results in the formation of donut-shaped cells called toroids with a lumen on the inside and referred to as the "Christmas tree" stage (Schindler and Sherwood, 2013; Sharma-Kishore et al., 1999). The final events of vulva formation start by the AC breaching the basement membrane and fusing with the VulF cells (Ihara et al., 2011; Schindler and Sherwood, 2013). This allows for the VulF cells to make connections with uv1 cells of the uterus (Schindler and Sherwood, 2013). Then the AC fuses with uterine cells to form the utse, a thin membrane separating the uterine from the vulval lumen (Schindler and Sherwood, 2013). Contacts are also established between vulval lips and sex muscles, four vm1 and four vm2 muscle cells, to control opening during mating or egg-laying (Schindler and Sherwood, 2013). The final step of vulva formation is called eversion, where the vulva turns inside-out with the guidance of motor neurons and the opening now forms a slit (Figure 2.3) (Schindler and Sherwood, 2013).

2.5.5 The characterization of VPC cytokinesis

The well-established events in *C. elegans* vulva formation make it a powerful organ system to characterize the mechanics of cytokinesis. The *C. elegans* VPCs are easy to follow under the microscope and allowed quantitative analysis of several aspects of cytokinesis, described in the following chapter. The work presented in this thesis builds on seminal discoveries, including the establishment of the invariant *C. elegans* lineage and RNAi (Fire et al., 1998; Kimble and Hirsh, 1979; Montgomery and Fire, 1998; Montgomery et al., 1998; Sulston and Horvitz, 1977; Sulston et al., 1983). Work with *Drosophila* epithelial cells provided insights into the mechanics of cytokinesis in intact tissues (Founounou et al., 2013; Guillot and Lecuit, 2013; Herszterg et al., 2013a; Higashi et al., 2016; Morais-de-Sa and Sunkel, 2013a). The following chapter further describes the mechanics of cytokinesis in cell of intact tissue using the *C. elegans* VPCs. The work presented below also illustrates the impact cell size has on many aspects of cytokinesis. Since cell size regulation is addressed in later chapters, it provides a link between cytokinesis and cell size, two processes essential for proper cell function.

3 Results Part 1 - Article 1

Quantitative analysis of cytokinesis *in situ* during *C. elegans* postembryonic development

Karine G. Bourdages[1], Benjamin Lacroix[1], Jonas F. Dorn[1], Carlos P. Descovich[2] & Amy S. Maddox[2]*

The work presented in the following chapter is reproduced from an article published in PLoS ONE in 2014, PLoS ONE 9(10): e110689. doi:10.1371/journal.pone.0110689.

Author contributions

B.L. performed initial experiments to establish the parameters for live imaging of the VPCs during *C. elegans* larval development. I joined the group of Dr. Maddox in January 2011 and conceived this study with B.L. and A.S.M. I designed and conducted the experiments presented in this article. B.L. provided technical support and insightful comments and suggestions throughout the project. J.F.D. designed the software for quantitative measurements of the dynamics of contractile ring closure and provided important insights for the analysis. C.P.D. performed the experiments described in Figure 3.5.3E-F and Figure 3.5.4B and generated the figures. I wrote the manuscript under the supervision of A.S.M.

Karine G. Bourdages[1], Benjamin Lacroix[1], Jonas F. Dorn[1], Carlos P. Descovich[2] & Amy S. Maddox[2]*

[1]Institute for Research in Immunology and Cancer, Université de Montréal P.O. Box 6128, Station Centre-Ville Montréal QC, H3C 3J7 Canada

[2]Department of Biology, University of North Carolina at Chapel Hill, NC 27599

Citation: Bourdages KG, Lacroix B, Dorn JF, Descovich CP, Maddox AS (2014) Quantitative Analysis of Cytokinesis In Situ during C. elegans Postembryonic Development. PLoS ONE 9(10): e110689. doi:10.1371/journal.pone.0110689

Editor: Rafael Garcia-Mata, University of Toledo, United States of America

Received August 18, 2014; Accepted September 24, 2014; **Published October 20, 2014**

Data Availability: The authors confirm that all data underlying the findings are fully available without restriction. All relevant data are within the paper.

Funding: This work was supported by operating funds from the National Science and Engineering Research Council of Canada (355657; http://www.nserc-crsng. gc.ca) and National Institutes of Health (NIH) (GM102390; http://www.nigms.nih.gov). The funders had no role in study design, data collection and analysis, decision to publish, or preparation of the manuscript.

Competing Interests: The authors have declared that no competing interests exist.

* Email: asm@unc.edu

Keywords: Cytokinesis, *C. elegans, in situ*, VPCs, tissue, scaling

3.1 Abstract

The physical separation of a cell into two daughter cells during cytokinesis requires cell-intrinsic shape changes driven by a contractile ring. However, *in vivo*, cells interact with their environment, which includes other cells. How cytokinesis occurs in tissues is not well understood. Here, we studied cytokinesis in an intact animal during tissue biogenesis. We used high-resolution microscopy and quantitative analysis to study the three rounds of division of the *C. elegans* vulval precursor cells (VPCs). The VPCs are cut in half longitudinally with each division. Contractile ring breadth, but not the speed of ring closure, scales with cell length. Furrowing speed instead scales with division plane dimensions, and scaling is consistent between the VPCs and *C. elegans* blastomeres. We compared our VPC cytokinesis kinetics data with measurements from the *C. elegans* zygote and HeLa and *Drosophila* S2 cells. Both the speed dynamics and asymmetry of ring closure are qualitatively conserved among cell types. Unlike in the *C. elegans* zygote but similar to other epithelial cells, Anillin is required for proper ring closure speed but not asymmetry in the VPCs. We present evidence that tissue organization impacts the dynamics of cytokinesis by comparing our results on the VPCs with the cells of the somatic gonad. In sum, this work establishes somatic lineages in post-embryonic *C. elegans* development as cell biological models for the study of cytokinesis *in situ*.

3.2 Introduction

Cytokinesis is the last step of cell division, physically partitioning the cytoplasm of a cell into two daughter cells. Cytokinesis failure results in tetraploidy, which promotes p53 activation and, in most cases, cell cycle arrest (Andreassen et al., 2001), but in several conditions, further proliferation (Fujiwara et al., 2005; Uetake and Sluder, 2004). Due to their supernumerary centrioles, dividing tetraploid cells exhibit errors in spindle bipolarity and chromosome segregation (Ganem et al., 2009; Godinho et al., 2014). The resulting aneuploidy implicates cytokinesis failure in oncogenic transformation (Ganem et al., 2009). Interestingly, regulated cytokinesis failure occurs during differentiation of several cell types including hepatocytes and cardiomyocytes (Lacroix and Maddox, 2012).

To initiate cytokinesis, the geometry of the anaphase spindle dictates the local activation of the small GTPase Rho. Active, GTP-bound RhoA activates formin actin nucleators and non-muscle myosin II, and recruits other effectors including the scaffolding protein Anillin (Eggert et al., 2006; Fededa and Gerlich, 2012; Glotzer, 2005; Green et al., 2012). Filament sliding and/or depolymerization are thought to drive closure of the actomyosin contractile ring and membrane furrowing (Fededa and Gerlich, 2012; Ma et al., 2012; Mendes Pinto et al., 2012). While it is well accepted that spindle signaling converges on Rho to elicit actomyosin ring assembly and closure, reports of cell-type specific requirements for spindle and contractile ring components (Fung et al., 2014; O'Connell et al., 1999; Piekny and Maddox, 2010; Verbrugghe and White, 2007) suggest that distinct mechanisms can achieve the common goal of cell division.

Recent comparative studies have yielded novel insights into the general principles of cytokinesis mechanics. One unifying concept is that actomyosin rings are built from discrete "contractile units" (Bement and Capco, 1991; Carvalho et al., 2009). This model was posed to explain how ring closure speed scales with cell size (Carvalho et al., 2009). Furrow speed scaling is observed in diverse cell types (Calvert et al., 2011; Carvalho et al., 2009), indicating that this phenomenon occurs as a result of a conserved feature of actomyosin rings.

Our current understanding of cytokinesis has been arrived at mainly using isolated cells including yeasts, mammalian cultured cells and invertebrate zygotes, such as that of *Caenorhabditis elegans*. However, it is not well known how the dogma of the molecular and mechanical mechanisms of cytokinesis applies to cells in the context of living tissues. Defining mechanistic differences in cytokinesis among cell types may help explain the tissue specificity of gene requirements during development and of drug sensitivity in some cancers. Here, we examined the impact of tissue context on cytokinesis as it occurred in the simple epithelium of a living animal.

Epithelia are ubiquitous tissues that regulate homeostasis and act as barriers against the surrounding environment (Knust and Bossinger, 2002). Epithelial cells are polarized, with their apical domain facing the lumen or outside environment and the basolateral surface contacting neighboring cells and the basement membrane. Cadherin-based adherens junctions delineate these domains and mechanically and biochemically connect epithelial cells (Lynch

and Hardin, 2009). When epithelial cells divide such that both daughter cells inherit the apical domain, their intercellular junctions must be remodeled. How epithelial integrity is preserved throughout this process is not fully understood.

Recent work with the *Drosophila* embryo, pupal notum and follicular epithelia has provided insights into the requirements for cytokinesis *in vivo* (Founounou et al., 2013; Guillot and Lecuit, 2013; Herszterg et al., 2013a; Morais-de-Sa and Sunkel, 2013a). These complementary studies described how intercellular adhesions mechanically oppose forces in the contractile ring, causing it to close non-concentrically. Thus, the geometry of contractile ring closure is not completely cell-autonomous and accordingly, ring asymmetry does not require Anillin and septins as it does in the *C. elegans* zygote (Founounou et al., 2013; Guillot and Lecuit, 2013; Maddox et al., 2007; Morais-de-Sa and Sunkel, 2013a). Interestingly, epithelial cells in these various tissues appear to differently regulate junction remodeling during division (Herszterg et al., 2013b; Morais-de-Sa and Sunkel, 2013b). Adhesions in the division plane become disengaged on both sides of the dividing cell in the embryo, on only one side in follicle cells, and not at all in the notum (Herszterg et al., 2013b; Morais-de-Sa and Sunkel, 2013b). The differences in how tissue context impacts cytokinesis among tissues may relate to their specialized functions.

Here, we characterize cytokinesis *in situ* using *C. elegans*, studying somatic cell divisions during post-embryonic development. We took advantage of the simplicity and thorough cell fate characterization of the egg laying apparatus in *C. elegans*, specifically, the vulval precursor cells (VPCs). VPC size reduced by half with each round of division, and the dimensions of the contractile ring scaled with cell size. Quantitative analysis of the kinetics of cytokinesis in the VPCs revealed acceleration and deceleration of the ring, which we also observed in diverse cell types including human HeLa and *Drosophila* S2 cultured cells. As in other epithelial cells, furrowing in the VPCs was asymmetric, terminating towards the apical domain. Examining furrow in HeLa and S2 cultured cells revealed that asymmetry also occurs in these "isolated" cells, and is polarized towards the substrate. Thus, asymmetry can arise from mechanical resistance originating from various cellular features. While the scaffolding protein Anillin was not required for the asymmetry of VPC furrowing, its depletion slowed cytokinesis in these cells. Depletion of conserved intercellular adhesion components did not

significantly alter the kinetics or geometry of VPC cytokinesis, suggesting that junctions are exceptionally robust in this tissue. In cells of the less organized somatic gonad, furrowing was more symmetric and slower than in the VPCs. Collectively, this work establishes tissues of the developing *C. elegans* as cell biological systems for studying cell division.

3.3 Results

3.3.1 Visualization of the vulval precursor cells (VPCs) *in situ*

To study cytokinesis *in situ*, we sought a simple, well-characterized epithelium. The nematode *C. elegans* lays eggs via the vulva, which starts as a simple epithelium, comprising the vulval precursor cells (VPCs; Figure 3.5.1A). The VPCs' lineage and placement are invariant, and the morphogenetic events of vulva formation are well understood (Greenwald, 1997; Kornfeld, 1997; Ririe et al., 2008; Sternberg and Horvitz, 1986; Sulston and Horvitz, 1977). At the third larval stage of *C. elegans* development, six cells (P3.p - P8.p) are competent to form the vulva (Kornfeld, 1997; Sternberg and Horvitz, 1986; Sternberg and Horvitz, 1989). Upon induction, only three of these cells, P5.p, P6.p and P7.p, adopt vulval fate (Kornfeld, 1997; Sternberg, 1988; Sternberg and Horvitz, 1986; Sternberg and Horvitz, 1989). Over the course of 6 hours at 25°C, they undergo three rounds of division to generate 22 descendants, which further go through morphogenesis to form the vulva (Horvitz and Sternberg, 1991; Sharma-Kishore et al., 1999) (Figure 3.5.1A).

To visualize VPC divisions in living animals, we performed high-resolution microscopy of a worm strain expressing GFP-tagged non-muscle myosin II (NMY-2; hereafter, "myosin"), a core component of the contractile ring, under the control of its own promoter. This transgenic strain has been widely used and is considered a faithful reporter of active myosin (Bringmann and Hyman, 2005; Carvalho et al., 2009; Munro et al., 2004; Roh-Johnson and Goldstein, 2009). At the beginning of the third larval stage (L3), which we denote as the 3 VPC stage, the P5.p, P6.p and P7.p cells' basal surfaces are internal and their apical domains lay against the worm's ventral cuticle (Figure 3.5.1A-C). In interphase, myosin was present at the cortex and enriched at apical junctions between VPCs that also likely contain cytokinetic midbody remnants (Figure 3.5.1C; see Figure 3.5.4). In the mid-L3 stage the three

VPCs divided in the plane of the epithelium, giving rise to 6 daughter cells (the 6 VPC stage; Figure 3.5.1A-C). Approximately two hours later they underwent a second round of division to produce 12 granddaughter cells. During the early 12 VPC stage prior to the last round of division and the L3/L4 molt, descendants of the P6.p cell invaginated dorsally by apical constriction (Figure 3.5.1A-C). 10 of 12 granddaughter cells undergo a third and final round of division, giving rise to 22 descendants (Figure 3.5.1A-C). Thus, high-resolution imaging of a fluorescent *C. elegans* strain allowed us to observe the organization of the VPCs during early vulva development.

To characterize the VPCs as a cell biological model, we first determined the dimensions of the VPCs (see Figure 3.5.1A). VPC length was reduced by approximately half from one round of division to the next, while the height (apical-basal cell axis) and thickness (left-right worm axis) of VPCs remained more constant (Figure 3.5.1D-E). Thus, cell volume was reduced by approximately half during each of the three rounds of VPC divisions (Figure 3.5.1F). Consistent with the decrease in VPC length, the three rounds of division occurred without appreciable growth of the tissue (Figure 3.5.1G). Thus, VPC divisions are reductional within the epithelium, providing an opportunity to study the effects of cell size on various aspects of cell division.

3.3.2 Contractile ring dimensions scale with cell size

We took advantage of the progressive reduction in VPC size to test how different aspects of cytokinesis scale with cell size. We first tested if the contractile ring scales with cell size, as has been demonstrated for meiotic and mitotic spindles (Brown et al., 2007; Hara and Kimura, 2009; Wuhr et al., 2008). We used worms expressing GFP-tagged myosin to visualize the contractile ring at each of the three rounds of VPC division. At cytokinesis onset, myosin was enriched in an equatorial band encircling the cell and visible on both the apical and basal domain of the dividing cell (Figure 3.5.2A). We measured the breadth of the contractile ring (how much of the cell long axis was occupied by myosin) along both the cell's apical and basal surfaces and compared it to cell length. As the VPCs become smaller from one round of division to the next, so do the apical and basal dimensions of the contractile ring (Figure 3.5.2B). This is consistent with the idea that contractile ring dimensions relate to spindle size,

which scales with cell length. Contractile rings were broader at the apical region than the basal domain of the cell (Figure 3.5.2C), indicating that apicobasal cell polarity generates differences in the mechanical or biochemical mechanisms that focus the contractile ring. The extent of this difference varied among the three rounds of VPC divisions; the apical region of the contractile ring was significantly broader than at the basal surface during the first two rounds of VPC division, but nearly identical during the last round of cytokinesis (Figure 3.5.2C). This result indicates that there is a lower bound to contractile ring breadth.

3.3.3 Furrowing speed scales with division plane dimensions

Another aspect of contractile ring biology that scales with cell size is furrowing speed, such that larger cells furrow more quickly than smaller cells of a given cell type (Calvert et al., 2011; Carvalho et al., 2009; Mendes Pinto et al., 2012; Turlier et al., 2014). One possibility was that speed scales with total available myosin or other contractile ring components and thus cell volume. According to this model, since VPCs halve their volume at each round of cell division (Figure 3.5.1F), furrow speed would decrease with decreasing VPC size. Alternatively, Calvert and colleagues presented evidence that furrowing speed scales with division plane dimensions (Calvert et al., 2011). VPC height and thickness, and therefore division plane circumference, remain roughly constant (Figure 3.5.1E-F), so furrowing speed would be expected to be similar among the three rounds of division. We performed time-lapse imaging through the thickness of the VPCs and measured contractile ring closure (Figure 3.5.3A-B). Indeed, furrowing speed, represented by the average speed between 20% and 80% ring closure, is relatively similar among rounds of VPC division, and does not scale with VPC volume (Figure 3.5.3B'). Maximum furrowing speed is significantly lower in the middle round of VPC divisions, but also does not scale with VPC size (see Figure 3.5.3D).

We next explored whether the scalability of furrowing speed with cell size extends outside of a given cell type. We compared our furrowing speed data from the VPCs (Figure 3.5.3B') with those measured previously in *C. elegans* blastomeres, where furrowing speed scales with cell size in general (Carvalho et al., 2009). Strikingly, our measurements from VPCs fit very well with the relationship between division plane diameter and furrowing speed in the much larger blastomeres Figure 3.5.3C). Thus, scaling is a conserved phenomenon

whose arithmetic relationship holds among different cell types in *C. elegans*. Our results indicate that furrow speed is dictated by a feature of the contractile ring that is universal among cells of varying sizes, shapes, fates and tissue contexts.

3.3.4 Contractile ring closure occurs via acceleration and deceleration

Measuring VPC contractile ring closure with high temporal resolution, we noticed that its speed is not constant but rather accelerated until reaching a maximum speed of approximately 18% per minute near 50% closure, and then decelerated until closure (Figure 3.5.3D). To examine whether contractile rings in well-studied model cell types also accelerate and decelerate, we measured ring closure over time in the *C. elegans* zygote, HeLa human cultured cells, and *Drosophila* S2 cells (Figure 3.5.3E). We then calculated how the speed of closure changed with time (Figure 3.5.3F). In all these cell types, contractile ring closure accelerated until the ring was approximately half closed, and then decelerated (Figure 3.5.3F). Thus, gradual change in ring closure speed appears to be a general characteristic of metazoan cytokinesis.

3.3.5 Asymmetric furrowing occurs towards the apical membrane of VPCs

Since contractile ring dimensions and closure speed scaled with VPC length and division plane dimensions, respectively, we next explored whether another feature of cytokinesis scaled with VPC size. Asymmetric cytokinesis (also called polarized, non-concentric, or unilateral cytokinesis) was first characterized in the *C. elegans* zygote, where confinement in the eggshell suggests it occurs cell-autonomously (Audhya et al., 2005; Maddox et al., 2007). Asymmetric cytokinesis has been observed in many epithelial cells and neuroepithelial cells *in situ* (Das et al., 2003; Dubreuil et al., 2007; Fleming et al., 2007; Founounou et al., 2013; Guillot and Lecuit, 2013; Herszterg et al., 2013a; Morais-de-Sa and Sunkel, 2013a; Reinsch and Karsenti, 1994). Recently, it was demonstrated with the *Drosophila* embryonic blastoderm and follicular epithelia that asymmetric furrowing in epithelial cells can be explained by apical junctions resisting the inward pulling forces of the contractile ring (Guillot and Lecuit, 2013; Morais-de-Sa and Sunkel, 2013a). Strikingly, ring closure is asymmetric and invariantly polarized to the substrate in human HeLa and

Drosophila S2 cells (Figure 3.5.4B). These results suggest that remnant substrate adhesions can also resist furrow forces and direct polarized ring closure. Thus, furrow asymmetry appears to be universal among metazoan cell types, but can occur by multiple mechanical means.

Contractile ring closure was asymmetric in the VPCs (Figure 3.5.4A and C; Movie 1). Ingression was polarized towards the apical membrane (Figure 3.5.4A; Movie 1), as in other epithelia (Das et al., 2003; Dubreuil et al., 2007; Fleming et al., 2007; Founounou et al., 2013; Guillot and Lecuit, 2013; Herszterg et al., 2013a; Morais-de-Sa and Sunkel, 2013a). The extent of asymmetry differed among the three rounds of VPC division (Figure 3.5.4C). Asymmetry increased from the first to the second round of division, but then decreased for the third round, where it was the most symmetric (Figure 3.5.4C). Thus, asymmetry did not scale with VPC dimensions.

The polarity of asymmetric furrowing suggested that the intercellular contiguity of apical junctions resists the inward pulling forces of the contractile ring, as was demonstrated with the *Drosophila* embryonic blastoderm and follicular epithelia (Guillot and Lecuit, 2013; Morais-de-Sa and Sunkel, 2013a). Unfortunately, technical difficulties prohibited us from drawing conclusions on the roles of intercellular adhesions in the geometry of VPC cytokinesis (Figure 3.6.1; see Discussion).

In the *C. elegans* zygote, ANI-1$^{\text{Anillin}}$ is required for asymmetric contractile ring closure (Maddox et al., 2007). Targeting of ANI-1 during post-embryonic development led to gross defects in vulval morphogenesis and vulval protrusion (Pvl), as previously seen (Field et al., 2008). Depletion of ANI-1 from the VPCs did not alter furrow asymmetry (Figure 3.5.4D and E), suggesting that furrow asymmetry is not ring-intrinsic but is caused by mechanical resistance by the apical junctions. Similar results and conclusions were obtained with *Drosophila* epithelial cells *in situ* (Founounou et al., 2013; Guillot and Lecuit, 2013; Morais-de-Sa and Sunkel, 2013a). ANI-1 depletion from VPCs slowed contractile ring closure (Figure 3.5.4D' and E'), as in mammalian cultured cells injected with an Anillin antibody (Oegema et al., 2000), and in the *Drosophila* embryonic and notum epithelial cells depleted of Anillin (Founounou et al., 2013; Guillot and Lecuit, 2013). Interestingly, this effect of ANI-1 depletion on furrowing speed is not seen in the *C. elegans* zygote (Maddox et al., 2007). Thus,

ANI-1^{Anillin} is differentially required for cytokinesis in epithelial cells versus early blastomeres in *C. elegans*.

3.3.6 Epithelial organization influences the kinetics of cytokinesis

The epithelium containing the VPCs is highly organized: the single layer of cells are all of similar size, with apparently similar contact with the basement membrane and neighboring epithelial cells (Sternberg, 2005) (Figure 3.5.1). In contrast, the *C. elegans* somatic gonad, located interior to the VPCs, is an ovoid collection of cells surrounded by a basement membrane (Figure 3.5.5A-B). The somatic gonad cells, which are segregated towards the worm midline from the two arms of the developing germline (Figure 3.5.5A-B), undergo several rounds of division to give rise to the cells that encase the germline, spermatheca and uterus (Kimble and Hirsh, 1979; Newman et al., 1996). To test how epithelial organization influences cytokinesis, we measured the kinetics and geometry of cytokinesis in the somatic gonad cells and compared them to our results with the VPCs.

The contractile rings of the somatic gonad cells could be observed via time-lapse imaging of GFP-tagged myosin, as for VPCs (Figure 3.5.5C; Movie 2). Contractile ring closure was slower in the somatic gonad cells than in the slowest VPCs (at the second round of division; (Figure 3.5.5D). Contractile ring closure was also more concentric, resembling that of the third round of VPC division (Figure 3.5.5E). Thus, as in the VPCs, furrowing speed is not strictly correlated with asymmetry, indicating that they are influenced by independent aspects of the contractile ring. These results suggest that tissue organization influences the dynamics of contractile ring closure.

3.4 Discussion

Here, we set out to establish a system for studying cytokinesis *in situ*. We used high-resolution microscopy of a strain expressing GFP-tagged myosin to follow contractile ring closure over the three rounds of vulval precursor cell (VPC) cytokinesis within developing *C. elegans*. We also examined a distinct tissue, the somatic gonad. By characterizing cytokinesis in multiple settings and taking a four dimensional view of the contractile ring, we defined

conserved features of cytokinesis, lending insight into general principles of contractile ring function.

We first established that the VPCs reduced in length by approximately half upon each division (Figure 3.5.1). This cell size reduction allowed us to investigate scalability of the contractile apparatus. The width of the contractile ring scaled with VPC length (Figure 3.5.2A-B), supporting the hypothesis that the dimensions of the mitotic spindle dictate the site of contractile ring assembly (Bringmann and Hyman, 2005), and parallels the finding that spindle length scales to cell size (Brown et al., 2007; Hara and Kimura, 2009), thus adding to a growing body of knowledge on organelle scaling.

When we investigated whether other aspects of cytokinesis scaled with cell size, we found that the speed of furrowing scaled with division plane dimensions and not with overall cell size. Whether furrowing speed scales with division plane size or cell volume had not been discernable from the study of *C. elegans* blastomeres (Carvalho et al., 2009), but had been arrived at using filamentous fungus (Calvert et al., 2011). Interestingly, the scaling of furrowing speed with the size of the division plane is consistent among the VPCs and blastomeres of *C. elegans* (Figure 3.5.3C). Carvalho and colleagues suggested that this scaling occurs because rings are constructed from standard sized contractile units, and large rings contain more contractile units than smaller cells (Carvalho et al., 2009). Our results thus suggest that different cell types of a given species possess that same contractile unit.

In measuring how the speed of contractile ring closure changes over time, we noticed that it first increases and then decreases (Figure 3.5.3D). Although this phenomenon is not widely appreciated, it has been reported (Bement and Capco, 1991; Bement et al., 1999; Mabuchi, 1990; Soto et al., 2013; Yoneda and Dan, 1972). Careful inspection of data from cells throughout phylogeny reveals that when ring size is plotted over time, the resulting curve is sigmoidal (first concave downward and later concave upward), belying acceleration and deceleration (Brennan et al., 2007; Calvert et al., 2011; Maddox et al., 2007). Acceleration may reflect progressive contractile ring compaction and organization, while deceleration may result from limitations on contractile ring disassembly. Understanding the structural bases of acceleration and deceleration and the switch between these two states will no doubt lead to insights into general principles of cytokinesis.

As observed in diverse epithelial cells (Das et al., 2003; Dubreuil et al., 2007; Fleming et al., 2007; Founounou et al., 2013; Guillot and Lecuit, 2013; Herszterg et al., 2013a; Morais-de-Sa and Sunkel, 2013a), VPC contractile rings close in a polarized, apically-directed fashion (Figure 3.5.4A; Movie 1). In *Drosophila* epithelia, the polarity of furrowing and resulting apical positioning of the midbody promote the formation of a long interface between daughter cells, important for epithelial integrity in a proliferating tissue (Herszterg et al., 2013a; Morais-de-Sa and Sunkel, 2013a). Thus, asymmetry results in this specific advantage for epithelial cells. However, we also observed asymmetry in non-epithelial cell types (Figure 3.5.4B). Together with several elegant mechanical perturbations of epithelial cytokinesis (Founounou et al., 2013; Guillot and Lecuit, 2013; Herszterg et al., 2013a; Morais-de-Sa and Sunkel, 2013a), our data suggest that asymmetry is an inevitable result of mechanical resistance in one region of the division plane.

Previous work in ectodermal and follicular epithelial cells of *Drosophila* established that mechanical resistance by apical adherens junctions dictates the polarity of asymmetric contractile ring ingression (Guillot and Lecuit, 2013; Morais-de-Sa and Sunkel, 2013a). Although we assume that the same principle holds for the *C. elegans* VPCs, we did not observe more concentric closure of the contractile ring upon depletion of either HMR-1$^{\text{E-cadherin}}$ or AJM-1, principal components of the two adhesion subdomains (Figure 3.6.1A-D). Simultaneous RNAi for these two targets did not exacerbate the effects on vulval morphogenesis and were not examined at the cell level (Figure 3.6.1E). These results suggest that VPC apical junctional integrity is robust due to redundant and/or persistent intercellular adhesion proteins. Cadherin- and AJM-1-based adhesion complexes are redundant during embryonic morphogenesis of the *C. elegans* gut epithelium (Segbert et al., 2004). In addition, junction proteins may have persisted despite RNAi, since the vulval epithelium is relatively insensitive to RNAi (Matus et al., 2014). Our attempts to circumvent this issue using a mutant strain (*rrf-3* pk1426) with increased RNAi sensitivity (Simmer et al., 2002) did not enhance the penetrance of terminal vulval defects (Figure 3.6.1F) and thus were not pursued further. It is possible that the VPCs' junctions with the Hyp7 hypodermis (orange in Figure 3.5.2A), which lie in the division plane for longitudinal VPC divisions, are generally more compliant and/or less depleted by RNAi. Lastly, the VPCs' apical association with the cuticle could

contribute to mechanical resistance by the apical aspect of these cells. Indeed, the cuticle-associated apical ECM was implicated in the maintenance of apical junction integrity in the *C. elegans* excretory system (Mancuso et al., 2012).

In sum, our characterization of cytokinesis in the VPCs of *C. elegans* lays the foundation for applying the wealth of knowledge that exists on vulval genetics and morphogenesis to the study of cytokinesis. It also provides insights into the differences in mechanisms and geometry of cell division *in situ* versus in isolated cells. These distinctions could aid the understanding and development of cancer therapies, since one of the major challenges of anti-mitotic agents is their unexplained tissue specificity (Gascoigne and Taylor, 2009).

3.5 Figures and legends

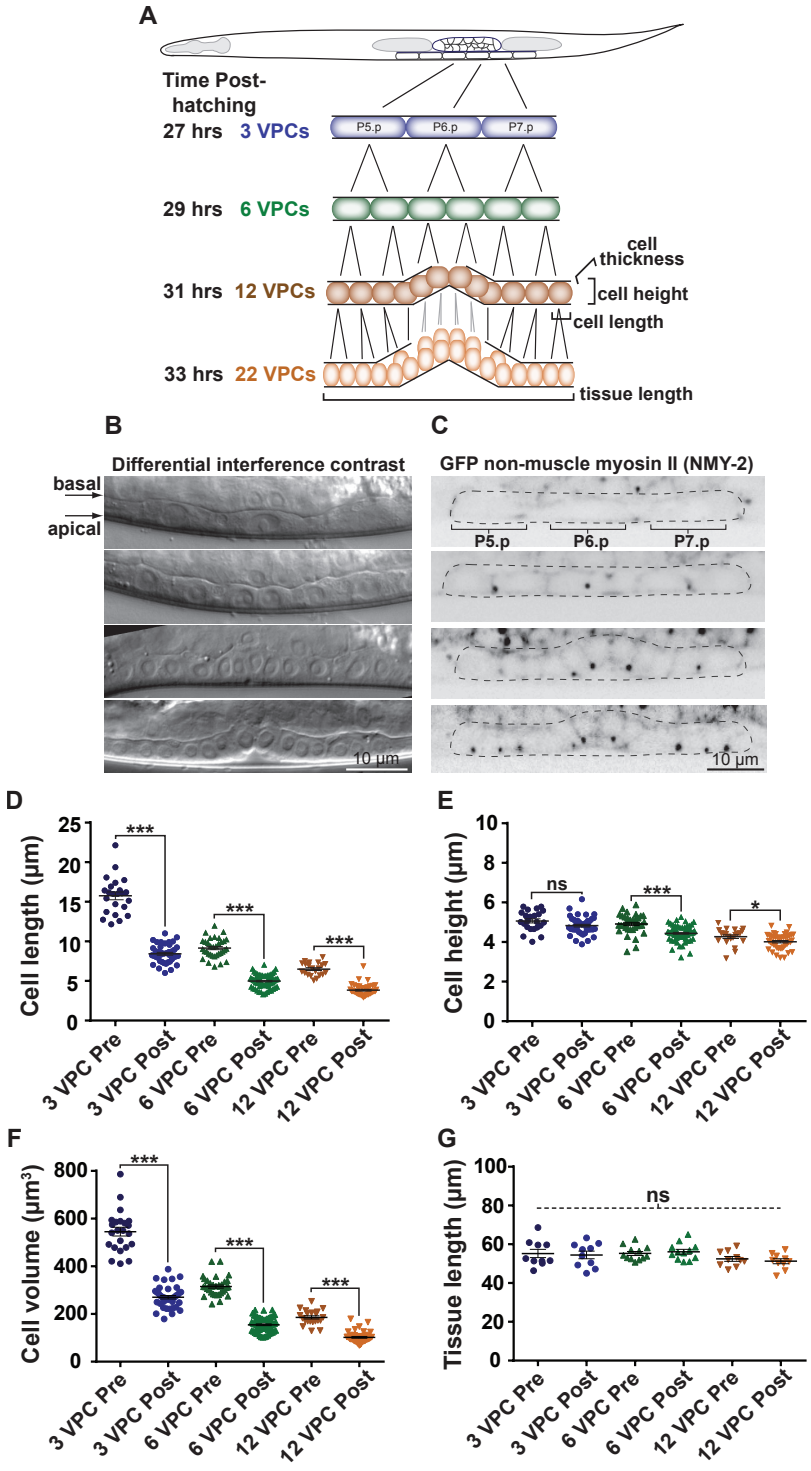

Figure 3.5.1 The C. elegans vulval precursor cells (VPCs) inside the living and developing animal

(A) Schematic representation of the VPCs (P5.p, P6.p and P7.p cells) in a third larval stage (L3) worm. 3 VPC stage: undivided precursors (purple); daughter cells: 6 VPC stage (green); 12 granddaughter cells: 12 VPC stage (orange); final 22 descendants = 22 VPC stage. (B) DIC images of the VPCs at the corresponding stages shown in A. For all images, anterior is to the left and dorsal is to the top. Scale bar = 10 μm. (C) Maximal intensity projection images of worms expressing GFP-tagged non-muscle myosin II (NMY-2) in the VPCs (dotted lines) at the 3, 6, 12 and 22 VPC stages. Scale bar = 10 μm (D-E) Scatter plots of individual VPC measures before (pre) and after (post) each round of VPC division. Cell length: ***: $p < 0.0001$, unpaired t test. Cell height: n.s.: $p = 0.06$, ***: $p < 0.0001$, *: $p = 0.02$, unpaired t test. Bars = mean with SEM. n(cells) > 20 and n(worms) ≥ 8 for each VPC stage. (F) VPC volume = length (D) x height (E) x thickness (number of 0.6 μm steps occupied by the cells). ***: $p < 0.0001$, unpaired t test. Bars = mean with SEM. n(cells) > 20 and n(worms) ≥ 8 and for each VPC stage. (G) Length of region occupied by the VPCs and their descendants. n.s.: $p > 0.1$, one-way analysis of variance. Bars = mean with SEM. n(worms) ≥ 10 for each stage.

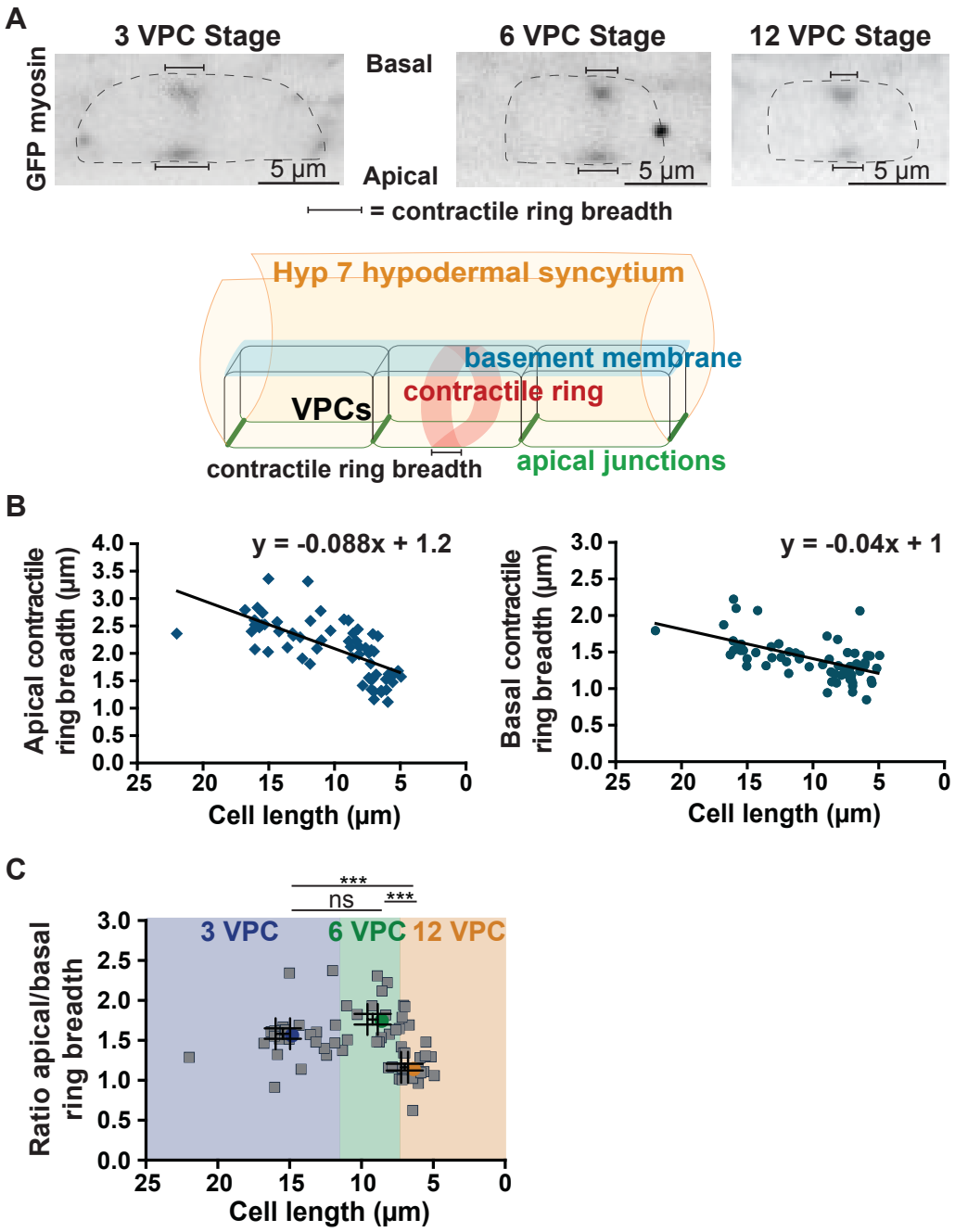

Figure 3.5.2 Contractile ring dimensions scale with the length of VPCs

(A) GFP-tagged myosin worms at the 3 (left), 6 (middle) and 12 (right) VPC stages. Images are maximal projections taken at < 150 seconds following cytokinesis onset. Myosin is enriched in the contractile ring at both the basal (upper) and apical (lower) domain of the cells. Dotted lines: dividing cells. Scale bar = 5 µm. Right: 3D schematic of a dividing VPC showing contractile ring breadth in brackets. (B) Apical (left) and basal (right) contractile ring breadth plotted against VPC length for all three rounds of division. The x-axis was inverted to

show the decrease in cell length through divisions. Best-fit linear regressions and their equations are shown. (C) Scatter plot of apical versus basal contractile ring breadth (data from B) for cell lengths at the 3 (purple), 6 (green) and 12 (orange) VPC stages. Colored dots: average for each stage. Scale bars = mean with SEM for both axes. n.s.: p value = 0.05, ***: p < 0.0001, unpaired t test.

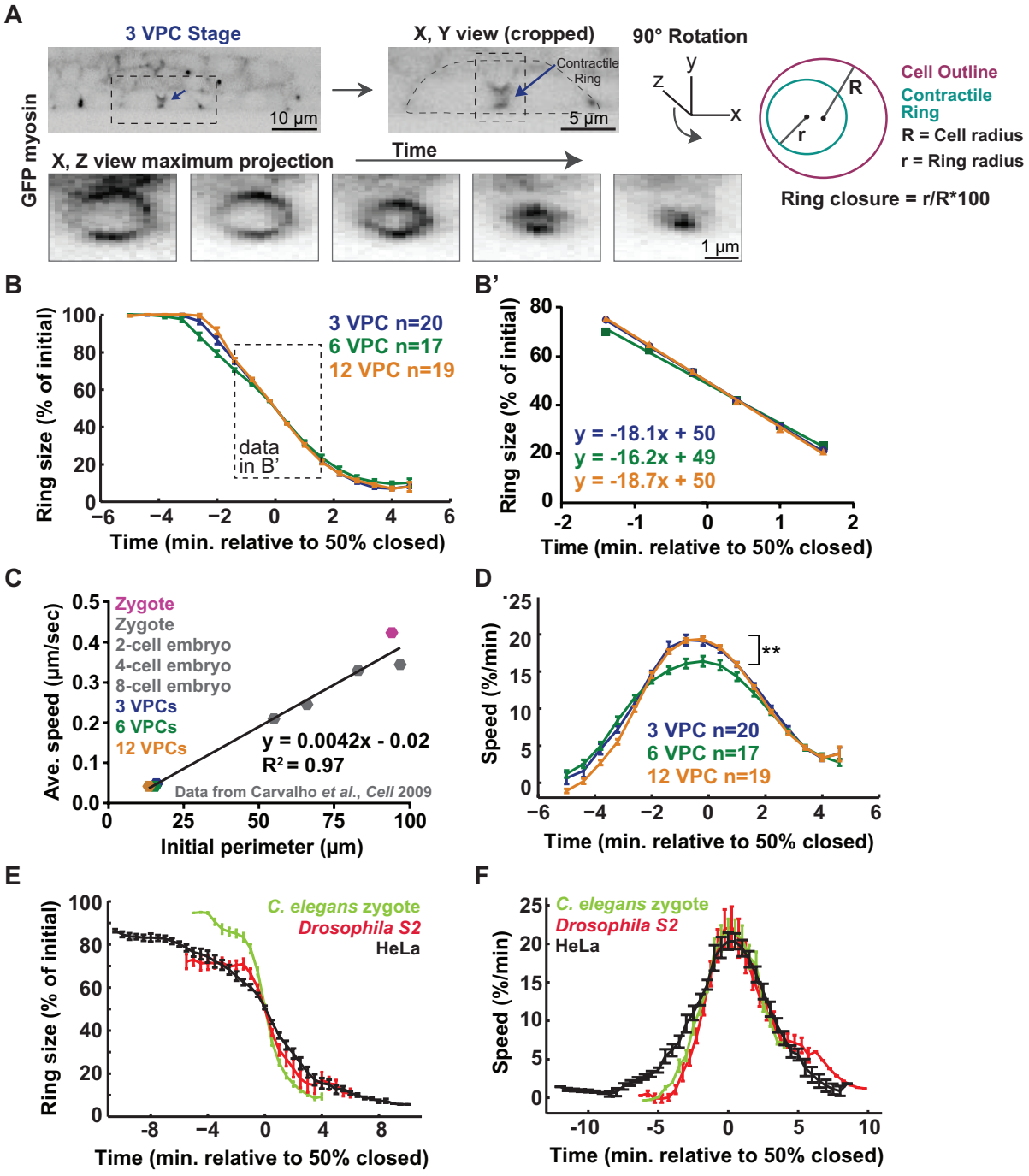

Figure 3.5.3 Quantitative analysis of the kinetics of contractile ring closure in the VPCs

(A) Maximal intensity projection images of a worm expressing GFP-tagged myosin at the 3 VPC stage. Left: dotted box: dividing cell; arrow: contractile ring. Scale bar = 10 µm. Middle: enlargement of the dividing cell (dotted outline); dotted box and arrow: contractile ring. Scale

bar = 5 μm. The cropped contractile ring is rotated 90° to generate a z, x maximum projection. Bottom: contractile ring closure over time. Scale bar = 1 μm. Right: representation of ring annotation and the parameters quantified: red = cell outline; green = contractile ring; R = cell radius; r = ring radius; Ring closure = r/R*100. (B) Average percentage of contractile ring closure over time aligned at the midpoint of closure for the first (purple), second (green) and third (orange) rounds of VPC cytokinesis. Purple/first: n(cells) = 20, n(worms) = 11. Green/second: n(cells) = 17, n(worms) = 6. Orange/third: n(cells) = 19, n(worms) = 8. Error bars = SEM. Dotted box: data for B'. (B') Linear regression lines and their equations for 20% - 80% ring closure (data from B). (C) Furrowing speed versus division plane perimeter (3 VPC: purple, 6 VPC: green and 12 VPC: orange, grey: data from (Carvalho et al., 2009); pink: our zygote measurement). Linear regression fitted to all 8 data points. (D) Average speed of contractile ring closure over time for the three rounds of VPC cytokinesis. First round/purple, n(cells) = 20, n(worms) = 11, second/green, n(cells) = 17, n(worms) = 6, third/orange, n(cells) = 19, n(worms) = 8. **: p = 0.006 for 6 versus 12 VPC stage at time 0, unpaired t test. Error bars = SEM. (E-F) Graphs of average percentage of ring closure and speed over time for HeLa cells (black), *Drosophila* S2 cells (red) and the *C. elegans* zygote (light green). *C. elegans* zygote: n(cells) = 9, *Drosophila* S2: n(cells) = 5, HeLa: n(cells) = 8. Error bars = SEM.

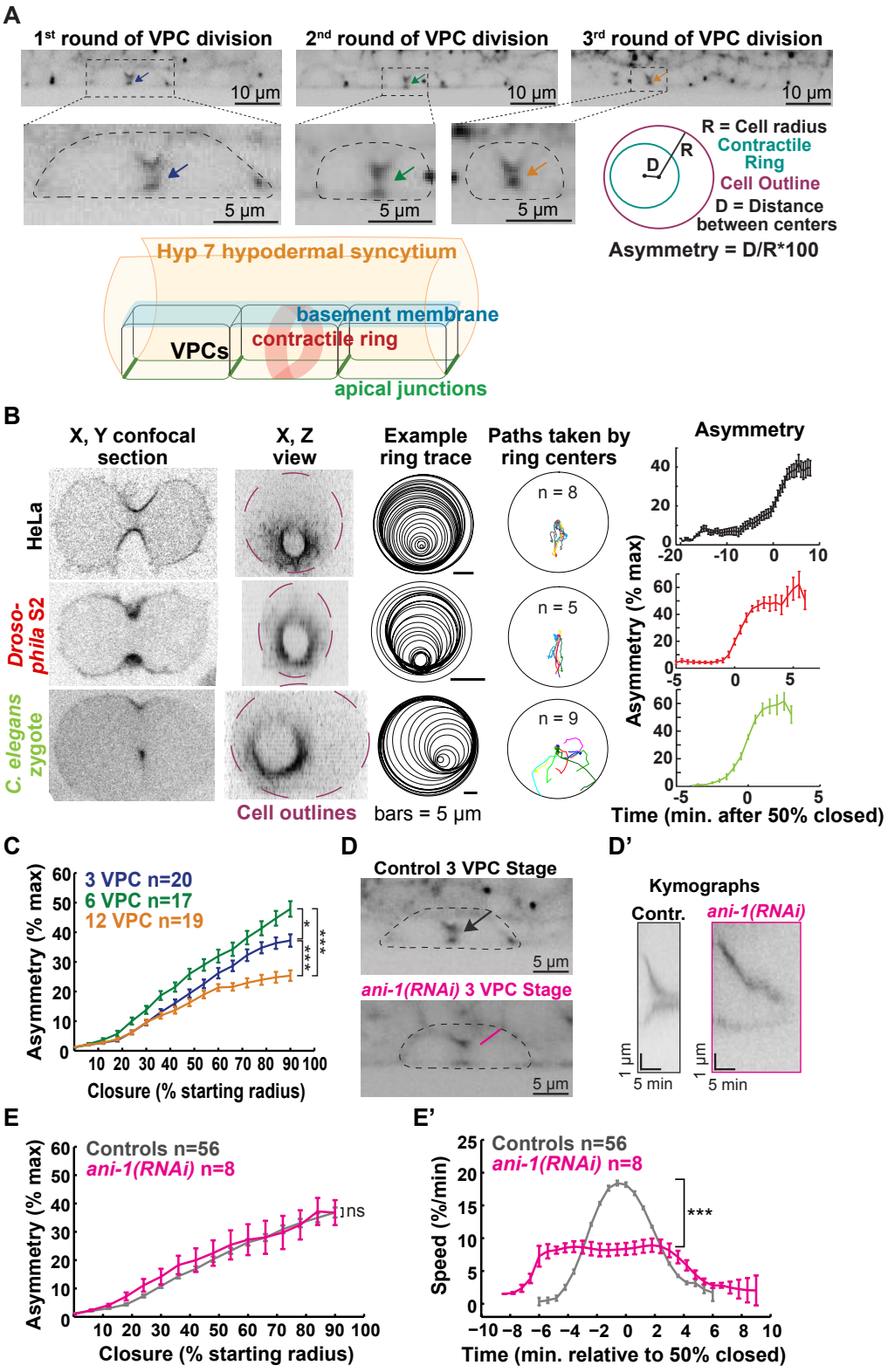

Figure 3.5.4 Strong intercellular adhesion leads to robust asymmetric contractile ring closure in the VPCs

(A) First (left), second (middle) and third (right) rounds of VPC cytokinesis in GFP::myosin worms. First round dividing cell reproduced from Figure 3A for ease of comparison. Scale bar = 10 μm. Dotted boxes and outlines: dividing cells; arrows: contractile rings. Scale bar = 5 μm. Representation of ring annotation and the parameters quantified: red = cell outline; green = contractile ring; R = cell radius; D = distance between cell and ring centers; Asymmetry = D/R*100. 3D schematic of contractile ring closure in the VPCs. (B) First column: x, y view of dividing HeLa cell (top), *Drosophila* S2 cell (middle), and *C. elegans* zygote (bottom). Second column: corresponding x, z views. Third column: example contractile ring location over time. Scale bar = 5 μm. Fourth column: the path taken by the ring for all examples of each cell type. Last column: asymmetry versus time. (C) Average asymmetry of furrowing over the percentage of VPC ring closure (first round; purple, second; green and third; orange). First: n(cells) = 20, n(worms) = 11. Second: n(cells) = 17, n(worms) = 6. Third: n(cells) = 19, n(worms) = 8. Error bars = SEM. ***: $p < 0.0001$, *: $p = 0.03$, unpaired t test calculated at 80% closed. (D) Confocal images of control and ANI-1 depleted worms expressing GFP::myosin (3 VPC stage). Dotted lines: dividing cells; arrows: ingressing furrows. Scale bar = 5 μm. (D') Kymographs of contractile ring closure for control (black) and ANI-1 depleted (fuchsia) worms expressing GFP::myosin. Vertical scale bar = 1 μm. Horizontal scale bar = 5 min. (E-E') Average furrow asymmetry and ring closure speed (all three rounds of VPC cytokinesis). Control (grey), n(cells) = 56, n(worms) = 25. *ani-1(RNAi)* (fuchsia), n(cells) = 8, n(worms) = 4. Error bars = SEM. n.s.: $p > 0.1$, unpaired t test. ***: $p < 0.0001$, unpaired t test.

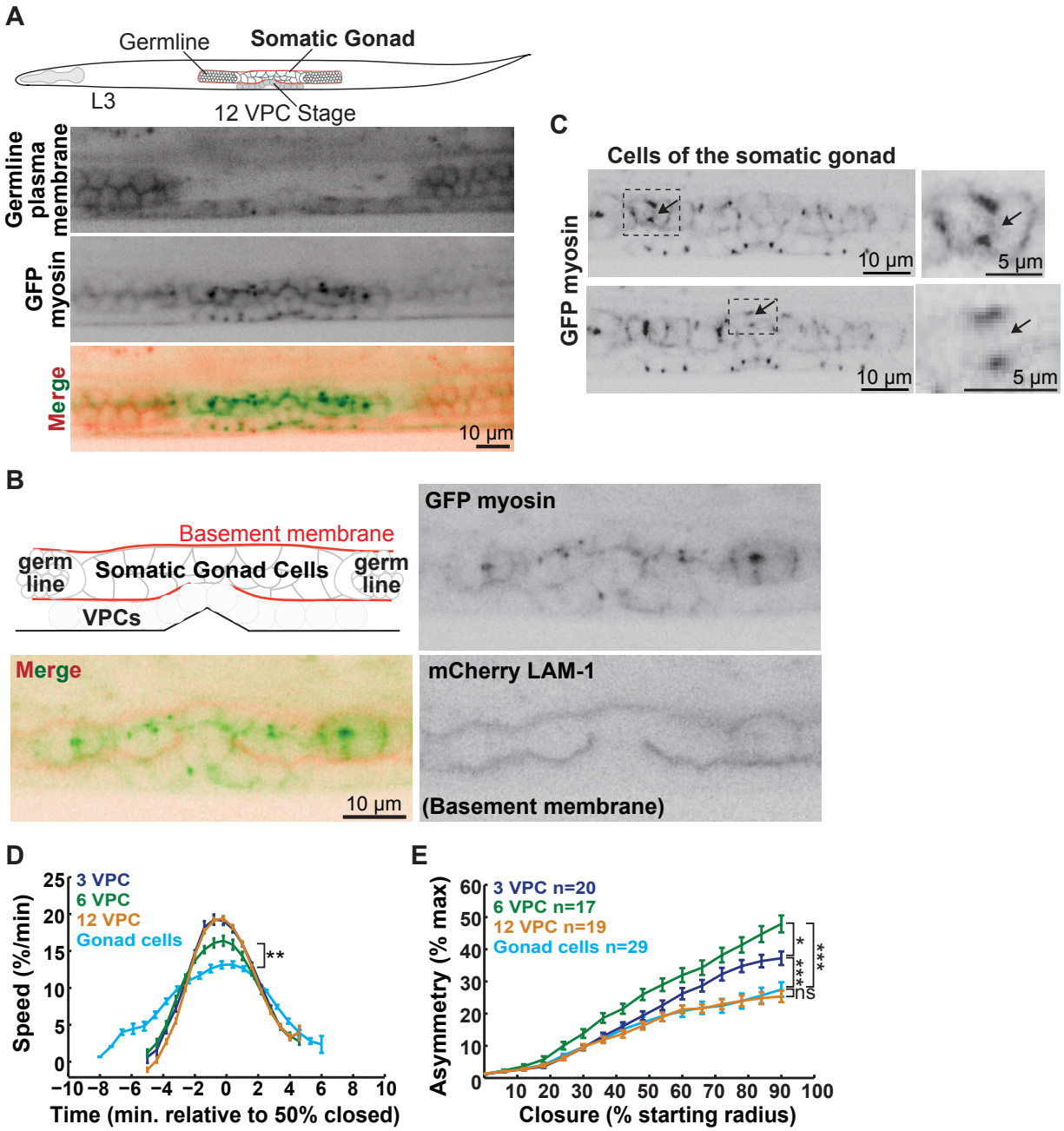

Figure 3.5.5 Tissue geometry influences the kinetics of cytokinesis in the cells of the somatic gonad

(A) Schematic representing an L3 worm (~31 hours post-hatching), showing the somatic gonad, VPCs and germline. Worm expressing mCherry-tagged phospholipase C (PLC) PH domain in the germline (top), GFP-tagged myosin in the VPCs and somatic gonad (middle), and merge image (bottom). Scale bar = 10 µm. (B) Schematic of the cells of the somatic gonad (middle) and the germline (extremities) surrounded by a continuous basement membrane (red). Worm at the 12 VPC stage expressing GFP::myosin and mCherry::LAM-1 (laminin-1)

to mark basement membrane. Scale bar = 10 μm. (C) Maximal projection images of the somatic gonad expressing GFP myosin. Dotted boxes: dividing cells, enlarged to the right; arrows: contractile ring. Scale bars = 10 μm (left); 5 μm (right). (D-E) Average ring closure speed and asymmetry (somatic gonad: teal blue, first VPC division: purple, second: green, and third: orange). Each VPC stage n(cells) ≥ 17, n(worms) ≥ 6. Gonad cells; n(cells) = 29, n(worms) = 12. Error bars = SEM. **: $p = 0.0023$, unpaired t test, gonad cells versus 6 VPC stage. *: $p = 0.06$, ***: $p < 0.0001$, n.s.: $p > 0.1$, unpaired t test.

Movie 1. Asymmetric furrowing to the apical membrane of VPCs

Time-lapse movie of a worm expressing GFP-tagged myosin during the second round of VPC division. Anterior is to the left and the apical membrane at the bottom. The contractile ring closes towards the apical membrane of all 6 daughter cells. Images were acquired every 2 minutes at 100x magnification, using a swept field confocal microscope (Nikon). A maximal projection of 0.6 μm z slices is shown. The movie is played at 5 frames/s. Scale bar = 10 μm. Time in minutes.

Movie 2. Cytokinesis in cells of the somatic gonad

Time-lapse imaging of a worm expressing GFP-tagged myosin, approximately 31 hours post-hatching. Same worm as shown in Figure 5C. Anterior is to the left and the ventral cuticle at the bottom. Above the 12 VPCs, four cells of the somatic gonad undergo cytokinesis, observed by myosin enrichment in the contractile ring. Images were captured every 30 seconds, at a magnification of 60x, using a swept field confocal microscope (Nikon). A maximal projection of 0.6 μm z slices is shown. The movie is played at 5 frames/s. Scale bar = 10 μm. Time in minutes.

3.6 Supplemental Figure and legend

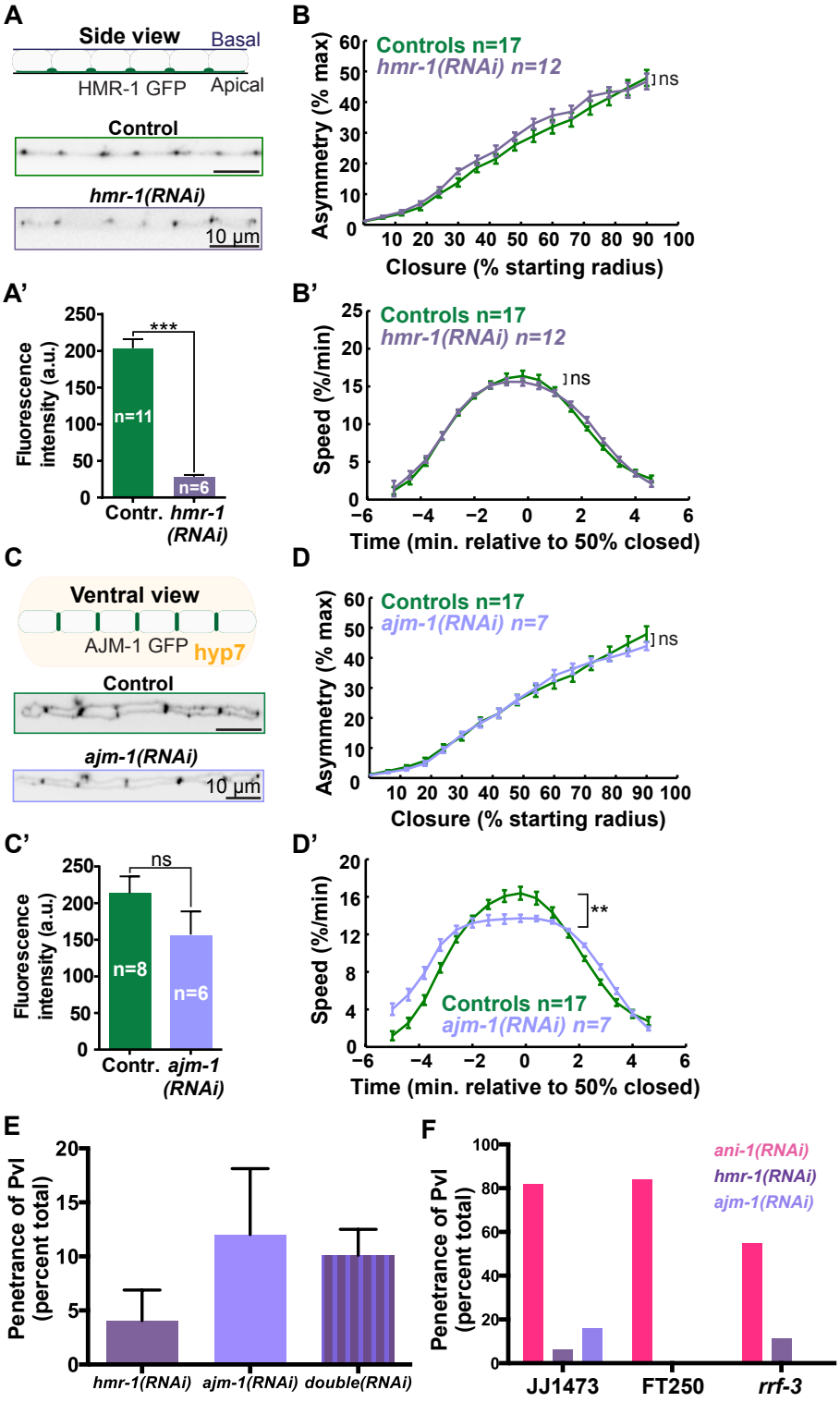

Figure 3.6.1 Supplemental Figure

(A) Schematic representation of HMR-1$^{E\text{-cadherin}}$ apical localization at the 6 VPC stage in an x, y view. Corresponding images of control and *hmr-1(RNAi)* worms. Scale bar = 10 μm. (A') HMR-1::GFP intensity in the entire VPC region (6 VPC stage). Green: average intensity for controls; purple: HMR-1 depleted worms. Bars = mean with SEM. ***: $p < 0.0001$, unpaired t test. (B-B') Average asymmetry and speed of contractile ring closure, respectively, in controls (green) and HMR-1 depleted worms (purple) during the second round of division. Controls n(cells) = 17, n(worms) = 6. HMR-1 depletions n(cells) = 12, n(worms) = 5. Error bars = SEM. n.s.: $p > 0.1$, unpaired t test. (C) Schematic of a ventral view of VPCs expressing GFP-tagged AJM-1. Corresponding maximal intensity projection images of 6 VPC stage AJM-1::GFP control and AJM-1 depleted worms. Scale bar = 10 μm. (C') AJM-1::GFP intensity in control (green) and AJM-1 depleted (light purple) worms (3 and 6 VPC stages). Bars = mean with SEM. n.s.: $p = 0.16$, unpaired t test. (D-D') Average asymmetry and speed of contractile ring closure for controls and AJM-1 depleted worms during the second round of division. Controls (green) n(cells) = 17, n(worms) = 6. *ajm-1(RNAi)* (light purple) n(cells) = 7, n(worms) = 3. Error bars = SEM. n.s.: $p > 0.1$. **: $p = 0.0026$, unpaired t test. (E) The penetrance of the protruded vulva (Pvl) phenotype was scored at least 72 hours post-feeding. *hmr-1(RNAi):* purple, *ajm-1(RNAi)*: light purple, *hmr-1+ajm-1(RNAi):* striped column. n(experiments): *hmr-1* = 6, *ajm-1* = 5, *hmr-1/ajm-1* = 2. Bars = mean with SEM. (F) Penetrance of the Pvl phenotype for three different worm strains; JJ1473 (NMY-2::GFP), FT250 (HMR-1::GFP) and *rrf-3* (pk1426). The average percentage of pvl is represented for *ani-1* (fuchsia), *hmr-1* (purple) and *ajm-1* (light purple) depleted worms. n(replicates): JJ1473/*ani-1* n = 5, JJ1473/*hmr-1* n = 6, JJ1473/*ajm-1* n = 5, FT250/*ani-1* n = 1, FT250/*hmr-1* n = 3, FT250/*ajm-1* n = 2 and *rrf-3*/*ani-1*, *rrf-3/hmr-1*, *rrf-3/ajm-1* n = 1.

3.7 Materials and methods

C. elegans strains

The following strains were used:

JJ1473 *(zuIs45 [nmy-2::NMY-2::GFP + unc-119(+)] V),*

FT250 *(xnIs96 [pJN455(hmr-1p::HMR-1::GFP::unc-54 3'UTR) + unc-119(+)]),*

SU93 *(jcIs1 [ajm-1::GFP + unc-29(+) + rol-6(su1006)] IV),*

OD183: OD70 *(ltIs44 [pAA173, pie-1p::mCherry::PH(PLC1delta1) + unc-119(+)])* x JJ1473, and JJ1473 x NK574 *(qyIs86 [cog-2::GFP]; lam-1::cherry)*.

C. elegans culture

C. elegans strains were maintained at 25°C using standard procedures (Brenner, 1974). For live imaging and feeding experiments worms were synchronized at the first larval stage (L1) using alkaline bleach (1.2% NaOCl, 250 mM KOH) (Stiernagle, 2006). Control L3 worms were mounted for imaging at 27 hours post-hatching. Somatic gonad imaging was performed using late L3 worms between 31 to 33 hours post-hatching (12 VPC stage).

RNA-mediated interference

Protein depletions were carried out by placing 10 to 15 worms on a plate seeded with the HT115 bacterial strain containing the L4440 vector inducing IPTG mediated dsRNA expression, as described (Kamath et al., 2003). Single bacterial clones from the Ahringer library (Fraser et al., 2000; Kamath and Ahringer, 2003), kindly provided by Jean-Claude Labbé (IRIC, Université de Montréal), were sequenced to confirm the presence of target genes. Synchronized L1 worms were fed dsRNA expressing bacteria for > 26 hours at 25°C before imaging. To assess the effects of the RNAi on overall vulval morphogenesis, worms were grown for > 72 hours (to adulthood) and scored for protruded vulva (Pvl) phenotypes using a stereomicroscope.

Worm mounting and imaging

Worms anesthetized in 0.01% tetramisole in M9 buffer for 10 minutes were mounted on a 5% agarose pad bearing 20 to 80 μm wide grooves made by a custom nanofabricated silica plate. Worms were overlaid with a Poly-L-Lysine coated coverslip. To prevent desiccation, tetramisole solution was added between the coverslip and agarose pad and the chamber was sealed with VaLaP (1:1:1 Vaseline, lanolin and paraffin). Imaging was performed using a Swept Field Confocal (SFC, Nikon Canada, Mississauga, ON, Canada; and Prairie Technologies, Madison, WI, USA). The 50 μm slit mode was used with or without 2x2 binning on a CoolSnap HQ2 camera (Photometrics, Tucson, AZ). We used a 60X/1.4 NA Plan-Apochromat objective 0.6 μm z steps, 30 seconds intervals, and either 400 or 600 milliseconds exposures. All acquisition settings, including laser intensity, were controlled using NIS-Elements software (Nikon). Time-lapse imaging of VPCs and somatic gonad cells was performed for several hours to capture multiple divisions (each lasting approximately 10 minutes). Only one acquisition was made per worm. $n \geq 3$ worms per condition.

Cell and contractile ring dimension measurements

VPC and tissue dimensions were measured with NIS-Elements software (Nikon). The length and height of VPCs were measured before and after division. Cell thickness was estimated by counting the number of 0.6 μm z-slices occupied by the cell. Cell volume was calculated by multiplying length, height and thickness. Tissue length was determined by a longitudinal measure of the three VPCs and their descendants before and after each round of division. Measurements were recorded in Excel (Microsoft) and graphed using Prism (GraphPad software). Statistical analyses for cell height (unpaired t test) and tissue length (one-way ANOVA) were performed in Prism. For cell length and volume, unpaired t tests were performed in MATLAB. Contractile ring dimensions in the VPCs were assessed with a custom MATLAB-based software. Original acquisitions were processed (cell cropping) for analysis in NIS-Elements (Nikon). Contractile ring dimensions from maximal projection images were measured in the plane of imaging (x, y view). Apical and basal contractile ring breadths were measures of the equatorial region enriched for myosin. Myosin enrichment was defined by higher shades of grey compared with adjacent myosin at the cell perimeter. Breadth

measurements for the first five time points with detectable equatorial myosin were averaged. Measurements were compiled in Excel; statistical analysis and graphing were performed using Prism.

Fluorescence intensity measurements

To assess the extent of HMR-1 and AJM-1 depletions, the fluorescence intensity of GFP-tagged HMR-1 and AJM-1 was measured using FT250 and SU93 strains, respectively. All imaging parameters were held constant between control and RNAi animals. All measurements of fluorescence intensity were performed in the same way using Fiji (ImageJ 1.48a, NIH). Images were opened as 16-bit .nd2 files. A single confocal slice was selected for analysis. Images were rotated to align the VPCs horizontally. A box was drawn over the entire region of the VPCs. Each measurement was normalized to the fluorescence intensity of the background outside the worm. Mean fluorescence intensity was recorded in Excel. Graphing and statistical analysis were performed in Prism.

Cytokinesis kinetics analysis

Quantifications of the kinetics of cytokinesis were performed using custom MATLAB software cyanRing (CYtokinesis ANalysis of the contractile RING) (Dorn et al., 2010). Individual cells were first cropped from time-lapse z series in x and y using NIS-Elements. Using cyanRing, the contractile ring was cropped and rotated to generate a maximal projection image of the division plane (z, x view). The outline of the cell and contractile ring were annotated over time by marking three points (Figure 3A). Ring size and position were calculated from best-fit circles through these points. Graphs of ring closure timing, speed and asymmetry were made using cyanRing.

Statistical analysis

P values for cell length and cell volume measurements were obtained in MATLAB by performing unpaired t tests. Statistical analyses of cyanRing data were performed in MATLAB using a custom script. Unpaired t tests were calculated for each specified sets of data. For cell height (unpaired t test) and tissue length (one-way analysis of variance) measurements, statistical analyses were performed in Prism (GraphPad software). Statistical

analyses for fluorescence intensity quantifications were also performed in Prism, obtaining p values following unpaired t tests.

3.8 Acknowledgements

We thank Julie Canman, Dave Matus, Mark Peifer, and Joël Ryan for careful reading of the manuscript. We thank Xiaohu Wan, Joël Ryan and Jacques Boisvert for technical assistance and all members of the Maddox laboratories for helpful discussions. We thank Christian Charbonneau at the Bio-imaging facility of the Institute for Research in Immunology and Cancer for technical help with imaging.

4 Cell size regulation

The following chapter summarizes current knowledge on cell size regulation from yeasts to mammals, including the problem of how cellular structures are scaled according to cell size. This overview will be followed by a description of seminal work on cell size regulation in the budding yeast *S. cerevisiae*. The observation that several regulators of cell size are conserved between evolutionary divergent species motivated studies of size in higher eukaryotes, described later in the chapter. Finally, I will address an important void in the cell size field, namely the absence of large-scale analysis of mammalian cell size regulators. Revolutionary new gene editing technology based on the bacterial CRISPR/Cas9 system, described in detail in the next chapter, opens new frontiers for studies of size in higher eukaryotes. This leads to the work Thierry Bertomeu and I performed using the CRISPR/Cas9 technology to uncover genes implicated in human cell size regulation, the topic of Chapter 6.

4.1 Cell size scales with ploidy

In all organisms studied, a positive correlation between genome copy numbers and cell size has been reported. Scientists in the 1900's, including Boveri and Hertwig, were the first to note a correlation between ploidy level and cell size (Ycas et al., 1965). Since then, several studies across different eukaryotic species supported their preliminary observation.

Investigations in the budding yeast *S. cerevisiae* demonstrated a linear relationship between yeast size and genome copy numbers. Mundkur and Mortimer performed genetic manipulations to generate a yeast ploidy series from haploid to hexaploid. They observed that yeast volume increased proportionally to genome copy numbers, such that diploid yeast cells were nearly twice as large as their haploid equivalent (Mortimer, 1958; Mundkur, 1953). These studies provided compelling evidences that budding yeast cell size scales with ploidy.

Beyond unicellular organisms, higher eukaryotes exploit ploidy as a mechanism to increase cell size. In mammals, specialized cells of the bone marrow producing platelets called megakaryocytes achieve high levels of ploidy. These progenitors can reach up to one hundred and twenty-eight times the number of chromosomes in a haploid cell (Edgar and Orr-Weaver, 2001; Lacroix and Maddox, 2012). Other cell types including hepatocytes of the liver also

become polyploid, a process that contributes to most of the increase in liver mass (Lacroix and Maddox, 2012).

Early genetic studies in *Drosophila* uncovered a linear relationship between wing cell size and genome copy numbers (Dobzhansky, 1929). In addition, BrdU staining of various *Drosophila* larval tissues, such as the hindgut, imaginal disc and salivary glands, revealed a large range of DNA copy numbers (Smith and Orr-Weaver, 1991). *C. elegans* also employs increasing ploidy for the growth of its hypodermis lining the external surface of worm (Flemming et al., 2000; Lozano et al., 2006). Increasing genome copy numbers is a predominant mechanism in plants to promote an increase in cell size. For instance, dissection of somatic nuclei followed by flow cytometry analyses in different tissues of *Arabidopsis thaliana* revealed the presence of a large range in DNA copy numbers (Galbraith et al., 1991). These many examples suggest that ploidy increases represent a conserved mechanism across species to increase cell size.

Seminal work by Fankhauser in the salamander provided further strong evidence of a positive correlation between ploidy levels and cell size. The size of kidney tubule cells, and indeed cells from most other tissues, increased with increasing ploidy of the animal (Fankhauser, 1945). Strikingly, this study also revealed that neither organ size nor the body size of salamanders were altered in animals of different ploidies (Fankhauser, 1945). Similarly, nuclear volumes of cells within different tissues of tetraploid mice were twice the size of nuclei in diploid mice and again, regardless of ploidy, organ and body sizes of mice were unchanged (Henery et al., 1992). The basis for this compensation mechanism whereby organisms regulate cell number to compensate for increased cell size to maintain body size is unknown. These results clearly indicate that the coordination between cell growth and cell division includes multiple layers of regulation. These processes must be intricately regulated at the level of individual cells, organs, and the entire organism.

4.2 The existence of a cell size threshold

The size of an individual cell is dictated by its size at birth, how much it growths, and its status with respect to cell division. Early cell biological studies suggested that proliferating cells that fail to accumulate sufficient mass or attain a certain volume cannot proceed into the

division cycle. These observations and several other lines of evidence acquired since then, led to the proposition of the existence of a cell size threshold that must be achieved for a cell to trigger division.

The first indication for such a threshold came from a classical experiment performed in the unicellular organism *Amoeba proteus*. In his experiment, Hartmann periodically removed part of the cytoplasm of the cell preventing the ablated cell from dividing over 150 days (Hartmann, 1926). This remarkable experiment was later repeated by Prescott on a shorter timescale, which confirmed the results of Hartmann (Prescott, 1956a; Prescott, 1956b). In both experiments, *Ameoba* failed to divide upon removal of cytoplasmic content (Hartmann, 1926; Prescott, 1956a; Prescott, 1956b). Ablated *Ameoba* continued to grow but were of smaller sizes when compared to un-ablated equivalents (Prescott, 1956a; Prescott, 1956b). This simple experiment suggested that *Ameoba* needed to accumulate sufficient mass, volume or protein content before committing into division. Twelve years later, Donachie observed that *E. coli* cells individually growing reached initiation of DNA synthesis at similar sizes. He explained this observation by proposing that bacterial cells, like Ameoba, needed to gain sufficient mass before replicating their genome (Donachie, 1968).

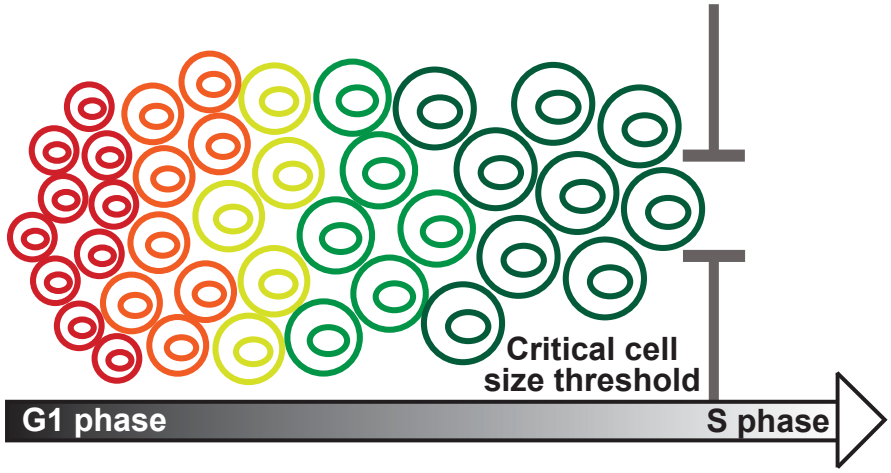

Figure 4.2 Cell growth in G1 to reach the cell size threshold and trigger S phase entry

Schematic depicting small cells at birth (red cells) that grow in G1 until they achieve sufficient growth (green cells) and pass a cell size threshold to trigger S phase entry. Adapted from (Ginzberg et al., 2015).

4.2.1 A critical cell size in yeasts

In the early 1970's, a seminal discovery made by Paul Nurse in the fission yeast *Schizosaccharomyces pombe* (*S. pombe*) and Lee Hartwell in the budding yeast *S. cerevisiae* propelled cell size studies in single-celled eukaryotes. Nurse and Hartwell sought to identify genetic mutations, in *S. pombe* and *S. cerevisiae* respectively, that led to the arrest of cells in different phases of the cell cycle. Many such genes were identified and accordingly named cell division cycle (CDC in *S. cerevisiae* and cdc in *S. pombe)* genes (Hartwell et al., 1970; Hartwell et al., 1973; Nurse, 1975). Following this discovery, Nurse, Fantes and Hartwell utilized these mutants to investigate the relationship between cell growth and cell division in both fission and budding yeast cells (Fantes, 1977; Hartwell et al., 1970; Hartwell et al., 1973; Nurse, 1975)

In the budding yeast, Hartwell and colleagues showed that cells with deficient cell division cycles continued to grow (Hartwell et al., 1970; Hartwell et al., 1973). Cdc mutant yeast cells reached volumes two- to three-fold greater than their wild type equivalents (Hartwell et al., 1970; Hartwell et al., 1973). Moreover, cells deprived of nutrients arrested in the early growth phase of the cell cycle (G1) suggesting insufficient mass or volume acquisition prevented cell cycle progression (Hartwell et al., 1970; Hartwell et al., 1973). Hartwell and colleagues were the first to infer that yeast cells needed to reach a "critical size" in order to proceed in the early events of cell division (Johnston et al., 1977). This work provided the first strong indication that yeast cells possess a cell size threshold (Figure 4.2). They named "Start" the commitment of budding yeast cells to cell division upon achieving this critical size at the end of G1 and subsequently showed that once past Start cells became refractory to arrest by mating pheromone (Johnston et al., 1977).

The work of Hartwell and colleagues led to an additional influential discovery. Since yeast cells with defective cell division genes kept on growing, the authors concluded that cell growth and cell division were largely separable processes. More recent work has shown that cells that grow to extreme sizes can actually inhibit division (Goranov et al., 2009). Nonetheless under physiological conditions, cell growth is the limiting factor for progression into the cell division cycle (Hartwell et al., 1970; Hartwell et al., 1973). These concepts are key to the understanding of cell size regulation and will be discussed in later sections.

4.2.2 A cell size threshold in animal cells

Seminal work by Killander and Zetterberg provided evidence for the existence of a cell size threshold in mammalian cells. Their work in mouse fibroblasts showed that cells with lower initial masses extended their G1 phase compared to heavier cells that proceeded into DNA synthesis (S phase) more rapidly (Killander and Zetterberg, 1965). This important observation led to the proposition that fibroblasts, like yeast, needed to reach sufficient mass in order to proceed into cell division (Killander and Zetterberg, 1965).

Several other groups provided supporting evidences for the existence of a size threshold in diverse mammalian cell types. Chinese hamster cells, oligodendrocytes, and mouse embryonic fibroblasts of smaller sizes increased the duration of the G1 phase to ensure sufficient total mass or volume was achieved to enter the division cycle (Gao and Raff, 1997; Kimball et al., 1971; Shields et al., 1978). In another experiment, when growth conditions were hampered by serum starvation or amino acid removal, Syrian hamster cells arrested in G1 and became quiescent a process that was reversed upon restoration of normal growth conditions (Pardee, 1974). This led to the proposition that mammalian cells possessed a "Restriction Point" analogous to Start in yeasts (Pardee, 1974). These results suggest that mammalian cells need to achieve sufficient growth to commit to cell division (Figure 4.2). This notion of a cell size threshold has been challenged by Raff and colleagues, who suggested that oligodendrocytes achieved cell size homeostasis by a mechanism of passive growth (Conlon and Raff, 2003; Lloyd, 2013).

4.3 Cell size regulation in budding yeast

Most of the current knowledge on how cells regulate their size comes from studies in yeasts. This model organism provided several advantages including ease of manipulation, well-established genetics and a relatively simple architecture. Studies in both budding yeast and fission yeast have generated a wealth of knowledge and a conceptual framework for cell size regulation at both the cellular and molecular levels, which has provided the foundation for work in higher eukaryotes. In the following sections, the molecular components involved in coordinating cell size in budding yeast are described.

4.3.1 Environmental conditions modulate cell growth

Proliferating cells need to achieve a sufficient amount of growth before committing into cell division (Figure 4.2). Early studies in yeast showed that environmental factors influence cell growth. Nurse and Fantes provided compelling evidences with experiments with *S. pombe* (Fantes and Nurse, 1977; Fantes, 1977). In their experiments, they investigated growth rates of fission yeasts under different culture conditions. Cells grown in glucose-rich media showed increased growth rates compared to yeast cells grown in nutrient-poor (glycerol) conditions (Fantes, 1977). Interestingly, changing growth conditions led to a rapid adjustment in growth rates of fission yeast cells (Fantes, 1977). For instance, cells shifted from nutrient-poor to a nutrient-rich media rapidly augmented cell growth during G1 (Fantes, 1977). In addition, fission yeast grown at lower temperatures were smaller and slower growing compared to larger fast-growing yeasts cultured at higher temperatures (Fantes and Nurse, 1977; Johnston et al., 1977). Thus, environmental conditions directly impact cell growth in fission yeasts. Similar results to those of Nurse and Fantes were obtained in budding yeast. Cells grown in the presence of rich nutrients, such as glucose, exhibited an increased size and growth rate. Conversely, cells grown in nutrients-poor media (glycerol) were smaller and exhibited slower growth rates (Johnston et al., 1977). Altogether, these findings illustrated the modulation of yeast cell growth and size by environmental conditions consistent with the notion that cell size is optimized to maximize fitness under different growth conditions (Jorgensen and Tyers, 2004).

4.3.2 Identification of the first cell size mutants in yeast

In the 1970's, genetic mutations resulting in small cell size phenotypes were first isolated in the fission yeast by Nurse and Fantes. These mutants were termed "wee", for small in Scottish English (Fantes and Nurse, 1977). Following this discovery, Bruce Carter and Peter Sudbery sought to identify analogous small mutants in *S. cerevisiae* and indeed isolated strains with a small cell size phenotype (Sudbery et al., 1980). These mutants were termed "Whi" for the bottle of whiskey bet on their successful isolation (Sudbery, 2002).

4.3.3 Start architecture

The G1 to S phase transition in budding yeast is orchestrated at the level of transcription. Two partially redundant transcription factors, called SBF and MBF coordinate the expression of over 200 genes implicated in budding, DNA replication and other processes at Start: SBF is composed of Swi4 and Swi6, whereas MBF is composed of Mbp1 and Swi6 (Baetz and Andrews, 1999; Bean et al., 2005; Dirick and Nasmyth, 1991; Iyer et al., 2001; Koch et al., 1993; Sidorova and Breeden, 1993; Simon et al., 2001). SBF and MBF exhibit functional overlap in transcriptional regulation as illustrated by the lethal G1 arrest of a swi4D swi6D or swi4D mbp1D double mutant (Dirick and Nasmyth, 1991; Koch et al., 1993). These transcriptional activators of Start must be repressed in G1 phase to prevent early entry into division under conditions of insufficient growth. Whi5 is an important repressor of Start that prevents activation of the SBF complex (Costanzo et al., 2004; de Bruin et al., 2004; Jorgensen et al., 2002; Jorgensen et al., 2004). Yeast cells deleted for WHI5 are small owing to the inability of the cell to repress Start in its absence (Jorgensen et al., 2002; Jorgensen et al., 2004). Nrm1 acts as an analogous repressor for the MBF after cells have passed Start (de Bruin et al., 2006). In turn, the MBF complex acts on Nrm1 to restrict transcription at the G1-S phase transition (de Bruin et al., 2008; de Bruin et al., 2006). MBF accumulates in G1 and at the DNA replication checkpoint, MBF expression peaks promoting Nrm1 inactivation and in turn activation of MBF-dependent transcription (de Bruin et al., 2008). In sum, early entry into Start is prevented by negative regulation of SBF/MBF transcription factors.

Commitment into Start requires that repression of SBF/MBF is alleviated in G1. This is achieved through the action of the partially redundant G1 cyclins, namely Cln1, Cln2 and Cln3 (Jorgensen and Tyers, 2004). These cyclins act in a dose-dependent manner to promote entry into Start by activation of the Cdk1 kinase (Cdc28) responsible for entry into S phase of the cell cycle (Cross, 1988; Dirick et al., 1995; Hadwiger et al., 1989; Nash et al., 1988; Richardson et al., 1989; Tyers et al., 1993). Cln3 was originally identified as WHI-1, the first cell size mutant in budding yeast (Sudbery et al., 1980) and is an essential regulator of Start acting upstream of Cln1/2 as an activator of the SBF complex (Tyers et al., 1993). Subsequent SBF activation occurs via phosphorylation of the Whi5 repressor and Swi6 (Costanzo et al., 2004; de Bruin et al., 2004). SBF activation occurs at CLN1/2 promoters further perpetuating

the Start signal in a positive feedback loop (Skotheim et al., 2008). A number of additional factors, including histone deacetylases and the transcriptional regulator Bck2, also contribute to the timing of G1/S transcription (Futcher, 2006). These studies in yeast helped to establish a framework for understanding cell size regulation in higher eukaryotes.

4.3.4 Systematic screens for size regulators in yeast

The development of a comprehensive set of deletion strains for every gene in *S. cerevisiae* (Winzeler et al., 1999) allowed the systematic identification of genes that affect yeast cell size. The Tyers groups carried out the first global analysis of yeast cell size with the deletion collection (Jorgensen et al., 2002). Using this collection, the authors quantitatively assessed each of the 6,000 deletion strains for effects on cell size in exponentially growing cultures (Jorgensen et al., 2002). This influential work revealed that 10% of gene deletions resulted in a cell size phenotype (Jorgensen et al., 2002). A parallel large-scale study, performed with stationary phase diploid yeast cultures, identified a similarly large set of genes that affect cell size (Zhang et al., 2002). Subsequent studies revealed additional gene deletion strains that alter the yeast cell size (Dungrawala et al., 2012).

Amongst gene deletions associated with a cell size phenotype, many were found to participate in ribosome biogenesis (Dungrawala et al., 2012; Jorgensen et al., 2002). Amongst these were the genes Sfp1 and Sch9 that when depleted caused a dramatic reduction in yeast cell size (Jorgensen et al., 2002). The transcription factor Sfp1 was identified as an important regulator of ribosomal protein and ribosome biogenesis genes and found to act as a sensor of the nutritional status of yeast cells (Jorgensen et al., 2002; Jorgensen et al., 2004; Lempiainen et al., 2009). Further characterization of the Sch9 gene revealed its involvement in ribosomal protein gene in parallel to Sfp1 (Jorgensen et al., 2002; Jorgensen et al., 2004; Urban et al., 2007). Sfp1 and Sch9 were subsequently identified as downstream regulators of the yeast target of rapamycin (TOR) gene (Jorgensen et al., 2004; Lempiainen et al., 2009; Urban et al., 2007). TOR is conserved from yeast to mammals and will be described in more detail in a later section (Gonzalez and Rallis, 2017). In budding yeast, the TOR network responds to nutrients and regulates ribosomal production and translational output via Sfp1 and Sch9 (Jorgensen et al., 2004; Lempiainen et al., 2009; Loewith and Hall, 2011; Singh and Tyers,

2009; Urban et al., 2007). The strong effect of ribosome biogenesis rate, but not protein translation rate per se, on the timing of Start suggested that the process of building ribosomes is linked to the G1/S cell cycle machinery (Jorgensen et al., 2004). As over 50% of the cell's biosynthetic capacity is directed towards the production of ribosomal RNA and protein, this model links the main requirements for growth to cell cycle commitment (Jorgensen and Tyers, 2004).

4.4 Mammalian cell size regulation

The discovery that molecular regulators of cell size in unicellular organisms were highly conserved, was important for subsequent studies in higher eukaryotes. In the following sections, molecular regulators of metazoan cell growth and cell proliferation will be first addressed separately. Later emphasis will be given to the increasing knowledge reconciling growth and cell division in mammalian systems. Finally, the lack of tools to perform large-scale studies that interrogate molecular regulators of size in mammalian cells will be discussed in the last section.

4.4.1 Mammalian cell growth

The presence of both nutrients and growth factors are required to promote an increase in mammalian cell size (Rathmell et al., 2000). Rathmell and colleagues showed that lymphocytes grown in nutrient-rich environments deprived of growth factors decreased in size and presented slower metabolism over time (Rathmell et al., 2000). Neurons also showed a marked reduction in size upon growth factor deprivation (Purves et al., 1988). Rat Schwann cells increased in size upon stimulation by insulin growth factors, as do many other mammalian cell types (Conlon et al., 2001). These studies demonstrated that mammalian cell growth requires the presence of growth factors. The majority of mammalian growth factors come in the form of growth hormones, including insulin (Lloyd, 2013). Some cell types require specific growth factors, such as neurotrophic factors for neurons and interleukins for lymphocytes (Lloyd, 2013). At the molecular level, growth factors trigger a cascade of events that ultimately result in cell growth modulation. A central player to the regulation of

mammalian cell growth is the mechanistic target of rapamycin (mTOR) gene, described in detail in the following section.

4.4.2 The target of rapamycin (TOR) growth regulatory network

TOR was first discovered in budding yeast, with the identification of TOR-1 and TOR-2 mutants that conferred resistance to the antifungal drug rapamycin (Heitman et al., 1991). Simultaneous inhibition of both yeast TOR genes caused a similar phenotype to nutrient deprivation (Barbet et al., 1996). Budding yeast cells treated with rapamycin arrest in G1 phase and enter quiescence (Barbet et al., 1996; Loewith et al., 2002). TOR function in growth regulation is conserved from yeast to humans (De Virgilio and Loewith, 2006; Loewith et al., 2002; Wullschleger et al., 2006). Growth modulation by TOR is important during development. *C. elegans* (ceTOR) and *Drosophila* (dTOR) mutants exhibit arrested development or severe developmental retardation, respectively (Long et al., 2002; Oldham et al., 2000). Embryos of mTOR-null mice die at an early stage of development due to severe cell growth defects (Gangloff et al., 2004). These findings support the important role of TOR in coordinating growth required for organism development (Gangloff et al., 2004; Long et al., 2002; Oldham et al., 2000).

Mammals possess a single TOR gene (mTOR) with a conserved sensitivity to rapamycin inhibition (Jefferies et al., 1997). However, mTOR functions as part of two different complexes, namely the mTOR complex 1 (mTORC1) and the mTOR complex 2 (mTORC2) (Laplante and Sabatini, 2013). mTORC1 is implicated in the control of macromolecular synthesis and is inhibited by rapamycin treatment, whilst mTORC2 functions in actin-dependent growth modulation (Zoncu et al., 2011). mTORC1 regulates several central metabolic processes, including mRNA translation, ribosome biogenesis, lipid synthesis and autophagy (Loewith and Hall, 2011; Sengupta et al., 2010; Wullschleger et al., 2006; Zoncu et al., 2011).

Importantly, mTORC1 functions as the central modulator of growth by sensing nutrients, growth factors, stress, oxygen and energy levels of the cell (Figure 4.4.3) (Loewith and Hall, 2011; Sengupta et al., 2010; Wullschleger et al., 2006; Zoncu et al., 2011). Under favorable growth conditions, mTORC1 promotes protein translation, suppresses autophagy

and activates transcription factors implicated in lipid synthesis and mitochondrial metabolism (Gonzalez and Rallis, 2017). mTORC1 stimulates anabolic processes such as ribosome translation and shuts down anabolic processes, including autophagy, to promote overall cell growth (Gonzalez and Rallis, 2017). Many studies have led to the identification of the molecular constituents associated with mTORC1 that coordinate mammalian cell growth, as described in the next section.

4.4.3 Signaling through mTORC1

The signaling pathways coordinating mammalian cell growth through mTORC1 have been well characterized. At the heart of this regulatory program is the PI3K/Akt signaling pathway. PI3K is activated upon binding of insulin or insulin growth factors to the insulin receptor, as well as upon the stimulation by other growth factor receptors (Figure 4.4.3.) (Leevers et al., 1996). The involvement of PI3K in growth control was shown by work in *Drosophila*. Null mutant flies for the PI3K *Drosophila* ortholog Dp110 and its adaptor protein p60 had smaller cells and showed aberrant cell numbers resulting in imaginal disc compartments of smaller sizes (Weinkove et al., 1999). PI3K promotes the conversion of the signaling lipid phosphatidylinositol (4,5)-bisphosphate (PIP2) to phosphatidylinositol (3,4,5)-trisphosphate (PIP3) (Leevers et al., 1996). The phosphatase PTEN antagonizes this process, thereby acting as a negative regulator of cell growth (Figure 4.4.3) (Backman et al., 2002). This lipid conversion at the plasma membrane stimulates the activation of Akt.

Akt is a key component to this signaling cascade, as it positively regulates cell growth (Figure 4.4.3). A study in *Drosophila* reported increased cell size in the wing imaginal disc upon Akt (Dakt1) overexpression (Verdu et al., 1999). A conserved function for Akt in mammalian cells was revealed by the observation of enlarged cardiac myocytes in transgenic mice harboring a constitutively active form of Akt (Shioi et al., 2002). Akt promotes cell growth by inhibiting the activity of the Tuberous Sclerosis Complex (TSC), a heterodimer of the TSC1 and TSC2 genes (Figure 4.4.3). Two simultaneous studies demonstrated the activity of Akt towards TSC1 and TSC2 genes (Inoki et al., 2002; Potter et al., 2002). Inoki and colleagues showed that Akt directly phosphorylated TSC2 *in vitro*, an event required for mTORC1 stimulation (Inoki et al., 2002). Potter and colleagues also reported TSC2

phosphorylation by Akt *in vitro* and demonstrated the importance of this interaction *in vivo* (Potter et al., 2002). Dakt1 overexpression caused an increase in *Drosophila* eye size; a phenotype partially rescued by the concomitant expression of TSC1 and TSC2 genes (Potter et al., 2002). This result suggested that TSC1 and TSC2 were negative regulators of cell growth.

Another study in *Drosophila* revealed the involvement of the GTPase Rheb in cell size regulation (Saucedo et al., 2003). Rheb overexpression in *Drosophila* wing cells led to an increase in cell size (Saucedo et al., 2003). Epitasis analysis suggested that Rheb acted upstream of mTORC1 but downstream of TSC genes (Saucedo et al., 2003). Indeed, TSC1 and TCS2 *in vitro* expression promoted a decrease in Rheb activity towards mTORC1 (Inoki et al., 2003; Zhang et al., 2003). This result illustrated that TSC1 and TSC2 genes acted as negative regulators of Rheb activity. Therefore, the growth factor sensing branch of mTORC1 signaling requires inhibition of TCS1 and TCS2 genes by AKT that in turn promotes GTP-bound Rheb activity towards mTORC1 (Figure 4.4.3).

mTORC1 is also responsive to the nutritional status of the cell. Amino acids supplied to the cell can promote mTORC1 activity (Hara et al., 1998). Nutrient sensing through mTORC1 involves different molecular constituents than for growth factor-dependent signaling. Key regulators of the amino acid sensing branch of mTORC1 are Rag GTPases. Mammals possess four Rag genes, namely RagA through -D (Sancak et al., 2008). Rag proteins form heterodimers composed of one RagA or RagB and one RagC or RagD molecule (Sancak et al., 2008). Immunostaining experiments revealed that Rag heterodimers localized at lysosomal membranes independently of amino acid levels (Sancak et al., 2010; Sancak et al., 2008). In their active state (GTP-bound), Rag GTPases promoted the recruitment of mTORC1 at the lysosome (Sancak et al., 2010; Sancak et al., 2008). mTORC1 recruitment at the lysosomal membrane is required for growth stimulation by the presence of growth factors.

Several complexes act upstream of mTORC1 as part of the amino acids sensing signaling branch. Co-immunoprecipitation of Rag proteins followed by mass spectrometry analysis revealed the identity of the Ragulator complex (Figure 4.4.3) (Bar-Peled et al., 2012; Sancak et al., 2010). This complex includes five members (LAMTOR1-5 genes) that are responsible for recruiting Rag proteins at the lysosome (Bar-Peled et al., 2012; Sancak et al., 2010). The Ragulator complex acts as a GEF for RagA and RagB promoting their activity

towards mTORC1 (Bar-Peled et al., 2012). Depletion of Ragulator components by RNAi reduced the diameter of mammalian cells compared to controls (Bar-Peled et al., 2012; Sancak et al., 2010). These studies demonstrated that the Ragulator complex was a positive regulator of growth through mTORC1.

Mass spectrometry analysis of proteins associated with RagB revealed the presence of the GATOR complex upstream of mTORC1. Epistasis and cell size analysis suggested the presence of two distinct GATOR complexes (Bar-Peled et al., 2013). Members of the GATOR2 complex were identified in co-immunoprecipitation experiments and include MIOS, WDR24, WDR59, Seh1L and Sec13 (Bar-Peled et al., 2013). Members of the GATOR1 complex include DEPDC5, NPRL2 and NPRL3 genes (Bar-Peled et al., 2013). Mammalian cultured cells depleted of GATOR1 complex components individually showed increased cell diameters (Bar-Peled et al., 2013). Conversely, reduced activity of members of the GATOR2 complex, such as MIOS, caused a decrease in cell size, illustrating the antagonistic function of these two complexes. Therefore, the GATOR2 complex acts as an activator of mTORC1 by inhibiting the GATOR1 complex to stimulate growth upon amino acids availability (Figure 4.2).

In sum, the amino acid-sensing branch upstream of mTORC1 involves the activation of Rag proteins by the Ragulator and GATOR complexes (Figure 4.4.3). The Ragulator complex both recruits and participates in the activation of Rag proteins at the lysosomal surface (Figure 4.4.3). Amino acid sensing by the GATOR2 complex triggers the inhibition of the GATOR1 complex to keep Rag proteins in their GTP-bound state (Figure 4.4.3). The presence of growth factors activates mTORC1 at the lysosome to promote anabolic processes, including protein synthesis to stimulate growth (Figure 4.4.3). This recapitulates the events upstream of mTORC1.

Two key components relay information downstream of mTORC1. These conserved downstream targets of mTORC1 are the S6 kinase 1 (S6K1) and the eukaryotic translation initiation factor 4E (eIF4E)-binding protein 1 (4E-BP1) (Figure 4.4.3). mTORC1 phosphorylation of S6K1 and 4E-BP1 promotes their activation (Laplante and Sabatini, 2013; Ma and Blenis, 2009). Activated 4E-BP1 associates with the eIF4F complex to promote cap-dependent mRNA translation (Hara et al., 1998; Jefferies et al., 1997; Pende et al., 2004).

S6K1 activity also stimulates cap-dependent translation initiation by activating eIF4B and targets other effectors to promote protein synthesis (Hara et al., 1998; Jefferies et al., 1997; Pende et al., 2004).

The important role of S6K1 in growth control was supported by the observation of severe cell size defects caused by its loss-of-function. The few surviving S6K-null flies were tiny, reflected by an approximate 30% decrease in cell size (Montagne et al., 1999). Mammals possess two S6K genes (S6K1 and S6K2). Mice with homozygous deletions of both genes are inviable (Pende et al., 2004). However, S6K1-null mice are viable but are 15 to 20% smaller in size compared to wild type littermates (Shima et al., 1998). Thus, S6K1 is a key downstream regulator of mTORC1 signaling required for proper cell growth.

Altogether, these results define the known molecular regulators of cell growth through mTORC1 signaling. These signaling events are crucial for proper cell growth coordination and when de-regulated can lead to disease states. For example, several mTORC1 network constituents are frequently involved in oncogenic transformation. PI3K and Akt act as oncogenes and are often found to be constitutively active in human cancers (Laplante and Sabatini, 2013). In addition, TSC1/2 and PTEN, amongst others, can act as tumor suppressors (Backman et al., 2002; Bar-Peled et al., 2013). As previously mentioned (Chapter 1), mutations in TSC1/2 genes cause tuberous sclerosis where patients often present brain tumors (Goto et al., 2011). PTEN was originally discovered as a tumor suppressor frequently mutated in several types of cancer, including breast, kidney and glioblastomas (Backman et al., 2002). As a final example, cancer patients with loss of p53 function often present elevated mTORC1 levels (Laplante and Sabatini, 2013). These examples illustrate the importance of proper growth control through the mTORC1 network.

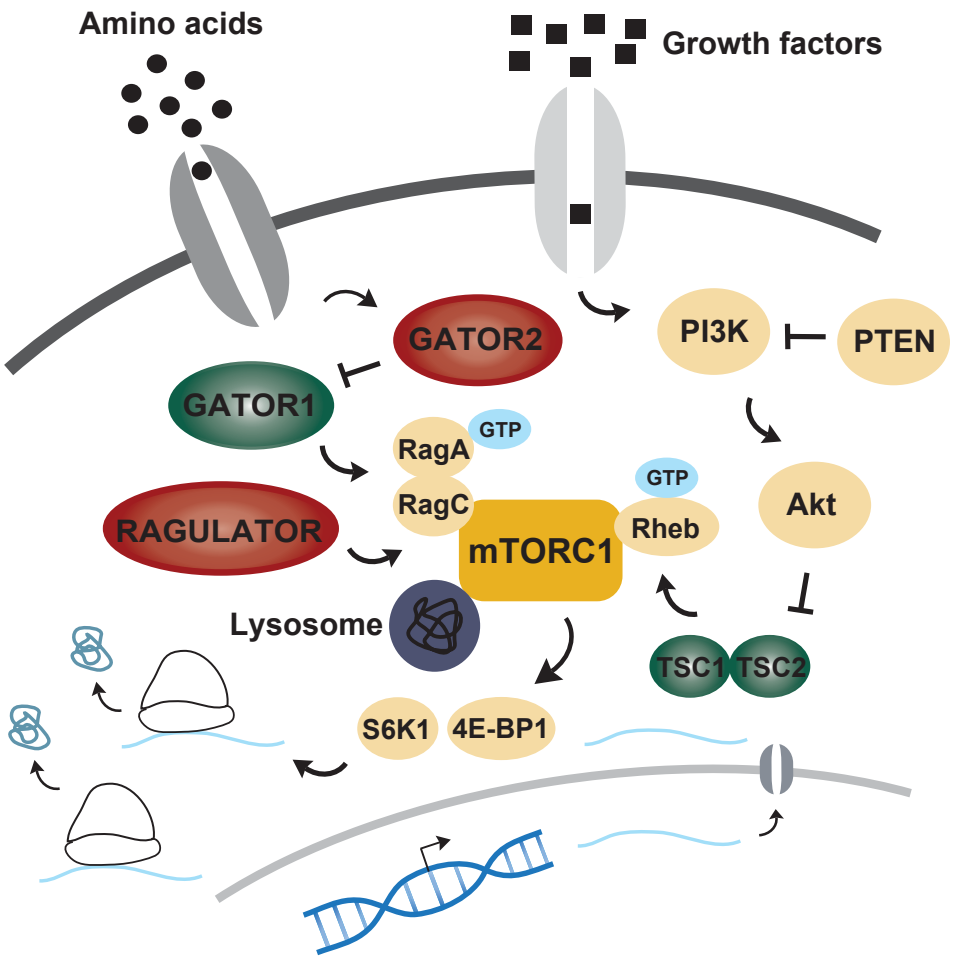

Figure 4.4.3 The molecular regulators of cell growth through mTORC1 signaling

Growth factors sensing via the PI3K/Akt signaling branch of mTORC1. Akt mediates the inhibition of TSC1/2 genes required for Rheb activation. The amino acid sensing branch depends on the GATOR complexes and the Ragulator complex for the activation of Rag GTPases and subsequent recruitment of mTORC1 at the lysosomal surface. The downstream mTORC1 targets S6K1 and 4E-BP1 to promote protein synthesis under favorable growth conditions. Adapted from (Guertin and Sabatini, 2006).

4.4.4 MYC participates in cell growth regulation

The MYC transcription factor also participates in metazoan cell growth regulation. The *Drosophila* ortholog of the mammalian MYC gene (dmyc) contributes to cell growth regulation during development (Johnston et al., 1999). Johnston and colleagues showed that *dmyc* mutant flies were smaller and had smaller wing cells (Johnston et al., 1999). Conversely, *dmyc* overexpression increased cell size without altering cell proliferation (Johnston et al.,

1999). Therefore, a role for *dmyc* in promoting cell growth was suggested (Johnston et al., 1999). Further investigation revealed that dmyc overexpression stimulated translation to increase ribosomal content (Grewal et al., 2005). These studies provided evidences of *dmyc* function as a regulator of cell growth.

Around the same time, work with B-lymphocytes supported a role for C-MYC in cell growth control. Iritani and Eisenman found that C-MYC overexpression increased B-lymphocyte size at all stages of differentiation and in all phases of the cell cycle (Iritani and Eisenman, 1999). Kim and colleagues also reported mice hepatocyte enlargement following exogenous C-MYC expression and observed an increase in ribosomal protein content following C-MYC overexpression (Kim et al., 2000). MYC associates with a variety of other effectors, including its obligate co-activator MAX, to induce transcription of a host of that gene that promotes cell proliferation (Adhikary and Eilers, 2005). At an overall functional level, MYC is the equivalent of the Sfp1 transcription factor in yeast (Jorgensen et al., 2004). The conserved transcriptional regulation of ribosome biogenesis underscores the central role of this process in cell growth regulation.

4.4.5 Metazoan cell cycle control

Cyclin-dependent kinases (CDKs) are conserved master regulators of the eukaryotic cell division cycle (Malumbres, 2014). Humans possess twenty distinct CDK enzymes whereas budding yeast only have six CDK family members (Malumbres, 2014). CDK activation requires association with the cyclins, which are obligate activators of the kinase catabolic domain. For instance, cyclin D associates with CDK4 and CDK6 to promote phosphorylation and subsequent inhibition of the retinoblastoma (Rb) gene required for entry into S-phase (Malumbres, 2014). CDK enzymes are subject to additional layers of regulation including suppression by inhibitory subunits and positive and negative phosphorylation events (Heim et al., 2017). In mammals, genetic loss of CDK1 inhibits cell proliferation (Santamaria et al., 2007). Organ hyperplasia and gigantism in mice was observed following p27 (CDK inhibitor 1B) deletion (Fero et al., 1996). p27 loss-of-function accelerated entry into S phase resulting in an increase in cell number rather than cell size (Fero et al., 1996).

The primary functions of the CDK enzymes are to activate G1/S transcription, to initiate DNA replication and to trigger various events associated with mitosis (Malumbres, 2014). With respect to G1/S regulation, once activated at the end of G1 phase, the CDK4/6 complexes phosphorylate the Rb tumor suppressor to alleviate repression of the E2F transcription factors that drive G1/S gene expression (Heim et al., 2017). This regulatory architecture is functionally analogous to the Cln2-Whi5-SBF pathway in yeast (Costanzo et al., 2004; de Bruin et al., 2004). The function of these conserved regulators of the cell cycle, including CDK1, the E2F transcription factors and Rb have been extensively studied in humans and metazoan systems. For example in flies, cells mutated for the transcription factor E2F (dE2F in *Drosophila*) underwent reduced proliferation over time (Weigmann et al., 1997). However, in the fly wing and imaginal disc, these cells continued to grow in size leading to an increase in cell volume to sustain organ size (Neufeld et al., 1998; Weigmann et al., 1997). Conversely, mutants for the *Drosophila* ortholog of the Rb gene (dRb) exhibited increased proliferation (Neufeld and Edgar, 1998). These functions are highly conserved in mammals, where Rb acts as a negative regulator of cell cycle progression that is inactivated at the G1-S phase transition upon CDK-mediated phosphorylation to promote E2F transcription (Lloyd, 2013).

4.5 Reconciling the coordination of growth with division

Most studies have addressed the molecular circuitry that regulates cell growth and cell proliferation separately. The achievement of cell size homeostasis depends on the tight coordination between cell growth and cell division. In the last ten years, several groups have developed improved experimental methods to precisely measure cell volume or mass to assess the kinetics of growth in individual mammalian cells. These studies will be described below. Higher temporal resolution of cell growth throughout the different phases of the cell cycle has provided valuable insights into the mechanisms that couple cell growth to cell division in higher eukaryotes.

4.5.1 Measuring growth rates

Improved techniques have been developed to measure the growth of individual mammalian cells over time, i.e. growth rate. Experimental approaches and mathematical calculations were combined to obtain quantitative measurements of mammalian cell volume as a function of either cell size or cell cycle position (Tzur et al., 2009). This analysis indicated that mouse and human lymphoblastic cells exhibited increased growth rates in G1 (Tzur et al., 2009). This is consistent with the notion that cells need to achieve sufficient growth before they can trigger cell division (Jorgensen and Tyers, 2004). However, despite considerable evidence, the concept of a size threshold per se has remained somewhat controversial (Lloyd, 2013)

In another approach, a microchannel mass-sensing device was developed to measure growth rates in different organisms (Godin et al., 2010). The buoyant mass of individual cells was measured over time by assessing resonance frequencies of cells trapped in the microchannel. Using this system, an increase in mass over time was reported in *E. coli*, *S. cerevisiae* and mouse lymphoblastic cells. In a later study, fine-tuning of the system led to improved mass measurements and over the entire cell cycle (Son et al., 2012). Supporting previous findings by Kafri and colleagues, these authors reported an increase in growth rate early in G1 (Son et al., 2012). As lymphoblastic cells approached S phase growth was slowed (Son et al, 2012). The authors observed a negative correlation between the growth rate in early G1 and the time at the G1-S phase transition (Son et al., 2012). Altogether, these studies provided insights onto the kinetics of growth of individual mammalian cells (Godin et al., 2010; Son et al., 2012).

In a different study, Park and colleagues acquired cell mass data over time for adherent cells grown on resonant sensors (Park et al., 2010). Measuring resonant frequencies over time revealed that individually growing colon cancer cells increased their mass over time (Park et al., 2010). Furthermore, cells that were heavier at birth presented increased growth rates compared to their smaller equivalents (Park et al., 2010). This result suggested that growth was proportional to initial cell size.

In a more recent study, growth rates at high temporal resolution were investigated (Kafri et al., 2013). Images of DNA content (DAPI), total protein content (succinimidyl ester) and cell cycle progression (mAG-hGEM) were acquired for a large set of individual HeLa and retinal pigment epithelial cells. A mathematical method called ergodic rate analysis (ERA) was applied to the data to confirm previous observations that the mass increased as cells progressed into the cell cycle (Kafri et al., 2013). This mathematical analysis also led to the proposition that the growth rate regressed at the G1-S phase transition (Kafri et al., 2013). This counter-intuitive observation suggests that cells possess a negative feedback mechanism to coordinate growth and closely modulate it (Kafri et al., 2013). Altogether, these studies suggest complex feedback mechanisms have evolved to allow the cell to coordinate cell growth with entry into the cell division cycle.

4.6 Knowledge gaps in mammalian cell size regulation

Large-scale analysis with the budding yeast deletion collection revealed the identity of numerous genes that affect yeast cell size (Dungrawala et al., 2012; Jorgensen et al., 2002; Zhang et al., 2002). Several findings illustrated the conserved nature of many of these genes, including TOR and its downstream targets, and propelled cell size studies in higher eukaryotes (De Virgilio and Loewith, 2006; Jorgensen et al., 2004). However, this list of conserved genes that participate in mammalian cell growth and cell division control has remained highly incomplete, due in part to the absence of robust genetic approaches in mammalian cells. An unexplored area of the mammalian cell size field is thus to interrogate the identity of additional genetics regulators of cell size at the genome scale. Large-scale screens that systematically address genes deletions that affect cell size, conceptually similar to those performed in budding yeast have yet to be undertaken in mammalian cells.

A global analysis of cell size regulators was reported in *Drosophila* S2 cultured cells using RNAi-based methods (Bjorklund et al., 2006). This study identified known regulators of cell cycle progression, including several CDKs, E2F transcription factors, Rb and MYC, as well as new functions (Bjorklund et al., 2006). The absence of large-scale studies on genes that affect cell size in mammalian cells can be attributed to the lack of tools to accurately assess gene function at a genomic scale. Genome-wide screens using small interfering RNA

(siRNA) or short hairpin RNA (shRNA) to silence gene often exhibit high rates of off-targets and variable degrees of gene depletion (Echeverri et al., 2006). From experience in the Tyers laboratory, large-scale analysis of cell size regulators in mammalian cells using shRNA methods resulted in largely non-reproducible hits that proved difficult or impossible to deconvolve (T. Bertomeu, unpublished).

CRISPR/Cas9 gene editing technology has allowed robustly reproducible genome-wide interrogation of gene function in human cells (Shalem et al., 2014; Wang et al., 2014; Zhou et al., 2014). This technology has permitted our group to perform a genome-wide screen to identify regulators of human cell size, which will be the topic of Chapter 6. First, I describe the CRISPR/Cas9 system, the many advantages it provides and the multitude of applications it has enabled.

5 The CRISPR/Cas9 technology

The discovery of the clustered regularly interspaced short palindromic repeats (CRISPR) system in bacteria has been exploited to allow sequence-specific genome editing in virtually all species, including humans. This technique holds incredible promise for applications in personalized medicine and targeted therapies, as well as in fundamental research. In the following sections, the CRISPR/Cas9 technology will be described, with emphasis on genome-scale interrogation of gene function in higher eukaryotes.

5.1 CRISPR/Cas9 for precise gene editing

The CRISPR/Cas system is derived from the bacterial adaptive immune system (Brouns et al., 2008). Over the course of evolution, bacteria and archaea developed CRISPR for protection against foreign invaders (Brouns et al., 2008). Amongst the three types (I-III) of CRISPR systems, the type II derived from *Streptococcus pyogenes* is the best characterized (Cong et al., 2013; Jinek et al., 2012; Mali et al., 2013). The CRISPR/Cas system functions as an RNA-guided double-stranded DNA nuclease (Garneau et al., 2010), hence, it's reference as a molecular scissor (Jiang and Doudna, 2017). The Cas enzyme (Cas9 in *S. pyogenes*) is the nuclease that cuts both DNA strands via two distinct domains, the RuvC and HNH domains (Figure 5.1) (Cong et al., 2013; Jinek et al., 2012; Mali et al., 2013).

Cas9 cuts DNA at a specific location guided by a short stretch of 20 nucleotides that associates with a guide RNA (Figure 5.1) (Jiang and Doudna, 2017). The single guide or synthetic guide RNA (sgRNA) includes the CRISPR RNA (crRNA) and the trans-activating CRISPR RNA (tracrRNA) (Cong et al., 2013; Jinek et al., 2012; Mali et al., 2013). The crRNA contains the 20-nucleotide sequence complementary to the target DNA and requires association with the scaffold tracrRNA for Cas9 activity (Cong et al., 2013; Jinek et al., 2012; Mali et al., 2013). Early improvements were made on the system by fusing of the two RNA components resulting in a single chimeric RNA known as the single guide or sgRNA (Cong et al., 2013; Jinek et al., 2012; Mali et al., 2013). An additional requirement of the system is that the target DNA sequence be flanked at the 3' end by the Protospacer Adjacent Motif (PAM) sequence NGG specific to the type II system (Figure 5.1) (Cong et al., 2013; Jinek et al., 2012; Mali et al., 2013). Cas9 scans the DNA and the sgRNA pairs with the complementary DNA sequence for Cas9 to cut 3 to 4 nucleotides upstream of the PAM (Figure 5.1) (Jiang and Doudna, 2017).

DNA double-strand breaks created by Cas9 leads to activation of DNA repair mechanisms. Homology-directed repair (HDR) is a major repair pathway based on templated homologous recombination (HR) (Liang et al., 1998). In mammalian cells, HR occurs at low and somewhat variable rates and is mostly active in dividing cells (Saleh-Gohari and Helleday, 2004). In mammalian systems, HR is preferentially selected to repair DNA double-strand breaks when a donor template is provided (Ran et al., 2013). Otherwise, the cell utilizes non-homologous end joining (NHEJ) to repair DNA breaks caused by Cas9 (Ran et al., 2013). NHEJ is error-prone and consequently insertions or deletions (indels) accumulate at the break site (Cong et al., 2013; Mali et al., 2013). This often results in frameshift mutations that can cause insertion of a premature strop codon and non-sense mediated decay with the end result of near complete inactivation of a specified target gene function (Cong et al., 2013; Mali et al., 2013).

The advantages of CRISPR/Cas9 were rapidly exploited for genome editing in higher eukaryotes. Only a year after the first demonstration of CRISPR/Cas9 precise editing (Jinek et al., 2012) two groups concomitantly engineered the system for function in mammalian cells (Cong et al., 2013; Mali et al., 2013). These groups created a codon-optimized version of the

Cas9 nuclease and sgRNA for expression in mammalian systems. Both groups successfully used CRISPR/Cas9 to generate DNA double-strand breaks at desired loci. They observed the presence of indels at the target site with higher frequencies than previous gene editing technologies, such as zinc fingers nucleases (ZFNs) and transcription activator-like effector nucleases (TALENs) (Cong et al., 2013; Mali et al., 2013).

These groups provided compelling evidences for the greater versatility and flexibility of the CRISPR/Cas9 system (Cong et al., 2013; Mali et al., 2013)). Not only was it possible to generate loss-of-function mutations, it was also feasible to introduce specific DNA fragments, including GFP or other protein fusions, into a desired locus (Cong et al., 2013; Mali et al., 2013). Indels could be efficiently generated in a diverse set of genes in several different cell lines (Cong et al., 2013; Mali et al., 2013). In sum, this seminal work established CRISPR/Cas9 as a novel tool that can be used to precisely and effectively modify any genome, including in humans (Cong et al., 2013; Garneau et al., 2010; Jinek et al., 2012; Mali et al., 2013). The CRISPR/Cas9 system confers many advantages, including simplicity of use, low cost, ease of design, versatility and precise gene editing.

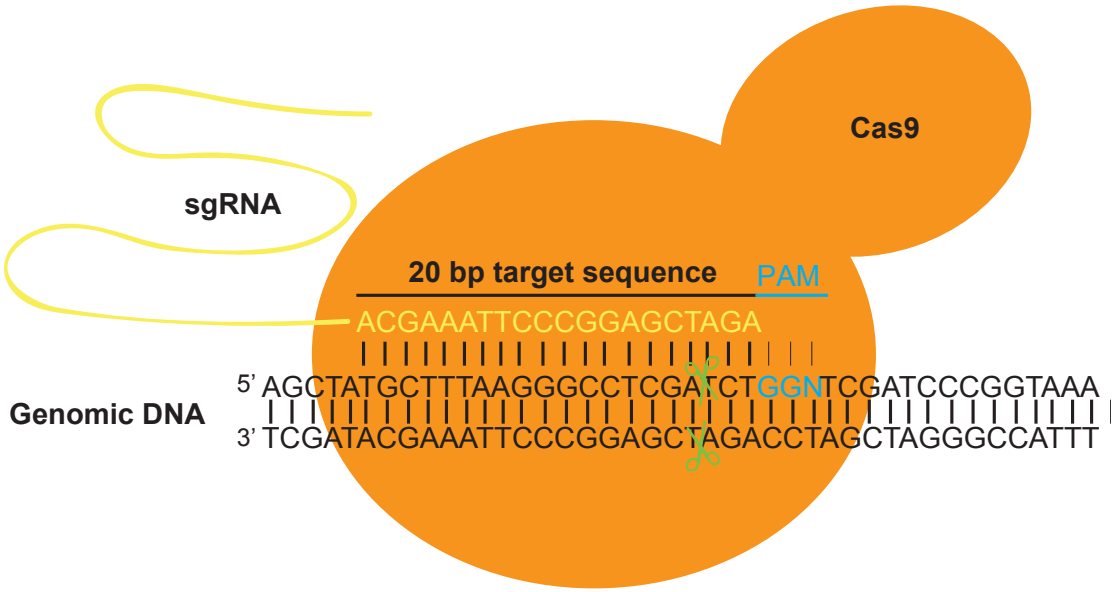

Figure 5.1 The CRISPR/Cas9 system

The Cas9 enzyme (orange) is brought to a specific site on the DNA by the sgRNA (yellow). The small 20 bp sgRNA (yellow) sequence binds to the complementary DNA sequence and the Cas9 enzyme generates a double-strand break 3 to 4 nucleotides upstream of the PAM sequence (blue). As the cell tries to repair the DNA double-strand break at this location, indels are introduced that can lead to frame-shift mutations or the introduction of a stop codon resulting in complete loss of gene function. Adapted from (Ran et al., 2013).

5.2 Genome-wide CRISPR/Cas9 pooled screens

The CRISPR/Cas9 technology immediately generated great interest in the functional genomics field because of the potential to rapidly interrogate gene function at a large-scale. Two groups were successful in performing large-scale loss-of-function screens in mammalian cells (Shalem et al., 2014; Wang et al., 2014). Shalem and colleagues created the GeCKO (Genome-scale CRISPR/Cas9 KO) library of sgRNAs targeting approximately 18,000 RefSeq genes with a coverage of 3 sgRNAs per gene (Shalem et al., 2014). Wang et al. targeted a smaller number of genes (approximately 7000) but with a higher coverage of 10 sgRNAs per genes and including 100 non-targeting sgRNAs as controls (Wang et al., 2014). Both sgRNA libraries were used in pools for global analysis of genetic functions. These groups observed high drop-out scores for classes of genes essential for cell proliferation and survival, including several RNA processing and ribosomal protein genes (Shalem et al., 2014; Wang et al., 2014). In another concomitant study, Zhou and colleagues performed a CRISPR/Cas9 pooled screen

using a subset of sgRNAs targeting 291 human genes of interest for resistance to specific toxins (Zhou et al., 2014). Altogether, these three studies laid the foundation for large-scale genomics studies in higher eukaryotes using the CRISPR/Cas9 technology.

Gene deletion collections available in microorganisms allowed the establishment of a benchmark map of genes essential for cell fitness (Baryshnikova et al., 2010; Giaever et al., 2002). However, the greater complexity of mammalian systems has made it difficult for researchers to define gene essentiality. Several research groups thus performed genome-wide loss-of-function CRISPR/Cas9 screens to identify genes conferring fitness defects in higher eukaryotes. Pooled libraries of sgRNAs with similar design but variable coverage, were utilized to screen several cell lines derived from different disease backgrounds. Wang and colleagues generated an improved version of their GeCKO library to target 18,000 genes for knockout in two chronic myeloid leukemia (KBM7 and K562) and two B lymphocyte-derived cell lines (Raji and Jiyoye) (Wang et al., 2015). In a similar study, Blomen and colleagues used a gene-trap system for large-scale gene inactivation in a haploid chronic myeloid leukemia-derived cell line (KBM7) and its non-hematopoietic derivative (HAP1) (Blomen et al., 2015). Hart and colleagues generated an sgRNA library targeting 17,661 human genes called the Totonto knockout (TKO) collection (Hart et al., 2015). This group screened for gene knockouts resulting in cell proliferation and growth defects in HeLa cells, two colon carcinoma cell lines HCT116 and DLD1, one retinal epithelial cell line RPE1, a melanoma cell line A375 and a glioblastoma-derived cell line GBM (Hart et al., 2015).

Two groups performed further large-scale CRISPR/Cas9 pooled screens to identify genes required for cell viability. The first group screened 33 cancer cell lines with a library of sgRNAs targeting 19,050 genes (Aguirre et al., 2016). This work revealed an important factor to consider when performing deletion screens, namely that cells with too many un-repaired DNA double strand breaks caused by Cas9 cutting in genes with high copy number drop out of the pool irrespective of a function in cell viability (Aguirre et al., 2016). Munoz and colleagues confirmed this observation while performing loss-of-function screens in five different cell lines (Munoz et al., 2016). These screens helped better define the network of genes essential for optimal mammalian cell fitness and revealed a potential pitfall of

CRISPR/Cas9 screens that must be accounted for in all screens (Aguirre et al., 2016; Munoz et al., 2016).

The Tyers groups developed an independent in-house extended knockout (EKO) library of 278,754 sgRNAs that targets 19,084 RefSeq annotated genes (Bertomeu et al., 2017). The extended part of this sgRNA library includes 20,852 sgRNAs targeting alternative exons and 3,872 hypothetical genes (Bertomeu et al., 2017). This work contributed to a greater characterization of human genes essential for viability and cell fitness in a pre-B ALL-derived cell line called NALM-6 (Bertomeu et al., 2017). The extensive coverage of this library provided additional information on the potential functions of alternative exons and hypothetical genes (Bertomeu et al., 2017).

All these libraries of sgRNAs were used in pooled CRISPR/Cas9 deletion screens to identify genes essential for optimal cell fitness (Aguirre et al., 2016; Bertomeu et al., 2017; Blomen et al., 2015; Hart et al., 2015; Munoz et al., 2016; Wang et al., 2015). These studies provided a comprehensive list of approximately 2,000 genes required for mammalian cell viability or optimal cell fitness in different cell line contexts. Important correlates of essential genes were revealed by these screens, including a high degree of gene conservation and a strong propensity for protein-protein interactions (Aguirre et al., 2016; Bertomeu et al., 2017; Blomen et al., 2015; Hart et al., 2015; Munoz et al., 2016; Wang et al., 2015).

5.3 Applications of CRISPR/Cas9

The immense potential of the CRISPR/Cas9 system can be exploited for studies in virtually any organism. Amongst model organisms commonly used in research, the application of the technology began in yeasts (DiCarlo et al., 2013), followed by *Drosophila* (Gratz et al., 2013) and *C. elegans* (Friedland et al., 2013). CRISPR/Cas9 has also been implemented in *zebrafish* and mice, illustrating its potential for *in vivo* studies (Hwang et al., 2013a; Hwang et al., 2013b; Wang et al., 2013). Altogether, these many applications in different species illustrate the versatility of the CRISPR/Cas9 technology.

The flexibility and versatility of the CRISPR/Cas9 system have been exploited in diverse context. For instance, CRISPR/Cas9 has been engineered to tag genes with fluorescent

proteins. Using the CRISPRainbow technology, inactive Cas9 can tag specific loci with fluorescent proteins coupled to sgRNAs (Ma et al., 2016). A group performed live imaging of up to six chromosomal loci simultaneously and in a single cell (Ma et al., 2016). In another application, CRISPR/Cas9 has been used to modulate transcription levels. Konermann and colleagues adapted the CRISPR/Cas9 system to boost transcription of target genes (Konermann et al., 2015). In another study, the technology was modified to efficiently repress transcription (CRISPRi) (Larson et al., 2013). Both technologies were used in pooled screens to better define gene functions associated with variations in expression levels, complementing pooled loss-of-functions screens (Gilbert et al., 2014).

A main application of the CRISPR/Cas9 technology is for the identification of cancer-specific vulnerabilities. A CRISPR/Cas9 pooled knockout screen in mice revealed the identity of several gene deletions that promote cancer cell proliferation and metastasis (Chen et al., 2015). A pool of lung cancer cells with CRISPR/Cas9 gene knockouts was injected into immunocompromised mice that developed tumors that further metastasized (Chen et al., 2015). Analysis of lung metastasis in these mice revealed enriched sgRNAs, including those targeting *Nf2*, *Pten* and *Cdkn2a*, all of which are known tumor suppressors (Chen et al., 2015). This *in vivo* screen identified loss of gene function associated with an acceleration of lung metastasis (Chen et al., 2015). Another genome-wide CRISPR/Cas9 pooled loss-of-function screen revealed the identity of genes essential for viability of glioblastoma stem-like cells (GSCs) and neuronal stem cells (NSCs) derived from patients (Toledo et al., 2015). PKMYT1 and WEE1 regulators of the cell cycle were observed to be important factors promoting GSCs and NSCs survival (Toledo et al., 2015). These candidate target genes offer potential therapeutic targets for this aggressive form of brain cancer (Toledo et al., 2015).

Recent elegant CRISPR/Cas9 loss-of-function screens demonstrated the potential of this system in the context of immunotherapy. These screens led to the identification of genes conferring either resistance or sensitivity to PD-1 immune checkpoint blockade, an immunotherapy treatment currently used in the clinic to treat melanoma, non-small-cell-lung carcinoma and renal cell carcinoma (Manguso et al., 2017; Patel et al., 2017). In the first study, a pooled knockout screen in melanoma cells that were injected into mice treated with PD-1 blockade (Manguso et al., 2017). sgRNAs targeting genes that were depleted in these

mice compared to control mice were suggested to confer sensitivity to immunotherapy treatment (Manguso et al., 2017). Amongst these genes, PTPN2 caused an increase in sensitivity to immunotherapy by promoting interferon gamma signaling for antigen presentation to T cells (Manguso et al., 2017). In the second study, T cells were first engineered to recognize a specific antigen and then co-cultured with melanoma cancer cells undergoing genome-wide CRISPR/Cas9 pooled gene knockouts (Patel et al., 2017). This new system, called 2CT-CRISPR, allowed screening for gene knockouts that conferred resistance to T cell activity (Patel et al., 2017). The authors recovered a subset of genes, including APLNR a gene of the G-protein coupled receptor family, whose loss-of-function promoted cell survival indicative of resistance to T cell function (Patel et al., 2017). This study provided important insights into the genetic circuitry associated with immunotherapy treatment resistance (Patel et al., 2017). Taken together, these studies illustrated the potential of the CRISPR/Cas9 technology to better define the genomic landscape associated with the response to immunotherapy.

The CRISPR/Cas9 technology holds great promises for personalized medicine and in the fast-moving field of immunotherapy. The above examples showed that CRISPR/Cas9 pooled loss-of-function screens can be applied in different contexts to address specific biological questions. In the following chapter, I describe the use of the CRISPR/Cas9 system to interrogate the identity of the genes associated with human cell size regulation.

6 Results Part 2 - Article 2

A genome-wide CRISPR/Cas9 knockout screen reveals that TLE4 participates in the maintenance of pre-B cell size homeostasis

Karine G. Bourdages[1*], Thierry Bertomeu[1*], Jasmin Coulombe-Huntington[1] and Mike Tyers[1]

* K.G.B. and T.B. contributed equally to this work

[1]Institute for Research in Immunology and Cancer, Department of Medicine, Université de Montréal, Montréal, Québec H3C 3J7, Canada

Keywords: CRISPR/Cas9, pooled screens, cell size, TLE4, pre-B lymphocytes, BCR signaling and B cell differentiation

Author contributions

T.B. generated the EKO library, performed the cell culture work for CRISPR/Cas9 pooled screens (Figure 6.5.1A) and counterflow centrifugal elutriation experiments (Figure 6.5.1B-C). T.B. extracted DNA from cell size fractions for the first screen replicate and prepared samples for Illumina sequencing, while I performed those steps for the second screen (Figure 6.5.1D). J.C-H. developed the RANKS algorithm and performed screen analyses to establish gene rankings based on the ability of each individual gene to affect cell size (Figure 6.5.2A). T.B. selected the list of candidate genes to validate and designed the cell size assays. T.B. cloned single sgRNAs into lentiviral vectors, performed lentiviral infections and selection. T.B. and I performed cell volume measurements for each round of cell size gene validations for all selected candidates (Figure 6.5.3). I designed and performed all the experiments for the characterization of TLE4 in NALM-6 cells (Figures 6.5.4-6). J.C-H. generated gene rankings for RNA-Seq results and performed the GO term analysis (Figure 6.5.5). I prepared samples for the flow cytometry experiment and analyzed the results with the help of T.B. (Figure 6.5.6).

6.1 Abstract

How mammalian cells achieve cell size homeostasis remains enigmatic due to a lack of large-scale genomics studies on cell size regulation in mammalian cells. However, recently developed CRISPR/Cas9 technology now allows for global analysis of cell size regulators in higher eukaryotes. In the current study, I characterized a candidate gene identified in the first genome-wide CRISPR/Cas9 pooled knockout screens that interrogated cell size regulation in mammalian cells. I confirmed the transcriptional repressor TLE4 as a potent developmental regulator of cell size. Genes characteristic of B cell hematopoietic lineages were up regulated in NALM-6 TLE4 knockout cells, including genes associated with functions in B cell differentiation. I propose that TLE4 contributes to the maintenance of pre-B cell size homeostasis by participating in the B cell activation program. The genome-wide CRISPR/Cas9 screen provides one of the first examples of a size regulator that is linked to a developmental lineage.

6.2 Introduction

Cell size is intricately modulated since proliferating cells must acquire sufficient mass or volume to trigger cell division and increase the number of cells within a population over time. Thus, cell size homeostasis is achieved by balancing cell growth and cell division. In recent years, improvements in genome-wide technologies have permitted important discoveries on the identity of the genes that regulate cell growth and cell division. *S. cerevisiae* gene deletion collections allowed large-scale interrogations of genes implicated in cell size regulation, revealing that approximately ten percent of genes in budding yeast are associated with a cell size phenotype (Dungrawala et al., 2012; Giaever et al., 2002; Jorgensen et al., 2002; Zhang et al., 2002). Genes associated with the target of rapamycin (TOR) kinase such as its downstream targets Sfp1 and Sch9, were identified as central players in yeast cell size control (Jorgensen et al., 2002). Sfp1 and Sch9 sense nutritional status signals of the cell and modulate the translational output and participate in ribosomal production (Jorgensen et al., 2002; Lempiainen et al., 2009; Urban et al., 2007).

TOR is conserved from yeast to mammals and is a key regulator of cell growth (De Virgilio and Loewith, 2006; Gonzalez and Rallis, 2017; Loewith and Hall, 2011; Zoncu et al., 2011). In mammals, the mechanistic target of rapamycin complex 1 (mTORC1) functions as the central regulator of cell growth and is sensitive to rapamycin treatment (Bar-Peled and Sabatini, 2014; Loewith et al., 2002; Zoncu et al., 2011). mTORC1 integrates external signals, including growth factors, hormones, amino acids, energy status of the cell, oxygen and stress levels (Gonzalez and Rallis, 2017). At the lysosome, mTORC1 activates downstream S6K1 and 4E-BP1 genes that in turn stimulate the activity of translation initiation factors at the 5' end of mRNAs, including eIF4B and the eIF4F complex, to promote cap-dependent translation initiation (Ma and Blenis, 2009). This causes a global increase in protein production under favorable conditions resulting in cell growth.

Many molecular constituents of the mTORC1 signaling network are well characterized. These include Rheb and Rag GTPases that are key activators of mTORC1 at the lysosome (Inoki et al., 2003; Sancak et al., 2008; Zhang et al., 2003). Upstream events occur through two main signaling pathways. The insulin-sensing branch of mTORC1 begins by activation of PI3K upon intake of insulin growth factors (Leevers et al., 1996). PI3K activates Akt that mainly functions to inhibit the TSC complex, composed of a heterodimer of TSC1 and TSC2 molecules (Inoki et al., 2002; Potter et al., 2002). This inhibitory event is crucial to Rheb activation at the lysosome to promote mTORC1 activity at this location. The nutrients sensing branch of mTORC1 mediates the recruitment of mTORC1 at the lysosome. Amino acids intake stimulates the activation of the Ragulator complex, which is a key activator of Rag proteins (Bar-Peled et al., 2012; Sancak et al., 2008). GTP-bound Rags mediate the recruitment of mTORC1 at the lysosome where it is activated by Rheb upon growth factor stimulation (Bar-Peled et al., 2012). Essential for Rag activity are the GATOR1 and GATOR2 complexes. GATOR1 functions as an inhibitor of Rag proteins, whereas GATOR2 antagonizes this function by directly inhibiting GATOR1 under conditions of high amino acid levels (Bar-Peled et al., 2013). Therefore, the mTORC1 network plays a major role in cell growth control.

Nonetheless, this is far from the complete list of genes implicated in mammalian cell size regulation. An approach to better define molecular regulators of size is to perform

genome-wide genetics studies. Large-scale screens to identify cell size regulators in mammalian cells remain inexistent. An RNAi-based screen for cell size regulators in *Drosophila* cultured cells is the only genome-wide study of size in higher eukaryotes (Bjorklund et al., 2006). Use of RNA interference (RNAi) for large-scale studies in mammalian cells is prone to high off-target rates and variable levels of gene knockdown, limiting their effectiveness (Echeverri et al., 2006). Thus, improvements in genome-wide technologies are needed to perform global analysis of mammalian cell size regulators.

The revolutionary clustered regularly interspaced short palindromic repeats (CRISPR) and CRISPR/Cas9-associated technology provides just that. CRISPR/Cas9 derived from the *Streptococcus pyogenes* adaptive immune system was adapted for gene editing in mammalian cells (Cong et al., 2013; Jinek et al., 2012; Mali et al., 2013; Ran et al., 2013). CRISPR/Cas9 allows for complete loss-of-function of target genes with great precision, efficiency and versatility (Cong et al., 2013; Jinek et al., 2012; Mali et al., 2013; Ran et al., 2013). The design of genome-wide pooled libraries of sgRNAs for gene deletion is conceptually similar to gene deletion collections of budding yeast strains, aside from being in a pooled format. CRISPR/Cas9 pooled loss-of-function screens were proven successful in mapping genes essential for cell viability and optimal fitness (Bertomeu et al., 2017; Blomen et al., 2015; Hart et al., 2015; Wang et al., 2015). In a recent publication, we carried out a CRISPR/Cas9 pooled knockout screen that identified genes essentials for optimal NALM-6 cell fitness (Bertomeu et al., 2017). In the current study, we conducted similar CRISPR/Cas9 pooled knockout screens to identify genetics regulators of human cell size.

We present the first genome-wide CRISPR/Cas9 pooled knockout screen that addresses molecular regulators of human cell size. We conducted CRISPR/Cas9 loss-of-function screens in NALM-6 pre-B lymphocytes followed by counterflow centrifugal elutriation for physical separation of cells by size. Our screening method allowed us to identify several known regulators of growth, including those associated with the mTORC1 network. Interestingly, we identified the transcriptional repressor TLE4 as a candidate gene identified in the screen, which had not been previously associated with cell size functions. Further investigations revealed that transcripts associated with B cell activation and differentiation functions were up-regulated upon loss of TLE4 function. The differentiation

program of NALM-6 cells was also modified in TLE4 knockout cells and accompanied by a reduction in cell size. These results suggest that TLE4 participates in the developmental program of NALM-6 cells to maintain size homeostasis.

6.3 Results

6.3.1 Whole-genome CRISPR/Cas9 cell size screens in NALM-6 cells

In order to investigate the molecular regulators of human cell size, genome-wide CRISPR/Cas9 loss-of-function screens were conducted. These screens were initiated and carried-out by Thierry Bertomeu, who recently reported with co-workers, the design of the custom extended knockout (EKO) library of pooled sgRNAs (Bertomeu et al., 2017). The EKO library is composed of a total of 278,754 sgRNAs that target 19,084 RefSeq protein-coding genes, and included 2,043 non-targeting sgRNAs as controls (Bertomeu et al., 2017). For the purpose of this study, we will not be addressing the extended part of the library targeting 20,852 unique alternative exons and 3,872 hypothetical genes. T. Bertomeu. had previously generated a clone of the pre-B lymphocytic NALM-6 cell line expressing Cas9 under a doxycycline-inducible promoter. The NALM-6 cell line was initially chosen for its diploid status and the ability to grow these cells in suspension, allowing for the use of counterflow centrifugal elutriation.

The EKO sgRNA library was introduced into the NALM-6 Cas9 clonal cell line to generate an inducible pooled gene knockout library within a human cell line model. The inducible nature of the system was exploited and allowed screens to be done in multiple contexts without depletion of sgRNAs targeting essential genes. In the current study, the previously generated pool of NALM-6 cells with Cas9 and sgRNA expression was used to perform cell size screens. T. Bertomeu performed two replicates of the CRISPR/Cas9 pooled knockout screens. In the first screen, gene knockouts were induced for 7 days with doxycycline treatment following by 13 days of outgrowth. This timing depletes sgRNAs targeting essential genes from the pool and subsequently favors size scorings of non-essential genes (Bertomeu et al., 2017).

In parallel, the screen was repeated using the same library but inducing Cas9 expression by doxycycline treatment for 8 days and followed by 4 days of recovery and expansion without doxycycline (Figure 6.5.1A). At all times, cells were kept under exponentially growing conditions to maintain an asynchronous population of cells and to avoid cell size bias from cell cycle arrest. Next, T. Bertomeu performed counterflow centrifugal elutriation to physically fractionate the pool of cells, from the smallest cells that exit the elutriation chamber at low flow to the largest cells that escape the chamber at a high flow rate (Figure 6.5.1B). A total of 13 fractions were collected and containing cells of increasing sizes as assessed by Coulter counter volume measurements from readings of a portion of cells from each fraction (Figure 6.5.1C). These measurements represent the pattern of size distribution of each fraction (Figure 6.5.1C). This was followed by large-scale genomic DNA extractions of each separate fractions and PCR amplification of sgRNA sequences (Figure 6.5.1D). sgRNA frequencies from each fraction was assessed by Illumina sequencing, as previously described (Bertomeu et al., 2017).

Using our in-house scoring method for CRISPR dropout screens named RANKS (Bertomeu et al., 2017), gene knockouts depleted and enriched in the smallest and largest cell size fractions were determined. Gene rankings for the tendency of a gene knockout to make cells smaller or larger were obtained by comparing sgRNA frequencies from the combination of the three smallest fractions versus the three largest. All the sgRNAs present in the pool and targeting RefSeq annotated genes were used as internal controls (see Materials and Methods for details). Genes were ordered from those that are more likely to make cells smaller when knocked out (negative RANKS scores) to loss of gene function that are more likely to give rise to larger cells (positive RANKS scores).

6.3.2 Many hits were identified in the cell size screens including the strong candidate gene TLE4

The screens revealed that several gene knockouts potentially conferred either a small or large cell size phenotype (Figure 6.5.2A). sgRNAs targeting the Transducin Like Enhancer of split 4 (TLE4) were amongst the most enriched sgRNAs in small cell size fractions from both screen replicates (Figure 6.5.2A). TLE4 is known as a co-repressor for a variety of

transcription factors, including LEF/TCF, PAX and MYC, mostly involved in Notch and Wnt/beta-catenin signaling (Cinnamon and Paroush, 2008; Jennings and Ish-Horowicz, 2008). Interestingly, TLE4 has never been previously associated with cell size functions. These results suggest that CRISPR/Cas9 pooled knockout screens can detect gene knockouts that potentially confer cell size phenotypes and have not been previously addressed in cell size functions.

In parallel to TLE4, many other top scoring genes with known functions in mTORC1 signaling were identified in the screens (Figure 6.5.2A). sgRNAs enriched in large cell size fractions included those targeting TSC1 and TSC2 genes, negative regulators of growth through mTORC1 (Figure 6.5.2A-B) (Inoki et al., 2002; Zhang et al., 2003). TSC1 and TSC2 genes scored high in both screen replicates (Figure 6.3.2A-B). This was also the case for components of the GATOR1 complex NPRL2/3 and DEPDC5 whose sgRNAs were enriched in large cell size fractions in both screen replicates (Figure 6.5.2A-B). The loss-of-function of GATOR1 components caused an increase in cell growth and consequently larger cell size consistent with the function of the complex as a negative regulator of mTORC1 (Bar-Peled et al., 2013).

sgRNAs targeting RPTOR were also enriched in small cell size fractions (Figure 6.5.2A). RPTOR is part of the mTOR complex 1 and participates in the recruitment of mTORC1 substrates upon amino acid or growth hormone uptake (Hara et al., 2002). We also identified three of the five members of the GATOR2 complex, namely MIOS, WDR59 and WDR24, as high scoring genes in small cell size fractions (Figure 6.5.2A-B). Upon amino acids stimulation, the GATOR2 complex inhibits GATOR1 to promote cell growth (Bar-Peled et al., 2013). These results are consistent with GATOR2 function as a positive regulator of growth since sgRNAs targeting genes member of the GATOR2 complex were enrichment in small cell size fractions (Figure 6.5.2A-B). Additional regulators of the amino acid sensing branch of the mTORC1 network are LAMTOR genes part of the Ragulator complex (Bar-Peled et al., 2012). LAMTOR2 and LAMTOR4 were amongst the high scoring genes in small cell size fractions in both screen replicates (Figure 6.5.2A-B). These screen results are indicative of the role of LAMTOR genes as activators of mTORC1 (Figure 6.5.2A-B).

We also recovered all four members of a newly identified complex associated with mTORC1 signaling, named KICSTOR (Wolfson et al., 2017). This complex was found to interact with the GATOR1 complex, together acting as negative regulators of mTORC1 (Wolfson et al., 2017). KICSTOR includes four members: KPTN, ITFG2, C12orf66 and SZT2 (Wolfson et al., 2017). sgRNAs targeting all four constituents of the complex had high positive scores in both screen replicates (Figure 6.5.2A). KPTN, ITFG2, C12orf66 and SZT2 showed a high tendency to give rise to large cell sizes (Figure 6.5.2A-B). These results demonstrated that our cell size screens well reconstituted many of the molecular constituents of the mTORC1 growth network (Figure 6.5.2B). Consistency of the data between the two screen replicates illustrated the robustness of the screens for the identification of genes potentially regulating human cell size. Notably, sgRNAs targeting TLE4 were top scoring in small cell size fractions (Figure 6.5.2A). Since TLE4 has no known cell size functions, I decided to focus my efforts on TLE4.

6.3.3 The cell size phenotype conferred by loss of TLE4 function and several other candidates was validated

We next sought to confirm the small cell size phenotype of TLE4 knockout cells and more generally to assess the reliability of our cell size screens. In order to do so, we interrogated the ability of TLE4 gene knockouts to affect NALM-6 cell size. In parallel, T. Bertomeu selected over 120 genes for individual validation based on high RANKS scores from both screen replicates (Figure 6.5.2A) and a few genes of interest to the field. Most of the genes selected by T. Bertomeu were amongst the top 100 scoring genes whose sgRNAs were enriched in either small or large cell size fractions from at least one replicate of the screen. For each gene, two independent sgRNAs were cloned in the all-in-one LentiCRISPR v2 vector for single gene knockouts in NALM-6 cells. NALM-6 cells were infected and selected for integration following puromycin selection. These single gene knockout populations were kept under asynchronous growth conditions by daily diluting cells to 400,000 cells per ml for a minimum of 4 consecutive days before assessing cell volume. Changes in cell volume were measured on a Coulter counter.

Using this assay, we validated a total of 64 genes that conferred either a small or large cell size phenotype upon deletion. This subset of validated genes is likely to underestimate the total number of genes that affect NALM-6 cell size since most selected genes for validation were ranked within the first 100 small or large ranked genes. Genes were considered validated when two independent sgRNAs provided the same answer for at least three volume measurements. Our stringent analysis identified 39 genes that when loss-of-function gave a small cell size phenotype and 25 loss of gene function associated with a large cell size phenotype. Amongst those validated genes, were the four members of the KICSTOR complex. KPTN (Figure 6.5.3A), ITFG2 (Figure 6.5.3B), C12orf66 (Figure 6.5.3C), and SZT2 (Figure 6.5.3D), gene knockouts all resulted in an increase in cell volume when compared to control sgRNA populations. Unfortunately, the C12orf66 knockout cell population with the second independent sgRNA could not be assessed in this experiment (Figure 6.5.3C). Other examples of validated genes include WDR24 whose deletion with two independent sgRNAs caused a decrease in cell volume compared to larger volumes of control populations (Figure 6.5.3E). As a member of the GATOR2 complex, this result is consistent with a function as an activator of cell growth. Loss of WDR24 function likely prevented growth resulting in reduced cell size (Figure 6.5.3E).

The small cell size phenotype attributed to TLE4 loss-of-function was validated using this assay (Figure 6.5.3F). Both sgRNAs targeting TLE4 reduced cell volume compared to control sgRNAs (Figure 6.5.3F). To further confirm the small cell size phenotype conferred by TLE4 loss of function, two additional sgRNAs from the EKO library and targeting TLE4 were used in an independent cell size assay. TLE4 loss-of-function caused by these two additional sgRNAs also conferred a small cell size phenotype (data not shown). These results confirmed that TLE4 knockout leads to a decrease in NALM-6 cell size.

Following this result, I sought to determine the role of TLE4 in mammalian cell size regulation. I first wanted to know if the cell size phenotype conferred by TLE4 loss-of-function was specific to NALM-6 pre-B lymphocytes. To test this, cell size assays were carried out in two additional cell lines using the same two independent sgRNAs targeting TLE4 (Figure 6.5.3F). I selected two other blood cancer cell lines: Jurkat T lymphocytes and Raji B lymphocytes derived from Burkitt's lymphoma. TLE4 knockout in both Jurkat and Raji

cell lines did not affect their size whereas it reduced cell volume in NALM-6 cells (Figure 6.5.4A-C). The possibility that TLE4 knockout affects the size of other cell lines cannot be excluded. Cell size assays in other B lymphocytes derived from acute lymphoblastic leukemia (ALL), such as RCH-ACV and SMS-SB cell lines, would have to be performed to assess cell type specificity of TLE4 knockout. A broader panel of cell lines would also need to be tested. Nonetheless, this result suggested that the small cell size phenotype associated with TLE4 loss-of-function is specific to pre-B NALM-6 cells.

6.3.4 Transcripts associated with B cell-specific functions are up-regulated following TLE4 knockout

I next wanted to gain insights into the role of TLE4 in NALM-6 cell size regulation. Very few published studies have addressed TLE4 function in mammalian cells. The mammalian TLE4 gene mostly serves context-dependent functions (Dayyani et al., 2008; Wheat et al., 2014). For instance, TLE4 act as tumor suppressor in AML carrying the AML1-ETO translocation (Dayyani et al., 2008). TLE4 also plays a role in murine bone development (Wheat et al., 2014). TLE4-null mice show growth retardation due to severe bone marrow defects partly attributed to deficient B cell development (Wheat et al., 2014). TLE4 was reported to interact with the transcription factor PAX5, whose expression is essential early in B cell lymphopoiesis (Eberhard et al., 2000; Linderson et al., 2004; Nutt et al., 2001). In this context, TLE4 interacts with PAX5 to repress genes of inappropriate B-cell lineages (Eberhard et al., 2000; Linderson et al., 2004).

Since TLE4 acts at the transcription level, I used RNA-sequencing (RNA-Seq) to transcriptionally profile TLE4-null NALM-6 cells. I generated two independent populations of NALM-6 cells carrying TLE4 knockouts using the two previously validated sgRNAs from cell size assays (Figure 6.5.3F). I also included for comparison two NALM-6 cell populations with control sgRNAs, one targeting the AAVS1 locus and the other targeting the azami-green fluorescent marker with no matching DNA in the genome.

Since TLE4 is a known co-repressor of transcription, I hypothesized that transcripts of interest would be enriched in populations depleted of TLE4 when compared to controls. Indeed, I observed enrichment of transcripts associated with B cell-specific functions (Figure

6.5.5 and Table 1). Gene ontology enrichment for biological processes analysis performed by Jasmin Coulombe-Huntington revealed that the fraction of genes associated with pre-BCR signaling was increased in the absence of TLE4 (Figure 6.5.5). Genes implicated in B cell activation were also over-represented in TLE4 knockout populations when compared to other functions (Figure 6.5.5).

Amongst the top scoring genes with highest transcripts levels upon TLE4 knockout, BANK1 and CD45 were identified and are known to participate in pre-B cell receptor (pre-BCR) signaling (Table 1). Pre-BCR signaling is essential for B cell survival, development and differentiation (Rickert, 2013). Strong BCR expression is required at the pre-B cell stage to promote differentiation (Rickert, 2013). The BCR functions to modulate extracellular survival factors via the immunoglobulin gene and its adapters immunoglobulin alpha (CD79a) and beta (CD79b) chains (Rickert, 2013). Downstream signals are transmitted via the PI3K and ERK/MAPK signaling networks to specific transcription factors that coordinate B cell lymphopoiesis (Muschen, 2015; Rickert, 2013). Amongst the top 1000 scoring genes, I identified CD79a and CD79b transcripts that showed a moderate increase in TLE4 knockout cells (data not shown). Transcripts associated with the LYN gene, an important kinase that transmits signals from the BCR, were also slightly increased in TLE4 knockout cells (data not shown). Genes with transcript enrichments in TLE4 knockout NALM-6 cell populations also included CD23 and CD37 both implicated in B cell activation (Table 1). CD23 is as a receptor for immunoglobulin E that also participates in the differentiation program of B cells (Bonnefoy et al., 1995). Immunoglobulin gene rearrangements are characteristics of B cell development involving specific re-arrangement at different stages of differentiation (van Zelm et al., 2005). In one study, TLE4 was identified as part of a subset of genes implicated in specific immunoglobulin gene rearrangements during human B cell differentiation (van Zelm et al., 2005).

These results showed that several components involved in B-cell specific functions, including pre-BCR signaling, B cell activation and differentiation, had elevated activities following loss of TLE4 function. Thus, the small cell size phenotype resulting from TLE4 deletion in NALM-6 cells seems to be related to B cell specific functions.

6.3.5 CD19 differentiation factor is over-expressed following TLE4 deletion

Since I observed overexpression of several genes implicated in B cell differentiation in the RNA-Seq analysis (Figure 6.5.5 and Table 1), I sought to investigate the possibility that TLE4 knockout can promote B cell differentiation. Cluster of differentiation (CD) genes, including CD23 and CD37 identified in the RNA-Seq experiment, are expressed at the surface of cells derived from hematopoietic lineages and function in the differentiation program. For B cells derived from the bone marrow, differentiation stages are discriminated by the expression of specific cell surface proteins (CD markers). In the bone marrow, human pro-B cells transition to the pre-B I cell stage upon CD19 expression (van Zelm et al., 2005). Loss of CD34 marks the passage to the pre-B II stage where cells are larger (van Zelm et al., 2005). These large pre-B cells express strong pre-BCR signaling (Rickert, 2013). The next stage of B cell development is associated with a reduction in size at the pre-B II (small) stage (van Zelm et al., 2005). Finally, strong CD20 expression promotes the transition to immature B cells that further differentiate outside of the bone marrow (van Zelm et al., 2005). Since NALM-6 cells are derived from the pre-B stage, I hypothesized that TLE4 knockout might promote the transition to the small pre-B II stage, explaining the reduction in cell size.

In order to test this hypothesis, I looked at the expression level of proteins associated with specific stages of B cell differentiation. Protein expression was assessed by fluorescence-activated cell sorting (FACS) and compared between TLE4 knockout and wild type NALM-6 cell populations. I assessed immunoglobulin M (IgM) levels reported to show reduce expression at the pre-B II small stage compared to the pre-B II large stage (van Zelm et al., 2005). TLE4 knockout cells, using two independent sgRNAs, exhibited a small reduction in IgM expression as compared to wild type NALM-6 cells (Figure 6.5.6A). I also observed an increase in CD19 expression upon TLE4 knockout (Figure 6.5.6B). CD19 is expressed starting from the pre-B I stage and remains throughout B cell differentiation (van Zelm et al., 2005; Wang et al., 2012). CD19 is an important factor of B cell lymphopoiesis, actively participating in pre-BCR signaling (Fujimoto et al., 2000; Wang et al., 2012). A study suggested that strong CD19 expression could promote progression from early pre-B stages to the small pre-B stage (Wang et al., 2012). The possibility that loss of TLE4 function drives CD19 overexpression that in turn promotes the transition to the pre-B II small stage of differentiation needs to be

further addressed. These results remain preliminary and additional replicates of the experiment are required to reach a conclusion on the differentiation status of TLE4 knockout cells. Taken together with the RNA-Seq analysis of TLE4 knockout changes in transcription profiles involving BCR signaling, these data suggest that TLE4 promotes the activity of cell surface proteins essential to the B cell developmental program. Therefore, I propose that loss of TLE4 function causes a de-regulation in pre-B cell homeostasis that translates into a reduction in cell size.

6.4 Discussion

In the current study, I examined a candidate gene from the first genome-wide CRISPR/Cas9 pooled knockout screens that interrogated the molecular regulators of human cell size. The pipeline consisted in CRISPR/Cas9 dropout screens followed by counterflow centrifugal elutriation to physically separate cells grown in suspension by size. We provided a reliable method to identify genes that regulate mammalian cell size. Our cell size screens recovered many genes associated with the mTORC1 network implicated in cell growth regulation. The data we obtained was consistent between the two biological replicates of the screens, illustrating the robust nature of our screens. Interestingly, a candidate gene was identified in the screen, TLE4, and had not been previous associated with cell size regulation. Therefore, it was of interest to further investigate the function of TLE4 in cell size regulation. As a repressor of transcription, TLE4 knockout led to an increase in transcript expression for many genes associated with B cell activation and differentiation functions (Figure 6.5.5 and Table 1). CD19 protein expression was up-regulated in TLE4 knockout cells compared to wild type NALM-6 cells suggesting that the loss of TLE4 function alters the developmental program of these cells.

Our CRISPR/Cas9 pooled loss-of-function screens served as a basis for the identification of genes that regulate human cell size. They allowed us to discover TLE4, a gene with no previous association with cell size regulation functions. TLE4 deletion resulted in a reduction in NALM-6 cell size when compared to controls (Figure 6.5.3F). The RNA-Seq analysis showed that the transcriptome of TLE4-null cells reflected B cell-specific functions, including pre-BCR signaling, B cell activation and differentiation (Figure 6.5.5 and Table 1).

Increased CD19 expression in TLE4 deleted NALM-6 cells further supported the participation of TLE4 in the pre-B cell program (Figure 6.5.6B). A previous study had showed that transformed cell lines might possess the potential to differentiate (Liu et al., 2014). The restoration of PAX5 expression in pre-B ALL-derived cells lines mutated for this gene led to an increase in CD19 expression levels, described as promoting differentiation (Liu et al., 2014). Additional experiments are required to reach a conclusion about the differentiation status of TLE4 knockout cells. CD19 overexpression is not sufficient to state that TLE4 knockout cells differentiate to the pre-B II small stage of B cell differentiation (van Zelm et al., 2005). It would be of interest to look at CD38 expression levels in TLE4 knockout cells, an important factor of B cell differentiation in mice (Donis-Hernandez et al., 2001), or CD23 and CD37 markers uncovered in our RNA-Seq experiment (Table 1). The results presented in this study suggest that TLE4 loss of function influences the developmental program of NALM-6 cells and this causes an imbalance in cell size homeostasis reflected by a decrease in cell size. To our knowledge, this is the first study that describes a gene that participates in the maintenance of cell size homeostasis by affecting the developmental program of a specific cell type.

Since cell size regulation was explored at large, our CRISPR/Cas9 screens revealed the nature of many other genes that affect human cell size. Amongst those were genes associated with the mTORC1 network key to growth control. All four members (KPTN, ITFG2, C12orf66 and SZT2) of the newly identified KICSTOR complex were recovered in both replicates of our cell size screens (Figure 6.5.2A). We confirmed the increased cell size phenotype associated with loss-of-function for all four members of the KICSTOR complex (Figure 6.5.3A-D). Interestingly, we had uncovered the role of C12orf66 in our first cell size screen prior to the publication of the study on KICSTOR (Wolfson et al., 2017). These results supported the efficacy and robustness of our screens to identify regulators of human cell size. The validated genes that affected cell size and presented in the current study only represent a small subset of the potential regulators of NALM-6 cell size. We only proceeded with the validation of 120 genes that scored amongst the top 100 genes potentially affecting NALM-6 cell size. Genes outside of this boundary might also affect cell size and could further expand the landscape of genes contributing to mammalian cell size regulation.

In sum, we presented the first whole-genome CRISPR/Cas9 pooled knockout screen that interrogated the genetic regulators of mammalian cell size. A candidate gene identified in the screen, TLE4, was characterized. This investigation showed that TLE4 knockout affects the developmental program of pre-B cells by causing an increase in transcript expression primarily associated with B cell activation and differentiation functions. This study presents the first characterization of a gene that participates in the maintenance of human cell size homeostasis via lineage-specific developmental program coordination.

6.5 Figures and Legends

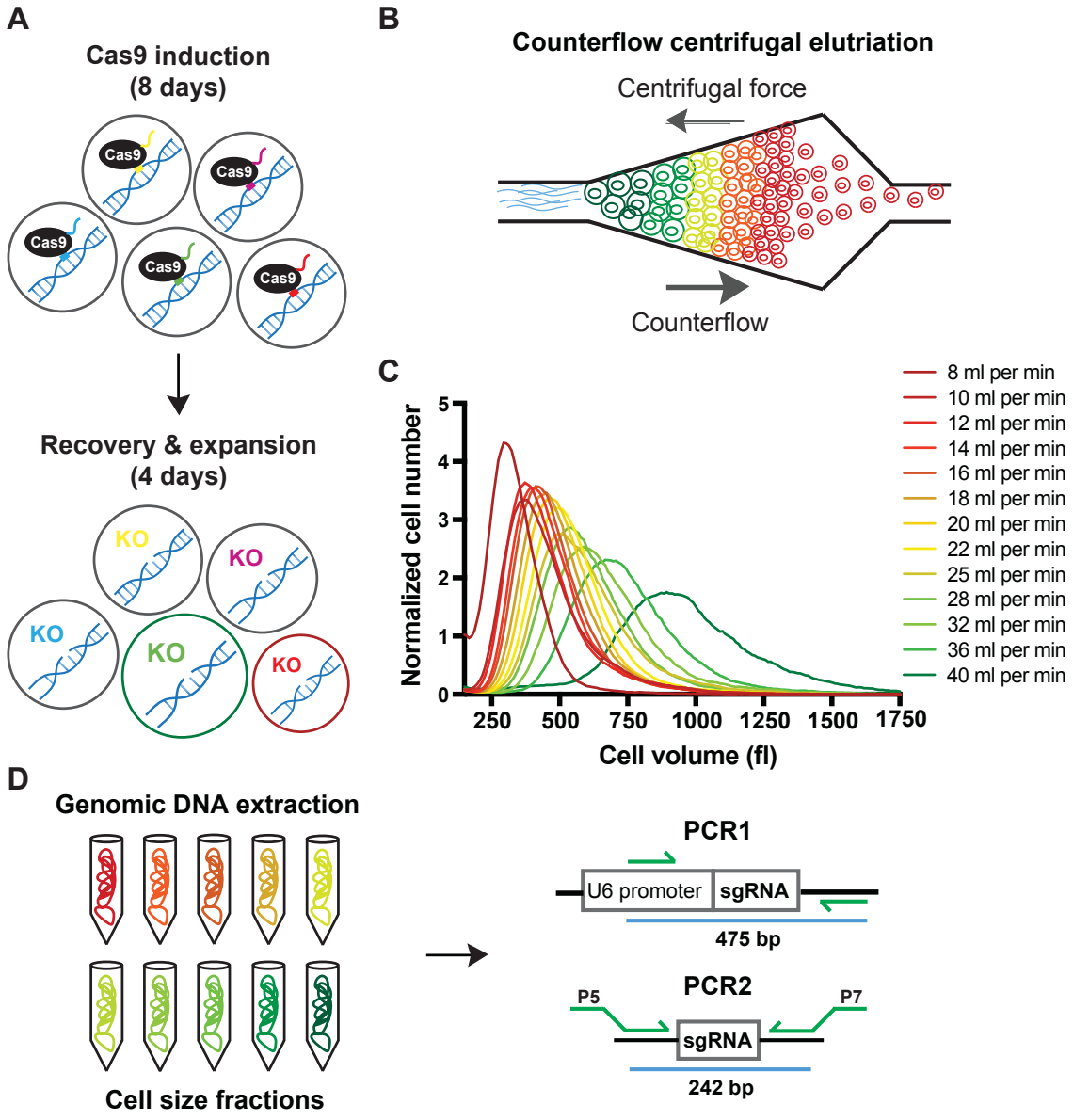

Figure 6.5.1 Outline of genome-wide CRISPR/Cas9 cell size screens in NALM-6 pre-B lymphocytes

(A) Schematic representation of the pool of NALM-6 cells each expressing Cas9 and a different sgRNA (Top). During the second replicate of the screen, cells were treated with doxycycline for 8 days to allow gene knockouts to take place followed by a period of 4 days without doxycycline to allow expansion of the pool and recovery from doxycycline treatment (Bottom). Gene knockouts present in the pool and causing either a small (red) or large (green) cell size phenotype. (B) The pool of 975 million cells was collected for counterflow

centrifugal elutriation. Schematic of the elutriation chamber that contains cells arranged in a size gradient from largest (dark green) to smallest (red) created by the opposing centrifugal and flow forces. Slowly increasing the flow rate pushes cells with increasing volumes (from red to green) outside of the chamber. This results in the physical separation of cells in separate size fractions. (C) Cell volume was monitored by Coulter particle counting of a small sample from each of the 13 fractions previously collected. The graph depicts the distribution of cell volumes from each fraction from smallest (red) to largest (dark green), corresponding to increasing flow rates. (D) Large-scale genomic DNA extractions were performed from each separate cell size fractions. A region of 475 base pairs of DNA including part of the U6 promoter and the sgRNA sequence was amplified in a first round of PCR. A second round of PCR served to add Illumina adaptors for NGS.

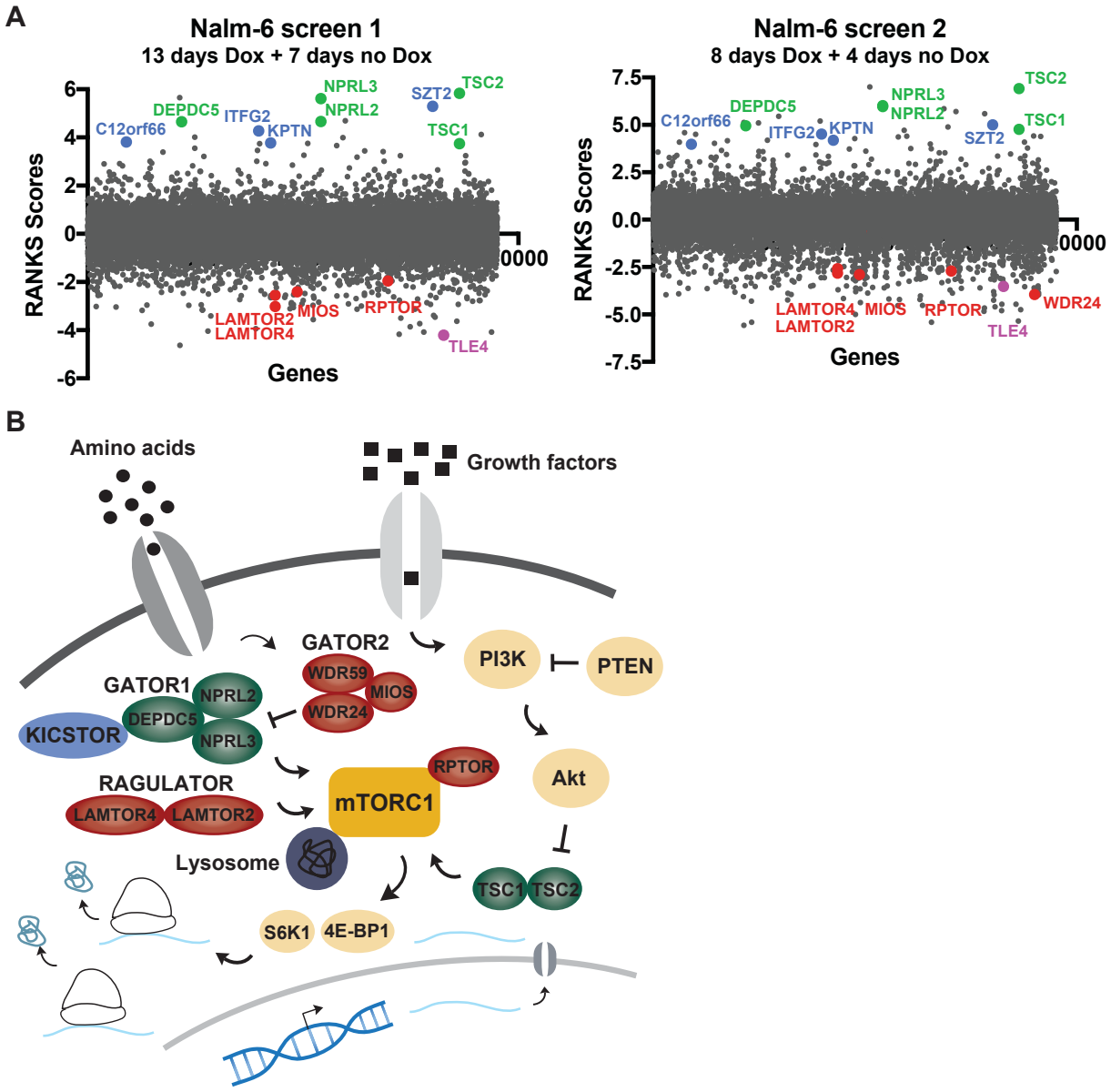

Figure 6.5.2 Mammalian cell growth regulators associated with mTORC1 identified in cell size screens

(A) Data from the first (left) and second (right) replicate of the CRISPR/Cas9 pooled knockout cell size screens. Genes are classified in alphabetical order (X axis) and their corresponding RANKS score is depicted (Y axis). Candidate genes whose knockout is predicted to result in small cell sizes have negative scores while genes whose knockout is predicted to make cells larger show positive scores. A total of 207 and 723 genes passed the FDR (<0.05) for the first and second screen replicates respectively. Candidate genes associated with mTORC1

signaling are represented (red and green). Gene members of the KICSTOR complex with high positive scores are also annotated (blue). (B) Schematic representation of the growth pathway associated with mTORC1 signaling. Key regulators of the network and essential for cell viability are represented (yellow). Genes highlighted in (A) are indicated and their location corresponds to their known function in the mTORC1 network. Color patterns follow results presented in (A).

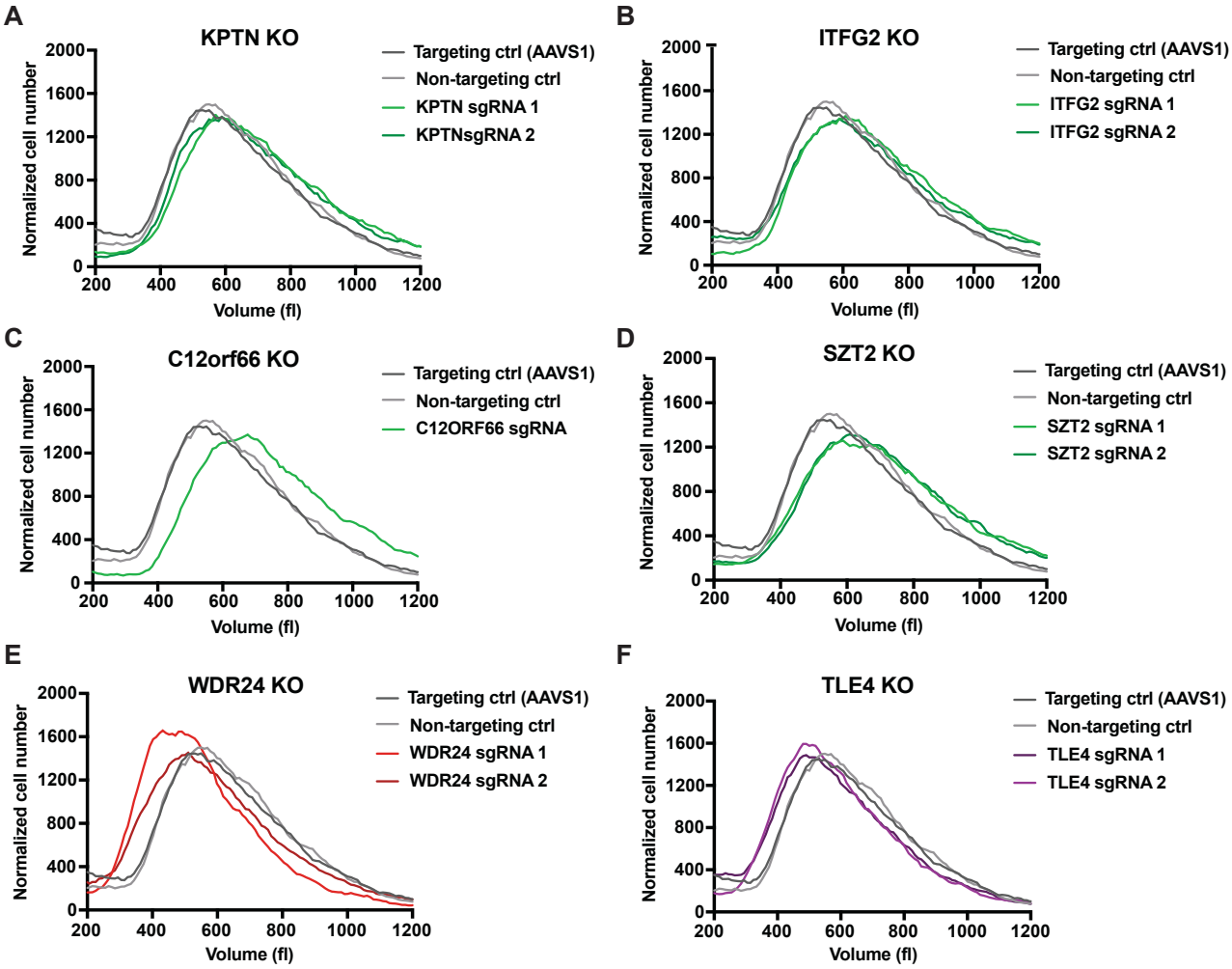

Figure 6.5.3 Cell size assays confirm phenotypes conferred by several candidates from the screens

(A-F) Graphs representing distributions of cell volume measured by Coulter particle counting. Single traces are depicted for the sgRNA targeting the AAVS1 locus (dark grey) and a non-targeting sgRNA (light grey) as controls and the two independent sgRNAs targeting the same gene of interest. (A-D) Population of NALM-6 cells with knockouts for the four members of the KICSTOR complex (green) compared to controls (grey), all causing an increase in cell volume (E) WDR24 knockout cells (red) have reduced cell volumes compared to controls (grey). (F) TLE4 knockout (purple) population of cells showing a reduction in cell volume compared to controls (grey).

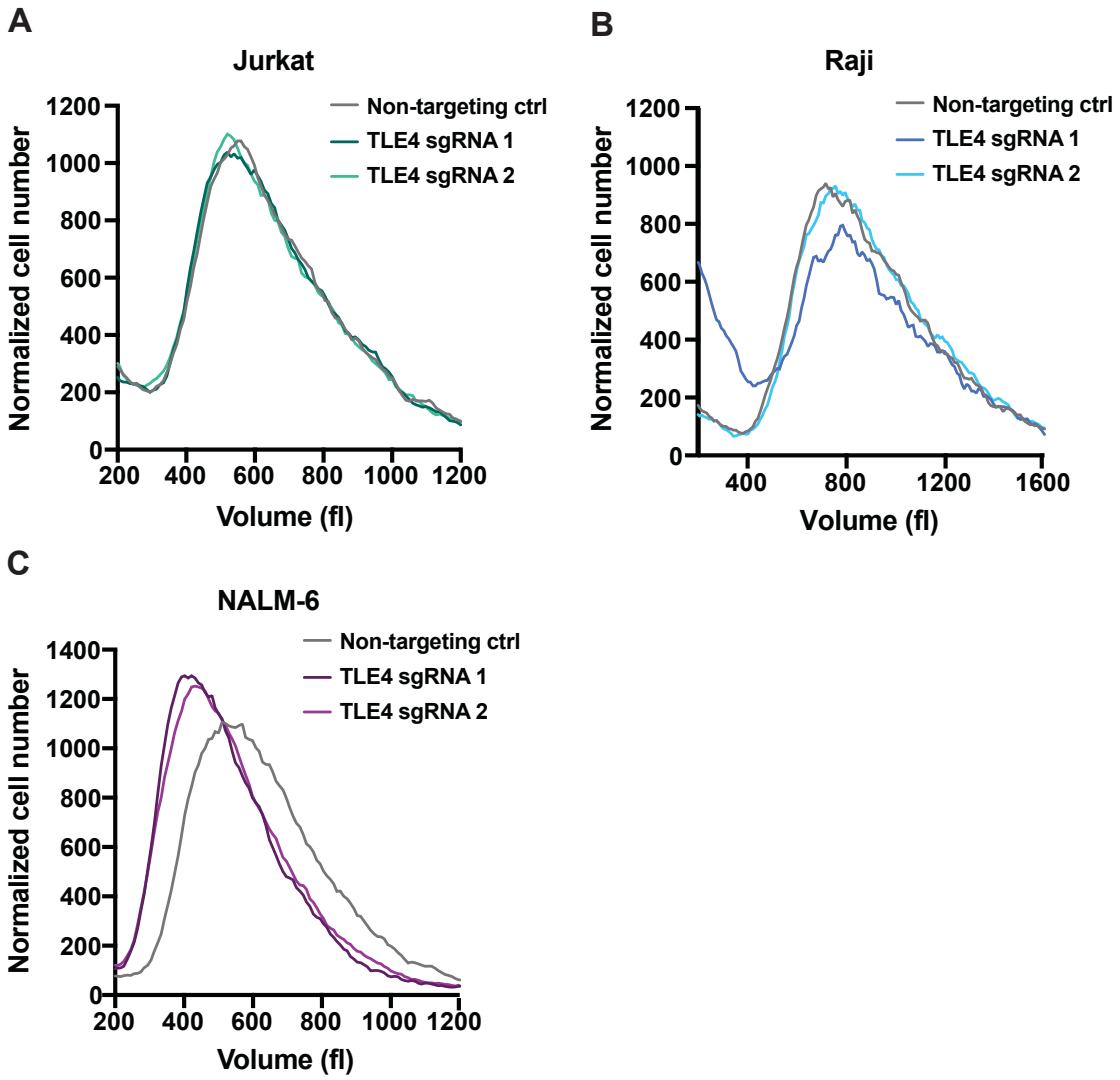

Figure 6.5.4 The small cell size phenotype resulting from TLE4 deletion seems NALM-6-specific

(A) Jurkat T lymphocytes were infected with two independent sgRNAs targeting TLE4 (turquoise). TLE4 knockout cells show no change in cell volume when compared to a non-targeting control population (grey). (B) Raji B lymphocytes derived from Burkitt's lymphoma do not observe any decrease in cell volume (blue) upon loss of TLE4 function. (C) Loss of TLE4 confers a reduction in NALM-6 cell volume as shown in Figure 3E.

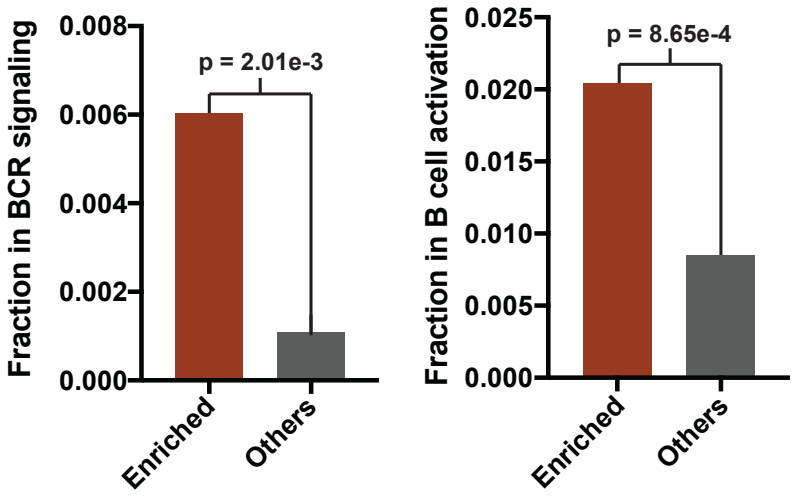

Figure 6.5.5 Genes associated with B cell-specific functions are up regulated upon TLE4 knockout

RNA-seq was performed on two independent populations of cells with TLE4 knockouts (two independent sgRNAs) compared to two control NALM-6 cell populations, one targeting the non-phenotypic AAVS1 locus and the other non-targeting control (azami-green fluorescent marker). TLE4 knockout cells were compared to control samples to determine $\log_2$ ratios for each gene (J.C-H.). A GO term analysis was performed by J.C-H. on these RNA-seq data. Graph showing genes associated with BCR signaling functions (GO terms) enriched upon TLE4 deletion when compared to any other function (left). Graph representing genes enriched for B cell activation functions (GO terms) in TLE4 knockout NALM-6 cell populations (right).

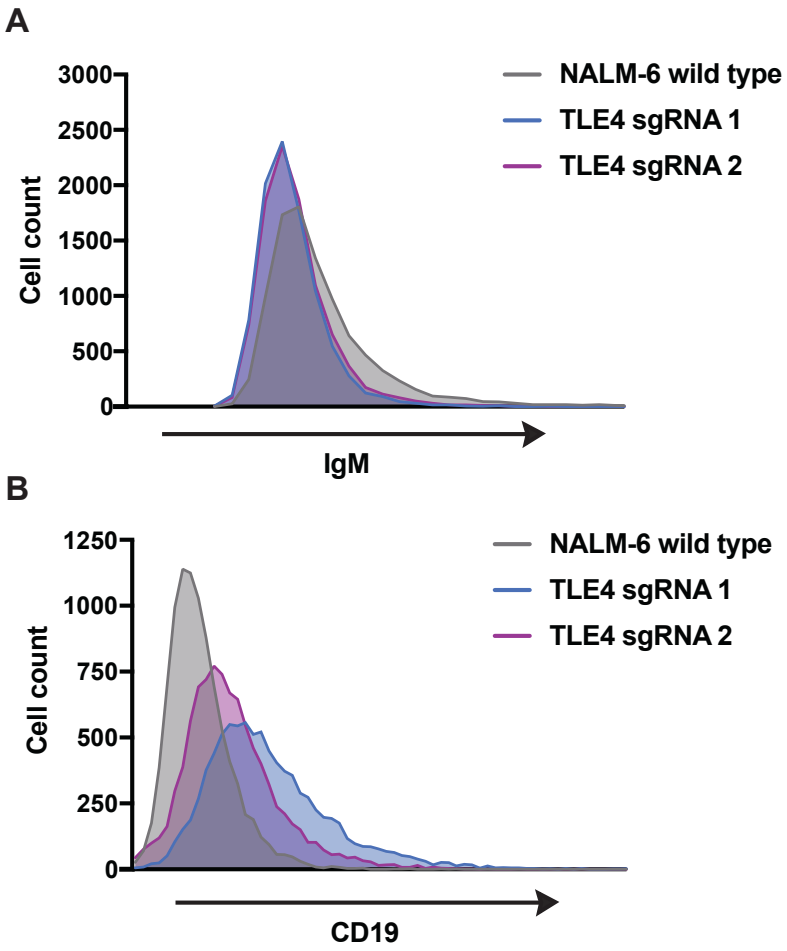

Figure 6.5.6 The loss of TLE4 function leads to an increase in CD19 expression

(A-B) FACS profiles corresponding to expression levels of two B cell-specific surface proteins. Fluorescence intensities of wild type NALM-6 (grey) versus NALM-6 infected by either of two lentiviruses inducing an sgRNA targeting TLE4 (sgRNA 1-blue and sgRNA 2-purple). (A) IgM (APC) expression slightly reduced in TLE4 knockout cell populations (blue and purple). (B) CD19 (PE-Cy7) protein expression levels are increased in TLE4 knockout cells (blue and purple) when compared to control wild type NALM-6 cells (grey).

Ranking	Gene name	Log_2 ratio	Description
1	MYBPC2	3.466	
2	CMTM3	3.158	
3	PARVG	3.013	
4	VPS26B	2.755	
5	PTPRC (CD45)	2.603	Important regulator of BCR signaling
6	CLEC12B	2.598	
7	ALDH3B2	2.378	
8	ADAMTS18	2.341	
9	BANK1	2.275	B cell-specific scaffold protein, BCR signaling
10	FMNL3	2.272	
11	CLEC12A	2.21	
12	FCER2 (CD23)	2.194	B cell-specific antigen, regulator of IgE production, differentiation
13	NAPSA	2.155	
14	RIMBP2	2.126	
15	CD37	2.109	Cell surface protein, might play a role in B cell interactions
16	ZFYVE28	2.094	
17	C7orf57	2.037	
18	ACY3	2.036	
19	NEIL1	1.982	
20	JAG1	1.978	
21	KLHL14	1.977	
22	CPNE5	1.936	
23	MFI2	1.93	
24	CLEC1B	1.923	
25	SPIB	1.833	Transcription factor enhancer of lymphoid-specific genes, BCR signaling
26	PSD2	1.809	
27	FCRLA	1.779	B cell-specific and potentially important for B cell development
28	SEMA5B	1.765	
29	FAM198B	1.721	
30	C16orf74	1.709	

Table Top scoring genes showing transcripts enrichment in TLE4 knockout cells

The top 30 genes showing transcript enrichments in TLE4 knockout cell populations from the RNA-Seq experiment. Gene names correspond to their official HGNC symbol. Log_2 ratios were calculated for each gene comparing TLE4 knockout to control samples. Genes associated with B cell-specific functions are highlighted (orange) and a brief description is provided.

6.6 Materials and Methods

Cell culture

293T (CRL-3216) cells were obtained from ATCC and the Nalm-6 cell line was a gift from Dr. Stephen Elledge (Harvard Medical School). 293T cells were cultured in DMEM medium supplemented with 10% FBS (Wisent). Nalm-6 cells were grown in RPMI medium supplemented with 10% FBS. Both cell lines were maintained at 37°C and 5% CO_2. The Jurkat (TIB-152) cell line was obtained from ATCC. The Raji cell line was kindly provided by Dr. Guy Sauvageau (IRIC, Université de Montréal). Jurkat and Raji were both maintained in 10% FBS RPMI medium and at 5% CO_2 in 37°C incubators.

NALM-6 cell size pooled screens

The uninduced version of the EKO library (MOI of 0.5) previously generated (Bertomeu et al., 2017) was used for the first cell size screen. 3 aliquots of the EKO library containing 45 million cells each were thawed with about 50% of mortality at thawing, unfortunately. Since the representation of the library (250 cells per sgRNA) was maintained, we proceeded with this screen. Knockouts were induced for 13 days of doxycycline (2 ug/ml). Cells were then expanded for an extra 7 days without doxycycline to allow cell size recovery. During that time, cells were diluted to approximately 300,000 cells per ml every day. For the second screen replicate, the library was re-made. 987 million cells of the same dox-inducible Cas9 NALM-6 clone (Bertomeu et al., 2017) were infected with the EKO sgRNA lentivirus library and the MOI evaluated by Q-PCR at 0.36 with the same methodology as described in Bertomeu 2017. Following 6 days of blasticidin selection, cells were frozen. Each vial contained 22.5 million cells in 4.5 ml of freezing media (50% FBS, 40% RPMI, 10% DMSO). 8 aliquots containing 22.5 million cells of this new version of the EKO library were thawed without significant mortality at thawing. This was followed by Cas9 induction with doxycycline (2 ug/ml) treatment for 8 days. Next, cells were cultured for an additional 4 days without doxycycline with daily dilution to 400,000 cells per ml to insure asynchronous exponential growth. Cells obtained from both pools were fractionated by counterflow centrifugal elutriation. A total of 352 million cells for the first screen and 975 million cells for

the second screen were slowly cooled down and maintained at 4°C. These cells were concentrated to 50 ml in 1% FBS RPMI media after 10 minutes of centrifugation at 300g. Cells were loaded in the elutriator (Beckman Coulter Avanti J-26 XPI centrifuge fitted with the JE-5.0 elutriation system using the small 4 ml chamber) at 6 ml per min using a Masterflex L/S Cole-Parmer peristaltic pump with centrifugation set at 2000 rpm (1st screen) and 2500 rpm (2nd screen). 200 ml fractions of cells were collected in 1% FBS RPMI media by increasing flow rate increments until reaching up to 40 ml per min. A total of 13 separate cell size fractions were generated. Cell volume for each fraction was measured by loading 1 ml from each 200 ml fraction on a Z2 Coulter counter (Beckman Coulter). Cells were centrifuged at 1000g for 15 min, washed with 10 ml PBS 1X, re-centrifuged and cell pellets kept at -20°C until genomic DNA extraction. DNA was extracted from each fraction separately using QIAamp DNA blood maxi and mini kits (Qiagen). sgRNA sequences were amplified by two rounds of PCR as previously described (Bertomeu et al., 2017). sgRNA sequencing was performed on an Illumina HiSeq 2000 instrument configured for 50 base pairs single reads. Sequencing was done at the Génome Innovation Center of McGill University (Montréal, Canada).

Screen results analysis

Gene rankings were obtained by using our in-house built RANKS algorithm for every RefSeq gene as previously reported (Bertomeu et al., 2017). RANKS computed gene scores were obtained by comparing the smallest cell size fractions versus the largest fractions and using all sgRNAs targeting RefSeq genes as the internal control. For the first screen, gene scores from the two smallest fractions (10 and 12 ml per minute) were compared to the three largest fractions (28, 32 and 36 ml per minute). For the second replicate, fractions 8, 10 and 12 ml per minute were compared to fractions 36 and 40 ml per minute. Lists of genes that when knocked out are predicted to give rise to smaller or larger cells were obtained from smallest to largest RANKS scores for both screen replicates.

Cell size validation assays

A list of candidate genes identified in cell size screens was established based on high rankings at both ends of the RANKS spectrum. Several other genes with slightly lower scores

were selected based on literature and possible association with cell size regulation in mammalian cells. Two sgRNA sequences for each gene to target were selected from the EKO library. For each round of validation, sgRNAs targeting the non-phenotypic AAVS1 locus and a non-targeting control (azami-green fluorescent marker) were included in the experiment. All sgRNAs were cloned in the all-in-one LentiCRISPR v2 (Addgene 52961) mammalian expression vector containing a puromycin selection cassette, Cas9 derived from *S. pyogenes* (SpCas9) expressed under the EFS promoter and an sgRNA expressed under the mammalian U6 promoter. Individual sgRNAs were designed and cloned into the LentiCRISPR v2 plasmid following the protocol from the Zhang lab (genome-engineering.org). Lentiviral preparations were produced in 293t cells for each corresponding sgRNA. A mixture of plasmids psPAX2 (6.5 ug), pCMV-VSV-G (3.5 ug), and LentiCRISPR v2 (9 ug) was prepared and supplemented with polyethyleneimine (1 mg/ml) in 1 ml total with water. After 15 min incubation, this mixture was added to 9 ml of fresh DMEM 10% FBS medium containing penicillin/streptomycin. Old media was removed from 293t cells at approximately 85% confluency and replaced with the transfection mixture. 16 hours post-transfection, the media was replaced with 10 ml 2% FBS DMEM. 48 hours post-transfection, lentiviruses were recovered, filtered through a 0.45 μm PVDF filter and filter-sterilized concentrated solution preserving lentivirus was added for a final concentration of 5% sucrose, 2 mM $MgCl_2$ and 10 mM HEPES pH 7.5. Lentiviruses were stored at 4°C until use and the rest of the preparation stored at -80°C for later use. 100 μl of lentiviral preparation was pre-mixed for 15 min at room temperature with 900 μl of 10% FBS RPMI medium, penicillin/streptomycin (1X) and protamine sulfate (20 ug/ml). The mixture was then added to 1 million NALM-6 cells in 1 ml of media in a 24-well plate format. A negative control without viral preparation was included per round of infection. 48 hours post-infection, cells were re-suspended and 1 ml was discarded. 2 ml RPMI 10% FBS containing puromycin (final concentration 1 ug/ml) was added to the cells. The next day, 1 ml of cell was transferred to a T-25 flask containing 4 ml of 10% FBS RPMI media supplemented with puromycin (1 ug/ml) and penicillin/streptomycin (1X). Cells were left under puromycin selection for a total of 6 days without them ever reaching 1 million cells per ml. Following selection, 1 ml of cells were put in 9 ml of isoton II diluent solution (Beckman Coulter) and counted within 5 minutes on a Z2 Coulter counter

(Beckman Coulter). NALM-6 cells post-selection were counted daily over the course of the experiment and diluted with 10% FBS RPMI media to a concentration of 400,000 cells per ml if they ever exceeded this concentration. Cells were read every day for a minimum of 3 days unless their concentration was too low. Around the same time each day, cell volume was measured by Coulter particle counting (Z2 Coulter). Cell volume measurements from the last day of the assay were used to assess cell size phenotypes associated with corresponding sgRNAs. Raw data were extracted from the Coulter counter to make corresponding cell volume graphs. Only data points ranging between volumes of 200 to 1200 fl were plotted to exclude debris. Cell counts attributed to bin volumes were normalized to an area under the curve equal to one.

RNA-Seq

Two NALM-6 TLE4 knockout cell populations (sgRNA 1 and 2) and two control populations (sgRNA targeting the AAVS1 locus and non-targeting sgRNA for the azami-green fluorescent protein) were cultured for 11 days in 10% FBS RPMI media. 1 million cells from all 4 separate conditions were collected, centrifuged at 1200 rpm for 5 min, washed with 1X PBS and re-centrifuged at 1200 rpm for 5 min. Cells were homogenized in 1 ml of Trizol solution. The presence of contamination with chemicals was assessed by nanodrop using 260/280 and 260/230 ratios. Quantification of total RNA was made by QuBit (ABI) and 1000 ng of total RNA was used for library preparation. Quality of total RNA was assessed with the BioAnalyzer Nano (Agilent) and all samples had a RIN above 9.6. Library preparation was done with the KAPA mRNAseq stranded kit (KAPA, Cat no. KK8420). Ligation was made with 11.4 nM final concentration of Illumina index and 9 PCR cycles was required to amplify cDNA libraries. Libraries were quantified by QuBit and BioAnalyzer. All libraries were diluted to 10 nM and normalized by qPCR using the KAPA library quantification kit (KAPA; Cat no. KK4973). Libraries were pooled to equimolar concentration. Sequencing was performed with the Illumina Hiseq2000 using the SBS v3 PE 200 cycles Kit (2x100bp). Around 53-60 M paired-end PF reads was generated per sample. Library preparation and sequencing was made at the Institute for Research in Immunology and Cancer's Genomics Platform (IRIC). Gene ranking was established by calculating the $\log_2$ ratio of the average read counts for each gene in TLE4 knockout populations over the average read counts of

corresponding genes in control cell populations. Each ratio was normalized by the total number of reads in each sample.

Antibody staining and FACS analysis

The antibody against IgM (APC clone G20-127) was obtained from BD Biosciences. The antibody for CD19 (PE-cy7 clone SJ25C1) was kindly provided by the lab of Dr. Guy Sauvageau (IRIC, Université de Montréal). 1 million NALM-6 cells per condition were harvested for antibody staining. NALM-6 cells were centrifuged at 1200 rpm for 5 min, washed with 1X PBS and re-centrifuged at 1200 rpm for 5 min to pellet the cells. NALM-6 wild type and NALM-6 TLE4 knockout (two independent sgRNAs) cell populations were used for the experiment after 8 days of knockout and after confirming the small cell size phenotype conferred by TLE4 knockout. Cells were washed with 1X PBS and blocked with 1% BSA for 10 minutes on ice. Next, corresponding antibodies were added to separate cell populations. The quantity of antibody suggested by the manufacturer was added for IgM (20 μl). CD19 (2 μl) were titrated by our providers and the volume of antibody suggested was added. Cells pre-mixed with antibodies were incubated for 30 minutes on ice in the dark. Cells where then washed with 1X PBS and transferred into FACS tubes for analysis. 10,000 events were recorded for each sample on a BD LSR II flow cytometer (BD Biosciences). IgM coupled to the APC fluorophore was excited with the 633-nm laser. CD19-PE-Cy7 was excited at 488 nm. The FSC-A parameter was adjusted for each sample. A negative control unstained sample was also included for each antibody measurement. Voltages were adjusted for each fluorophore. Data for each sample were compensated first for FSC-A and SSC-A parameters followed by FSC-H and FSC-W compensations and finally SSC-H and SSC-W. Data from compensated parameters were extracted for all 10,000 events acquired. Fluorophore intensity measurements were normalized to cell size values (FSC-A).

6.7 Acknowledgements

I thank Thierry Bertomeu who conceived and carried out the bulk of the work for the cell size screens. I also want to thank Jasmin Coulombe-Huntington for screen and RNA-Seq data analysis. I thank Luisa Izzi, Almer van der Sloot, Susan Moore and Andrew Chatr

Aryamontri for technical assistance and all members of the Tyers lab for helpful discussions. I want to thank Florent Guilloteau from the Genomic's platform (IRIC, Université de Montréal) for performing the RNA-Seq experiment. I am also thankful to all members of the Genomic platform and Gaël Dulude at the flow cytometry platform for technical assistance in RNA-Seq and FACS experiments, respectively. Finally, I want to thank Susan Moore, Thierry Bertomeu and Jasmin Coulombe-Huntington for their helpful comments and suggestions on the manuscript.

7 Discussion and perspectives

The first article (Chapter 3) presents data that demonstrated the scaling of several aspects of cytokinesis with cell size. This study reflects the influence cell size can have on cell division. This work also helped better define the mechanics of cytokinesis occurring in a living tissue. In the second article (Chapter 6), a genome-wide approach was taken to interrogate the genetic regulators of mammalian cell size by performing CRISPR/Cas9 pooled knockout screens. These screens presented the first global analysis of genetic regulators in mammalian cells. I characterized TLE4 not previously described in cell size regulation functions. Altogether, the findings presented in these chapters showed that cell size influences the kinetics of cytokinesis in living epithelial cells and is itself finely tuned at the molecular level. The necessary balance between cell growth and cell division underscores the intimate relationship between these two processes that were under study here.

The proper execution of cytokinesis and the maintenance of cell size homeostasis are both crucial to prevent pathologies, including cancer. Cytokinesis failure can result in the generation of tetraploid cells that are nearly twice as large as their diploid equivalent. When these tetraploid cells divide, chromosome segregation errors can occur, including aneuploidy an important hallmark of different cancers. Furthermore, increases in cell size are often used to detect cancer cells. It includes those that failed cytokinesis or large cells of brain tumors in tuberous sclerosis patients, amongst other examples (Goto et al., 2011; Lacroix and Maddox, 2012). Thus, a better understanding of how cell growth and cell division processes are regulated is crucial for the development of improved cancer therapies. The work presented in previous chapters contributes to the fundamental knowledge that provides the foundation for the design of improved cancer therapies in the future.

7.1 Future directions in cytokinesis studies

Most of the current knowledge on cytokinesis comes from studies with isolated systems, such as *C. elegans* zygotes, yeasts and mammalian cells in culture. Decades of work with these systems, have led to the establishment of the conserved regulators that orchestrate the different events in cytokinesis (described in Chapter 2). However, a large void remains in

the cytokinesis field and cell biology in general, as to whether molecular regulation is conserved in the context of living tissues. In addition, very little is known about the impact tissue properties have on cytokinesis. Recent work, including ours (Chapter 3), began to address this void in the cytokinesis field (Bourdages and Maddox, 2013; Founounou et al., 2013; Guillot and Lecuit, 2013; Herszterg et al., 2013a; Higashi et al., 2016; Morais-de-Sa and Sunkel, 2013a). Our work supports previous findings that suggested that there are different requirements for cytokinesis occurring in cells of living tissues.

To better understand how cytokinesis occurs in living epithelia, we developed a novel model to characterize cytokinesis. We assessed cytokinesis occurring in the developing *C. elegans* vulval precursor cells (VPCs) that undergo reductional divisions (Figure 3.5.1). We reported the occurrence of asymmetric contractile ring closure in the VPCs (Figure 3.5.4). In an attempt to determine the molecular regulators governing this property we investigated the role of Anillin during VPC cytokinesis. Work performed with isolated cells identified Anillin as a scaffolding protein of contractile rings required for proper cytokinesis (Piekny and Maddox, 2010). During *Drosophila* embryonic and pupal epithelial cells cytokinesis, Anillin depletion caused a reduction in the rate of contractile ring closure (Founounou et al., 2013; Guillot and Lecuit, 2013). We also observed a decrease in the speed of contractile ring closure during all three rounds of VPC cytokinesis upon Anillin (ANI-1) depletion (Figure 3.5.4). Our result supports a conserved function for Anillin during epithelial cell cytokinesis that is to contribute to the proper kinetics of contractile ring closure.

The same phenotype of reduced constriction rate was reported in *Drosophila* epithelia but following septin depletion (Founounou et al., 2013; Guillot and Lecuit, 2013). It would be of interest to address the function of septins during VPC cytokinesis. *C. elegans* possess two septin genes (*unc-59* and *unc-61*) that would be depleted concomitantly using RNAi by feeding and the speed of contractile ring closure quantified for all three rounds of VPC cytokinesis. This simple experiment would provide additional evidences regarding the function of septins during epithelial cell cytokinesis.

In the future, it would also be of interest to investigate the role of other conserved molecular regulators of cytokinesis in the living VPCs. These include components of the centralspindlin complex, namely ZEN-4 and CYK-4, and the RhoA activator, Ect2,

contributing to the establishment of the division plane in isolated systems (Chapter 2). I would deplete these components individually by soaking RNAi to increase phenotype penetrance and measure the kinetics of cytokinesis using GFP-tagged non-muscle myosin II to visualize the contractile ring by time-lapse microscopy, as previously described (Figure 3.5.2). The breadth of the contractile ring, asymmetry, speed and the duration of contractile ring closure would be quantified in the VPCs of worms depleted for these proteins.

An important question that remains poorly understood in the cytokinesis field is how tissue properties affect cytokinesis. In *Drosophila* epithelia, adherens junctions oppose the forces generated by the contractile ring to maintain tissue integrity during cytokinesis (Bourdages and Maddox, 2013; Founounou et al., 2013; Guillot and Lecuit, 2013; Herszterg et al., 2013a; Morais-de-Sa and Sunkel, 2013a). It would be of interest to investigate the contribution from adherens junctions during VPCs cytokinesis. This would help determine whether the mechanics of contractile ring closure, including properties such as speed and asymmetry, are conserved across metazoan. RNAi only partially disrupted *C. elegans* apical junctions and I did not observe any changes in the kinetics of contractile ring closure upon depletion of E-cadherin or AJM-1 components of adherens junctions (Figure 3.6.1). The use of CRISPR/Cas9 for complete gene loss-of-function might not result in viable progeny since both proteins are required for body elongation early during *C. elegans* development (Costa et al., 1998). Instead, I would propose to perform laser cell ablation to investigate the contribution from apical junctions during VPC cytokinesis. Apical junctions are juxtaposed to the worm's cuticle and would be ablated prior to VPC division and cytokinesis would be subsequently monitored by high-resolution time-lapse microscopy. This experiment would provide insights into the function of adherens junctions during cytokinesis in living epithelial cells of *C. elegans*.

Our study (Chapter 3) and that of others have provided insights into cell- and tissue-type differences in molecular or physical requirements for cell division (Bourdages et al., 2014; Founounou et al., 2013; Guillot and Lecuit, 2013; Herszterg et al., 2013a; Higashi et al., 2016; Morais-de-Sa and Sunkel, 2013a). I also examined the somatic cells constituting the *C. elegans* gonad to address differences in contractile ring dynamics between two different tissues. I found that these somatic cells divided more slowly than the VPCs with an asymmetry

of contractile ring closure resembling that of the final round of VPC cytokinesis (Figure 3.5.5). Thus, these findings demonstrated that the mechanics of cytokinesis differed depending on tissue-context.

Finally, our work revealed that several aspects of cytokinesis scaled with cell size. I found that the breadth of the contractile ring scaled with VPC length as the cells decreased in length from one round of division to the next (Figure 3.5.2). I hypothesize that larger cells contain more proteins and thus recruit more contractile ring constituents to form a broader contractile ring in cells of increasing length. As VPCs reduce in length from one round of division to the next, they recruit less contractile components since they have a small volume to partition and less force to generate compared to longer cells with increased volume.

Another finding from our work is that the speed of contractile ring closure scaled with VPC dimensions (Figure 3.5.3). In addition, the speed of constriction in the small VPCs positively correlated with the speed of contractile ring closure in larger *C. elegans* blastomeres (Figure 3.5.3). In *C. elegans* embryos, the duration of constriction was found to be independent of the initial perimeter of the cell, demonstrating the scaling of the speed of contractile ring closure with cell size (Carvalho et al., 2009). However, this study did not address whether the speed of furrowing scaled with cell dimensions or cell volume. Work with the filamentous fungi *N. crassa* showed that the speed of contractile ring closure scaled with the circumference of the cell (Calvert et al., 2011). In the VPCs, the speed of contractile ring closure also scaled with cell dimensions (Figure 3.5.3). Thus, our findings are consistent with that of others, demonstrating that a speed of contractile ring closure scales with cell size (Calvert et al., 2011; Carvalho et al., 2009). Altogether, these findings demonstrated that cell size influences the mechanics of cytokinesis. This brings about a different but related question as to how do cells regulate their size?

7.2 Global analysis of genetic regulators of mammalian cell size

The work described in Chapter 6, is derived from the first whole-genome screens for the effect of pooled gene knockouts on human cell size carried out in the Tyers laboratory. We performed genome-wide CRISPR/Cas9 pooled knockout screens followed by counterflow centrifugal elutriation to physically separate cells by size. Our CRISPR/Cas9 knockout screens

were robust and reliably identified many genes known to be involved in growth control associated with mTORC1 signaling (Figure 6.5.2). For instance, our screens recovered the four gene members of the KICSTOR complex, recently identified as a negative regulator of mTORC1 (Wolfson et al., 2017). We had also identified and confirmed the large cell size conferred by C12orf66 knockout, member of KICSTOR, prior to the publication by others (Wolfson et al., 2017). In sum, our work established the use of CRISPR/Cas9 pooled knockout screens to identify genes that regulate mammalian cell size.

Nonetheless, it is noteworthy to address two limitations to this method in the identification of genes affecting cell size. First, genes essential for cell viability rapidly dropped out of the pools when knocked out. This prevented us from recovering essential genes that also function as cell size regulators. This might explain why we failed to recover mTOR and its downstream targets S6K1 and 4E-BP1 essential for NALM-6 cell viability (Bertomeu et al., 2017). Secondly, counterflow centrifugal elutriation does not efficiently fractionate adherent cells by size. Therefore, only cells grown in suspension, mostly of lymphoid origins, can be well separated by size using this method. This adds the limitation that we might fail to identify genes that specifically regulate the size of adherent cell-types. In addition, we might fail to recover genetic regulators of size shared by most mammalian cell types. Instead, we would expect to find genes knockouts causing a cell size phenotype specifically in lymphocytes or cell type-specific regulators, such as TLE4. The caveat to defining the global or general regulators of cell size is that screens have to be carried out in many different cell types.

TLE4 had not been previous associated with cell size functions. The characterization of TLE4 function in cell size regulation suggested that it might be cell type-specific even though additional cell lines need to be examined. TLE4 knockout only reduced the size of NALM-6 pre-B lymphocytes and not Jurkat (T cells) and Raji (B cell derived from Burkitt's lymphoma) cell lines (Figure 6.5.4). This result suggested that the cell size phenotype associated with the loss of TLE4 function might be pre-B cell specific. Further investigating the function of TLE4 in NALM-6 cell size regulation, I found that several transcripts associated with B cell-specific functions, including B cell activation and differentiation and BCR signaling, were up regulated in TLE4 knockout cells (Figure 6.5.5 and Table 1). An increase in CD19 expression in TLE4

knockout cells (Figure 6.5.6) led to the proposition that TLE4 knockout potentially caused B cell activation that translates into a reduction in NALM-6 cell size. However, additional experiments are required to determine TLE4's function in the maintenance of pre-B cell size homeostasis. This includes the characterization of the direct transcriptional targets of TLE4. I recently obtained an antibody against TLE4 that would be used to perform chromatin immunoprecipitation sequencing (Chip-Seq).

In sum, Chapter 6 presented the characterization of a gene, TLE4 that participates in cell size regulation of pre-B cells by acting on the developmental program. This suggests that the molecular circuitry contributing to the cell size program is vast. Considering this broad diversity of genes regulating cell size, future work will be aimed at defining how they are coordinated to maintain cell size homeostasis. Once we establish an extensive list of genes that affect NALM-6 cell size it would be of interest to perform functional analysis to cluster genes with similar functions. This would be a first indication of how they work together to regulate cell size. Subsequent experiments include the generation of clonal cell lines for genes of interest that we seek to further characterize. In the future, we would use these cell lines to perform molecular biology experiments, including immunoprecipitation and genetic epistasis analysis, to gain insights into how they are coordinated to regulate cell size.

7.3 Do cells sense their size?

Several questions in the cell size field remain open ended. For instance, can cells "sense" their size? Work with erythroblasts supported the idea that a "size sensing" mechanism exists in mammalian cells (Dolznig et al., 2004). This work demonstrated that smaller genetically engineered erythroblasts grew at slower rates compared to their larger equivalents (Dolznig et al., 2004). Introducing unfavorable growth conditions to larger fast-growing erythroblasts shortened the time required to promote the G1-S phase transition (Dolznig et al., 2004). These results illustrated the rapid adaptation of erythroblasts to changing growth conditions and suggested the occurrence of size modulation in G1 dependent on cell size for these cells (Dolznig et al., 2004).

Studies that investigated growth rates at higher temporal resolution suggested that the growth rate was dependent on cell size. Large cells grew faster and entered S phase prior to

their smaller equivalent that grew more slowly and entered S phase at a later time (Godin et al., 2010; Kafri et al., 2013; Park et al., 2010; Son et al., 2012; Tzur et al., 2009). It is noteworthy to mention that a study in rat Schwann cells suggested that these cells exhibited growth rates independent of cell size (Conlon and Raff, 2003). In this study, cell size slowly adjusted to changes in growth conditions, which led to the proposal that these adherent cells of the nervous system lacked a "size sensing" mechanism (Conlon and Raff, 2003). However, this is the only study that reports cell growth independence on cell size. The TLE4 characterization I performed (Chapter 6) demonstrated the occurrence of developmental cell size regulation. These findings suggest that cell size is actively modulated and that cells possess a way to sense their size. Therefore, as most studies suggested the occurrence of a "size sensing" mechanism in mammalian cells, it is a generally well-accepted idea in the field.

These findings raised another question that is if cells possess a way to "sense" their size, what do they sense. Candidate metrics include protein content, the concentration or abundance of a specific factor, mass or volume in general. Since we are in the early phase of data analysis of our cell size screens, we are actively looking for genetic evidence of a "size sensing" factor. For instance, we hypothesize that a gene implicated in "size sensing" when knocked out would result in broadening of the cell size range in the population when compared to wild type cells. However, we have yet to identify a gene knockout causing this cell size phenotype. The cell size regulating genes validated from our screens either caused an increase or decrease in cell volume (Figure 6.5.3). It is also possible that our cell volume measurements on a population of cells are not sensitive enough to observe changes in cell size in both directions. In order to circumvent this issue and to gain better insights into the function of specific genes identified in our screens and validated, we plan to generate clonal cell lines for selected gene knockouts. This would ensure that only mutated cells remain in the population to robustly assess a specific gene function in cell size regulation.

7.4 Mammalian cell size; parts list and conservation

In the future, it would be of interest to perform additional genome-wide cell size screens in different cell lines to establish a robust list of genes implicated in mammalian cell size regulation. Additional screens would also allow us to define a set of core or "universal"

cell size regulating genes as opposed to cell-type specific regulators of cell size. Therefore, I propose to screen two additional cells lines, Raji cells derived from Burkitt's lymphoma and one cell line derived from chronic myeloid leukemia (K562). I would first generate Cas9 clones with strong expression following doxycycline induction for both cell lines, as described in Chapter 6. These Cas9-expressing cells would be infected with our EKO library of sgRNAs and knockout cells separated by size using counterflow centrifugal elutriation, as previously described for NALM-6 pre-B lymphocytes (Chapter 6). These additional screens would also allow us to define a better cut-off for genes affecting size. It would also provide a more complete and robust list of genes affecting cell size for subsequent investigation on their function in cell size regulation.

Further exploring cell size regulation at a system's level, it would be of interest to investigate the conserved nature of genes identified in our CRISPR/Cas9 pooled knockouts screens. First, I would, with the help of Jasmin Coulombe-Huntington, examine the degree of conservation with known regulators of budding yeast cell size (Jorgensen et al., 2002). We also have access to a list of approximately 2000 genes that affect budding yeast cell size under different growth conditions (data from our laboratory). Genes essential for optimal mammalian cell fitness exhibited a greater degree of conservation with distantly related species suggesting that the same could apply for regulators of mammalian cell size (Bertomeu et al., 2017). I will also investigate the degree of conservation with *C. elegans*. Identifying *C. elegans* orthologs or genes with similar functions between these two species, I could employ the VPC model to address questions of size. I would take advantage of the ease of protein depletions by RNAi in this system to quantify their effects on VPC size or the size of cells of the somatic gonad. This experiment would provide information on the evolutionary conservation of genes regulating cell size. It could also guide us for future experiments in mammalian cells to establish their specific function in cell size coordination.

Concluding remarks

The work presented in this thesis described a novel model to characterize cytokinesis occurring in living epithelial cells. The kinetics of cytokinesis occurring in the precursor cells of the *C. elegans* vulva (VPCs) were quantified. This revealed that several aspects of

cytokinesis, including the speed of constriction and the breadth of the contractile ring initially assembled, scaled with cell circumference and cell length, respectively. These findings reflect the influence cell size has on cytokinesis. This work also provided knowledge on the mechanics of cytokinesis occurring in a living epithelium. In the second part of this thesis, the long-standing question of how cells regulate their size was addressed. An unbiased approach was taken to identify genes that regulate mammalian cell size. Using the CRISPR/Cas9 technology to knockout, in a pool, every gene of the human genome, those that caused a cell size phenotype were identified. These genome-wide screens provided valuable insights into the nature of the genes that are implicated in human cell size regulation. TLE4, a candidate gene identified in the screen, was characterized. It was found that TLE4 is implicated in developmental cell size regulation of pre-B cells. Altogether, these studies contributed to the increasing knowledge on two processes that stand alone but that are intricately coordinated to ensure proper cell functioning. As fundamental building blocks of life, cells are sophisticated machines that must maintain an appropriate size and ensure the proper coordination of cell division that terminates by cytokinesis.

Bibliography

Adams, R.R., A.A.M. Tavares, A. Salzberg, H.J. Bellen, and D.M. Glover. 1998. pavarotti encodes a kinesin-like protein required to organize the central spindle and contractile ring for cytokinesis. *Genes Dev.* 12:1483-1494.

Adhikary, S., and M. Eilers. 2005. Transcriptional regulation and transformation by Myc proteins. *Nat Rev Mol Cell Biol*. 6:635-645.

Aguirre, A.J., R.M. Meyers, B.A. Weir, F. Vazquez, C.Z. Zhang, U. Ben-David, A. Cook, G. Ha, W.F. Harrington, M.B. Doshi, M. Kost-Alimova, S. Gill, H. Xu, L.D. Ali, G. Jiang, S. Pantel, Y. Lee, A. Goodale, A.D. Cherniack, C. Oh, G. Kryukov, G.S. Cowley, L.A. Garraway, K. Stegmaier, C.W. Roberts, T.R. Golub, M. Meyerson, D.E. Root, A. Tsherniak, and W.C. Hahn. 2016. Genomic Copy Number Dictates a Gene-Independent Cell Response to CRISPR/Cas9 Targeting. *Cancer Discov*. 6:914-929.

Altun, Z.F.H., D. H. 2017. Handbook of C. elegans anatomy. In WormAtlas.

Amodeo, A.A., and J.M. Skotheim. 2016. Cell-Size Control. *Csh Perspect Biol*. 8.

Andreassen, P.R., O.D. Lohez, F.B. Lacroix, and R.L. Margolis. 2001. Tetraploid state induces p53-dependent arrest of nontransformed mammalian cells in G1. *Mol. Biol. Cell*. 12:1315-1328.

Audhya, A., F. Hyndman, I.X. McLeod, A.S. Maddox, J.R. Yates, 3rd, A. Desai, and K. Oegema. 2005. A complex containing the Sm protein CAR-1 and the RNA helicase CGH-1 is required for embryonic cytokinesis in Caenorhabditis elegans. *J. Cell Biol.* 171:267-279.

Backman, S., V. Stambolic, and T. Mak. 2002. PTEN function in mammalian cell size regulation. *Curr. Opin. Neurobiol.* 12:516-522.

Baetz, K., and B. Andrews. 1999. Regulation of cell cycle transcription factor Swi4 through auto-inhibition of DNA binding. *Mol. Cell. Biol.* 19:6729-6741.

Baker, J., and D. Garrod. 1993. Epithelial cells retain junctions during mitosis. *J. Cell Sci.* 104 (Pt 2):415-425.

Bar-Peled, L., L. Chantranupong, A.D. Cherniack, W.W. Chen, K.A. Ottina, B.C. Grabiner, E.D. Spear, S.L. Carter, M. Meyerson, and D.M. Sabatini. 2013. A Tumor suppressor complex with GAP activity for the Rag GTPases that signal amino acid sufficiency to mTORC1. *Science*. 340:1100-1106.

Bar-Peled, L., and D.M. Sabatini. 2014. Regulation of mTORC1 by amino acids. *Trends Cell Biol.* 24:400-406.

Bar-Peled, L., L.D. Schweitzer, R. Zoncu, and D.M. Sabatini. 2012. Ragulator is a GEF for the rag GTPases that signal amino acid levels to mTORC1. *Cell*. 150:1196-1208.

Barbet, N.C., U. Schneider, S.B. Helliwell, I. Stansfield, M.F. Tuite, and M.N. Hall. 1996. TOR controls translation initiation and early G1 progression in yeast. *Mol. Biol. Cell*. 7:25-42.

Baryshnikova, A., M. Costanzo, Y. Kim, H. Ding, J. Koh, K. Toufighi, J.Y. Youn, J. Ou, B.J. San Luis, S. Bandyopadhyay, M. Hibbs, D. Hess, A.C. Gingras, G.D. Bader, O.G. Troyanskaya, G.W. Brown, B. Andrews, C. Boone, and C.L. Myers. 2010. Quantitative analysis of fitness and genetic interactions in yeast on a genome scale. *Nat Methods*. 7:1017-1024.

Basant, A., S. Lekomtsev, Y.C. Tse, D. Zhang, K.M. Longhini, M. Petronczki, and M. Glotzer. 2015. Aurora B kinase promotes cytokinesis by inducing centralspindlin oligomers that associate with the plasma membrane. *Developmental cell*. 33:204-215.

Basto, R., J. Lau, T. Vinogradova, A. Gardiol, C.G. Woods, A. Khodjakov, and J.W. Raff. 2006. Flies without centrioles. *Cell*. 125:1375-1386.

Baum, B., and M. Georgiou. 2011. Dynamics of adherens junctions in epithelial establishment, maintenance, and remodeling. *J. Cell Biol.* 192:907-917.

Bean, J.M., E.D. Siggia, and F.R. Cross. 2005. High functional overlap between MluI cell-cycle box binding factor and Swi4/6 cell-cycle box binding factor in the G1/S transcriptional program in Saccharomyces cerevisiae. *Genetics*. 171:49-61.

Bement, W.M., H.A. Benink, and G. von Dassow. 2005. A microtubule-dependent zone of active RhoA during cleavage plane specification. *J. Cell Biol.* 170:91-101.

Bement, W.M., and D.G. Capco. 1991. Analysis of inducible contractile rings suggests a role for protein kinase C in embryonic cytokinesis and wound healing. *Cell Motil. Cytoskeleton*. 20:145-157.

Bement, W.M., C.A. Mandato, and M.N. Kirsch. 1999. Wound-induced assembly and closure of an actomyosin purse string in Xenopus oocytes. *Curr. Biol.* 9:579-587.

Bertomeu, T., J. Coulombe-Huntington, A. Chatr-Aryamontri, K. Bourdages, E. Coyaud, B. Raught, Y. Xia, and M. Tyers. 2017. A high resolution genome-wide CRISPR/Cas9 viability screen reveals structural features and contextual diversity of the human cell-essential proteome. *Mol. Cell. Biol.*

Bieling, P., I.A. Telley, and T. Surrey. 2010. A minimal midzone protein module controls formation and length of antiparallel microtubule overlaps. *Cell*. 142:420-432.

Bjorklund, M., M. Taipale, M. Varjosalo, J. Saharinen, J. Lahdenpera, and J. Taipale. 2006. Identification of pathways regulating cell size and cell-cycle progression by RNAi. *Nature*. 439:1009-1013.

Blaxter, M., and D.R. Denver. 2012. The worm in the world and the world in the worm. *BMC Biol*. 10:57.

Blomen, V.A., P. Majek, L.T. Jae, J.W. Bigenzahn, J. Nieuwenhuis, J. Staring, R. Sacco, F.R. van Diemen, N. Olk, A. Stukalov, C. Marceau, H. Janssen, J.E. Carette, K.L. Bennett, J. Colinge, G. Superti-Furga, and T.R. Brummelkamp. 2015. Gene essentiality and synthetic lethality in haploid human cells. *Science*. 350:1092-1096.

Bonnefoy, J.Y., S. Lecoanet-Henchoz, J.P. Aubry, J.F. Gauchat, and P. Graber. 1995. CD23 and B-cell activation. *Curr. Opin. Immunol.* 7:355-359.

Bonner, J.T. 2011. Why size matters, from bacteria to blue whales. Princeton University Press.

Bourdages, K.G., B. Lacroix, J.F. Dorn, C.P. Descovich, and A.S. Maddox. 2014. Quantitative Analysis of Cytokinesis In Situ during C. elegans Postembryonic Development. *PloS one*. 9:e110689.

Bourdages, K.G., and A.S. Maddox. 2013. Dividing in epithelia: cells let loose during cytokinesis. *Developmental cell*. 24:336-338.

Brennan, I.M., U. Peters, T.M. Kapoor, and A.F. Straight. 2007. Polo-like kinase controls vertebrate spindle elongation and cytokinesis. *PloS one*. 2:e409.

Brenner, S. 1973. The genetics of behaviour. *Br. Med. Bull.* 29:269-271.

Brenner, S. 1974. The genetics of Caenorhabditis elegans. *Genetics*. 77:71-94.

Bringmann, H., and A.A. Hyman. 2005. A cytokinesis furrow is positioned by two consecutive signals. *Nature*. 436:731-734.

Brouns, S.J., M.M. Jore, M. Lundgren, E.R. Westra, R.J. Slijkhuis, A.P. Snijders, M.J. Dickman, K.S. Makarova, E.V. Koonin, and J. van der Oost. 2008. Small CRISPR RNAs guide antiviral defense in prokaryotes. *Science*. 321:960-964.

Brown, K.S., M.D. Blower, T.J. Maresca, T.C. Grammer, R.M. Harland, and R. Heald. 2007. Xenopus tropicalis egg extracts provide insight into scaling of the mitotic spindle. *J. Cell Biol.* 176:765-770.

Calvert, M.E., G.D. Wright, F.Y. Leong, K.H. Chiam, Y. Chen, G. Jedd, and M.K. Balasubramanian. 2011. Myosin concentration underlies cell size-dependent scalability of actomyosin ring constriction. *J. Cell Biol.* 195:799-813.

Canman, J.C., L.A. Cameron, P.S. Maddox, A. Straight, J.S. Tirnauer, T.J. Mitchison, G.W. Fang, T.M. Kapoor, and E.D. Salmon. 2003. Determining the position of the cell division plane. *Nature*. 424:1074-1078.

Cao, L.G., and Y.L. Wang. 1990. Mechanism of the formation of contractile ring in dividing cultured animal cells. II. Cortical movement of microinjected actin filaments. *J. Cell Biol.* 111:1905-1911.

Cao, L.G., and Y.L. Wang. 1996. Signals from the spindle midzone are required for the stimulation of cytokinesis in cultured epithelial cells. *Mol. Biol. Cell*. 7:225-232.

Carlsson, A.E. 2006. Contractile stress generation by actomyosin gels. *Phys Rev E Stat Nonlin Soft Matter Phys*. 74:051912.

Carvalho, A., A. Desai, and K. Oegema. 2009. Structural memory in the contractile ring makes the duration of cytokinesis independent of cell size. *Cell*. 137:926-937.

Cavey, M., and T. Lecuit. 2009. Molecular bases of cell-cell junctions stability and dynamics. *Cold Spring Harb Perspect Biol*. 1:a002998.

Chen, S., N.E. Sanjana, K. Zheng, O. Shalem, K. Lee, X. Shi, D.A. Scott, J. Song, J.Q. Pan, R. Weissleder, H. Lee, F. Zhang, and P.A. Sharp. 2015. Genome-wide CRISPR screen in a mouse model of tumor growth and metastasis. *Cell*. 160:1246-1260.

Cinnamon, E., and Z. Paroush. 2008. Context-dependent regulation of Groucho/TLE-mediated repression. *Curr. Opin. Genet. Dev.* 18:435-440.

Cong, L., F.A. Ran, D. Cox, S. Lin, R. Barretto, N. Habib, P.D. Hsu, X. Wu, W. Jiang, L.A. Marraffini, and F. Zhang. 2013. Multiplex genome engineering using CRISPR/Cas systems. *Science*. 339:819-823.

Conlon, I., and M. Raff. 1999. Size control in animal development. *Cell*. 96:235-244.

Conlon, I., and M. Raff. 2003. Differences in the way a mammalian cell and yeast cells coordinate cell growth and cell-cycle progression. *J Biol*. 2:7.

Conlon, I.J., G.A. Dunn, A.W. Mudge, and M.C. Raff. 2001. Extracellular control of cell size. *Nat Cell Biol*. 3:918-921.

Consortium, C.e.S. 1998. Genome sequence of the nematode C. elegans: a platform for investigating biology. *Science*. 282:2012-2018.

Cook, M., and M. Tyers. 2007. Size control goes global. *Curr. Opin. Biotechnol.* 18:341-350.

Corsi, A.K., B. Wightman, and M. Chalfie. 2015. A Transparent Window into Biology: A Primer on Caenorhabditis elegans. *Genetics*. 200:387-407.

Costa, M., W. Raich, C. Agbunag, B. Leung, J. Hardin, and J.R. Priess. 1998. A putative catenin-cadherin system mediates morphogenesis of the Caenorhabditis elegans embryo. *J. Cell Biol.* 141:297-308.

Costanzo, M., J.L. Nishikawa, X. Tang, J.S. Millman, O. Schub, K. Breitkreuz, D. Dewar, I. Rupes, B. Andrews, and M. Tyers. 2004. CDK activity antagonizes Whi5, an inhibitor of G1/S transcription in yeast. *Cell*. 117:899-913.

Cross, F.R. 1988. DAF1, a mutant gene affecting size control, pheromone arrest, and cell cycle kinetics of Saccharomyces cerevisiae. *Mol. Cell. Biol.* 8:4675-4684.

D'Avino, P.P., T. Takeda, L. Capalbo, W. Zhang, K.S. Lilley, E.D. Laue, and D.M. Glover. 2008. Interaction between Anillin and RacGAP50C connects the actomyosin contractile ring with spindle microtubules at the cell division site. *J. Cell Sci.* 121:1151-1158.

D'Arcy Wentworth, T. 1945. On growth and form. Cambridge: University Press: New York: Macmillan.

Das, T., B. Payer, M. Cayouette, and W.A. Harris. 2003. In vivo time-lapse imaging of cell divisions during neurogenesis in the developing zebrafish retina. *Neuron*. 37:597-609.

Dayyani, F., J. Wang, J.R. Yeh, E.Y. Ahn, E. Tobey, D.E. Zhang, I.D. Bernstein, R.T. Peterson, and D.A. Sweetser. 2008. Loss of TLE1 and TLE4 from the del(9q) commonly deleted region in AML cooperates with AML1-ETO to affect myeloid cell proliferation and survival. *Blood*. 111:4338-4347.

de Bruin, R.A., T.I. Kalashnikova, A. Aslanian, J. Wohlschlegel, C. Chahwan, J.R. Yates, 3rd, P. Russell, and C. Wittenberg. 2008. DNA replication checkpoint promotes G1-S transcription by inactivating the MBF repressor Nrm1. *Proc. Natl. Acad. Sci. U. S. A.* 105:11230-11235.

de Bruin, R.A., T.I. Kalashnikova, C. Chahwan, W.H. McDonald, J. Wohlschlegel, J. Yates, 3rd, P. Russell, and C. Wittenberg. 2006. Constraining G1-specific transcription to late G1 phase: the MBF-associated corepressor Nrm1 acts via negative feedback. *Mol. Cell*. 23:483-496.

de Bruin, R.A., W.H. McDonald, T.I. Kalashnikova, J. Yates, 3rd, and C. Wittenberg. 2004. Cln3 activates G1-specific transcription via phosphorylation of the SBF bound repressor Whi5. *Cell*. 117:887-898.

De Virgilio, C., and R. Loewith. 2006. The TOR signalling network from yeast to man. *Int. J. Biochem. Cell Biol.* 38:1476-1481.

Descovich, C.P., D.B. Cortese, S. Ryan, M. Werner, L. Zhang, K.N. Rehain, P.S. Maddox, and A.S. Maddox. 2016. Cytoskeletal crosslinkers both drive and brake cytokinetic ring closure. *Mol. Biol. Cell*. 27.

DiCarlo, J.E., J.E. Norville, P. Mali, X. Rios, J. Aach, and G.M. Church. 2013. Genome engineering in Saccharomyces cerevisiae using CRISPR-Cas systems. *Nucleic Acids Res*. 41:4336-4343.

Dirick, L., T. Bohm, and K. Nasmyth. 1995. Roles and regulation of Cln-Cdc28 kinases at the start of the cell cycle of Saccharomyces cerevisiae. *EMBO J.* 14:4803-4813.

Dirick, L., and K. Nasmyth. 1991. Positive feedback in the activation of G1 cyclins in yeast. *Nature*. 351:754-757.

Dobzhansky, T. 1929. The influence of the quantity and quality of chromosomal material on the size of the cells in drosophila melanogaster. *Wilhelm Roux Arch Entwickl Mech Org*. 115:363-379.

Dolznig, H., F. Grebien, T. Sauer, H. Beug, and E.W. Mullner. 2004. Evidence for a size-sensing mechanism in animal cells. *Nat Cell Biol*. 6:899-905.

Donachie, W.D. 1968. Relationship between Cell Size and Time of Initiation of DNA Replication. *Nature*. 219:1077-&.

Donis-Hernandez, F.R., R.M. Parkhouse, and L. Santos-Argumedo. 2001. Ontogeny, distribution and function of CD38-expressing B lymphocytes in mice. *Eur. J. Immunol.* 31:1261-1267.

Dorn, J.F., L. Zhang, V. Paradis, D. Edoh-Bedi, S. Jusu, P.S. Maddox, and A.S. Maddox. 2010. Actomyosin tube formation in polar body cytokinesis requires Anillin in C. elegans. *Curr. Biol.* 20:2046-2051.

Dorn, J.F., L. Zhang, T.T. Phi, B. Lacroix, P.S. Maddox, J. Liu, and A.S. Maddox. 2016. A theoretical model of cytokinesis implicates feedback between membrane curvature and cytoskeletal organization in asymmetric cytokinetic furrowing. *Mol. Biol. Cell*. 27:1286-1299.

Dubreuil, V., A.M. Marzesco, D. Corbeil, W.B. Huttner, and M. Wilsch-Brauninger. 2007. Midbody and primary cilium of neural progenitors release extracellular membrane particles enriched in the stem cell marker prominin-1. *J. Cell Biol.* 176:483-495.

Dungrawala, H., H. Hua, J. Wright, L. Abraham, T. Kasemsri, A. McDowell, J. Stilwell, and B.L. Schneider. 2012. Identification of new cell size control genes in S. cerevisiae. *Cell Div*. 7:24.

Earnshaw, W.C., and R.L. Bernat. 1991. Chromosomal passengers: toward an integrated view of mitosis. *Chromosoma*. 100:139-146.

Earnshaw, W.C., and C.A. Cooke. 1991. Analysis of the distribution of the INCENPs throughout mitosis reveals the existence of a pathway of structural changes in the chromosomes during metaphase and early events in cleavage furrow formation. *J. Cell Sci.* 98 (Pt 4):443-461.

Eberhard, D., G. Jimenez, B. Heavey, and M. Busslinger. 2000. Transcriptional repression by Pax5 (BSAP) through interaction with corepressors of the Groucho family. *EMBO J.* 19:2292-2303.

Echeverri, C.J., P.A. Beachy, B. Baum, M. Boutros, F. Buchholz, S.K. Chanda, J. Downward, J. Ellenberg, A.G. Fraser, N. Hacohen, W.C. Hahn, A.L. Jackson, A. Kiger, P.S. Linsley, L. Lum, Y. Ma, B. Mathey-Prevot, D.E. Root, D.M. Sabatini, J. Taipale, N. Perrimon, and R. Bernards. 2006. Minimizing the risk of reporting false positives in large-scale RNAi screens. *Nat Methods*. 3:777-779.

Eckley, D.M., A.M. Ainsztein, A.M. Mackay, I.G. Goldberg, and W.C. Earnshaw. 1997. Chromosomal proteins and cytokinesis: Patterns of cleavage furrow formation and inner centromere protein positioning in mitotic heterokaryons and mid-anaphase cells. *J. Cell Biol.* 136:1169-1183.

Edgar, B.A., and T.L. Orr-Weaver. 2001. Endoreplication cell cycles: more for less. *Cell*. 105:297-306.

Eggert, U.S., T.J. Mitchison, and C.M. Field. 2006. Animal cytokinesis: from parts list to mechanisms. *Annu. Rev. Biochem.* 75:543-566.

Fankhauser, G. 1945. Maintenance of Normal Structure in Heteroploid Salamander Larvae, through Compensation of Changes in Cell Size by Adjustment of Cell Number and Cell Shape. *J. Exp. Zool.* 100:445-455.

Fantes, P., and P. Nurse. 1977. Control of cell size at division in fission yeast by a growth-modulated size control over nuclear division. *Exp. Cell Res.* 107:377-386.

Fantes, P.A. 1977. Control of cell size and cycle time in Schizosaccharomyces pombe. *J. Cell Sci.* 24:51-67.

Fededa, J.P., and D.W. Gerlich. 2012. Molecular control of animal cell cytokinesis. *Nat Cell Biol*. 14:440-447.

Felix, M.A., and M. Barkoulas. 2012. Robustness and flexibility in nematode vulva development. *Trends Genet.* 28:185-195.

Felix, M.A., and F. Duveau. 2012. Population dynamics and habitat sharing of natural populations of Caenorhabditis elegans and C. briggsae. *BMC Biol*. 10:59.

Fero, M.L., M. Rivkin, M. Tasch, P. Porter, C.E. Carow, E. Firpo, K. Polyak, L.H. Tsai, V. Broudy, R.M. Perlmutter, K. Kaushansky, and J.M. Roberts. 1996. A syndrome of multiorgan hyperplasia with features of gigantism, tumorigenesis, and female sterility in p27(Kip1)-deficient mice. *Cell*. 85:733-744.

Field, C.M., and B.M. Alberts. 1995. Anillin, a contractile ring protein that cycles from the nucleus to the cell cortex. *J. Cell Biol.* 131:165-178.

Field, C.M., M. Coughlin, S. Doberstein, T. Marty, and W. Sullivan. 2005. Characterization of anillin mutants reveals essential roles in septin localization and plasma membrane integrity. *Development*. 132:2849-2860.

Field, C.M., A.S. Maddox, J.R. Pringle, and K. Oegema. 2008. Septins in the Metazoan Model Systems Drosophila Melanogaster and Caenorhabditis Elegans. *In* The Septins. P.A. Hall, S.E. Russell, and J.R. Pringle, editors. John Wiley & Sons, Ltd. 147-168.

Fire, A., S. Xu, M.K. Montgomery, S.A. Kostas, S.E. Driver, and C.C. Mello. 1998. Potent and specific genetic interference by double-stranded RNA in Caenorhabditis elegans. *Nature*. 391:806-811.

Fleming, E.S., M. Zajac, D.M. Moschenross, D.C. Montrose, D.W. Rosenberg, A.E. Cowan, and J.S. Tirnauer. 2007. Planar spindle orientation and asymmetric cytokinesis in the mouse small intestine. *J. Histochem. Cytochem.* 55:1173-1180.

Flemming, A.J., Z.Z. Shen, A. Cunha, S.W. Emmons, and A.M. Leroi. 2000. Somatic polyploidization and cellular proliferation drive body size evolution in nematodes. *Proc. Natl. Acad. Sci. U. S. A.* 97:5285-5290.

Foe, V.E., and G. von Dassow. 2008. Stable and dynamic microtubules coordinately shape the myosin activation zone during cytokinetic furrow formation. *J. Cell Biol.* 183:457-470.

Founounou, N., N. Loyer, and R. Le Borgne. 2013. Septins regulate the contractility of the actomyosin ring to enable adherens junction remodeling during cytokinesis of epithelial cells. *Developmental cell*. 24:242-255.

Fraser, A.G., R.S. Kamath, P. Zipperlen, M. Martinez-Campos, M. Sohrmann, and J. Ahringer. 2000. Functional genomic analysis of C. elegans chromosome I by systematic RNA interference. *Nature*. 408:325-330.

Friedland, A.E., Y.B. Tzur, K.M. Esvelt, M.P. Colaiacovo, G.M. Church, and J.A. Calarco. 2013. Heritable genome editing in C. elegans via a CRISPR-Cas9 system. *Nat Methods*. 10:741-743.

Fujimoto, M., J.C. Poe, M. Hasegawa, and T.F. Tedder. 2000. CD19 regulates intrinsic B lymphocyte signal transduction and activation through a novel mechanism of processive amplification. *Immunol. Res.* 22:281-298.

Fujiwara, T., M. Bandi, M. Nitta, E.V. Ivanova, R.T. Bronson, and D. Pellman. 2005. Cytokinesis failure generating tetraploids promotes tumorigenesis in p53-null cells. *Nature*. 437:1043-1047.

Fung, K.Y., L. Dai, and W.S. Trimble. 2014. Cell and molecular biology of septins. *International review of cell and molecular biology*. 310:289-339.

Futcher, B. 2006. Metabolic cycle, cell cycle, and the finishing kick to Start. *Genome Biol*. 7:107.

Galbraith, D.W., K.R. Harkins, and S. Knapp. 1991. Systemic Endopolyploidy in Arabidopsis-Thaliana. *Plant Physiol.* 96:985-989.

Ganem, N.J., S.A. Godinho, and D. Pellman. 2009. A mechanism linking extra centrosomes to chromosomal instability. *Nature*. 460:278-282.

Ganem, N.J., and D. Pellman. 2007. Limiting the proliferation of polyploid cells. *Cell*. 131:437-440.

Gangloff, Y.G., M. Mueller, S.G. Dann, P. Svoboda, M. Sticker, J.F. Spetz, S.H. Um, E.J. Brown, S. Cereghini, G. Thomas, and S.C. Kozma. 2004. Disruption of the mouse mTOR gene leads to early postimplantation lethality and prohibits embryonic stem cell development. *Mol. Cell. Biol.* 24:9508-9516.

Gao, F.B., and M. Raff. 1997. Cell size control and a cell-intrinsic maturation program in proliferating oligodendrocyte precursor cells. *J. Cell Biol.* 138:1367-1377.

Garneau, J.E., M.E. Dupuis, M. Villion, D.A. Romero, R. Barrangou, P. Boyaval, C. Fremaux, P. Horvath, A.H. Magadan, and S. Moineau. 2010. The CRISPR/Cas bacterial immune system cleaves bacteriophage and plasmid DNA. *Nature*. 468:67-71.

Gascoigne, K.E., and S.S. Taylor. 2009. How do anti-mitotic drugs kill cancer cells? *J. Cell Sci.* 122:2579-2585.

Giaever, G., A.M. Chu, L. Ni, C. Connelly, L. Riles, S. Veronneau, S. Dow, A. Lucau-Danila, K. Anderson, B. Andre, A.P. Arkin, A. Astromoff, M. El-Bakkoury, R. Bangham, R. Benito, S. Brachat, S. Campanaro, M. Curtiss, K. Davis, A. Deutschbauer, K.D. Entian, P. Flaherty, F. Foury, D.J. Garfinkel, M. Gerstein, D. Gotte, U. Guldener, J.H. Hegemann, S. Hempel, Z. Herman, D.F. Jaramillo, D.E. Kelly, S.L. Kelly, P. Kotter, D. LaBonte, D.C. Lamb, N. Lan, H. Liang, H. Liao, L. Liu, C. Luo, M. Lussier, R. Mao, P. Menard, S.L. Ooi, J.L. Revuelta, C.J. Roberts, M. Rose, P. Ross-Macdonald, B. Scherens, G. Schimmack, B. Shafer, D.D. Shoemaker, S. Sookhai-Mahadeo, R.K. Storms, J.N. Strathern, G. Valle, M. Voet, G. Volckaert, C.Y. Wang, T.R. Ward, J. Wilhelmy, E.A. Winzeler, Y. Yang, G. Yen, E. Youngman, K. Yu, H. Bussey, J.D. Boeke, M. Snyder, P. Philippsen, R.W. Davis, and M. Johnston. 2002. Functional profiling of the Saccharomyces cerevisiae genome. *Nature*. 418:387-391.

Gilbert, L.A., M.A. Horlbeck, B. Adamson, J.E. Villalta, Y. Chen, E.H. Whitehead, C. Guimaraes, B. Panning, H.L. Ploegh, M.C. Bassik, L.S. Qi, M. Kampmann, and J.S. Weissman. 2014. Genome-Scale CRISPR-Mediated Control of Gene Repression and Activation. *Cell*. 159:647-661.

Ginzberg, M.B., R. Kafri, and M. Kirschner. 2015. Cell biology. On being the right (cell) size. *Science*. 348:1245075.

Glotzer, M. 2005. The molecular requirements for cytokinesis. *Science*. 307:1735-1739.

Godin, M., F.F. Delgado, S. Son, W.H. Grover, A.K. Bryan, A. Tzur, P. Jorgensen, K. Payer, A.D. Grossman, M.W. Kirschner, and S.R. Manalis. 2010. Using buoyant mass to measure the growth of single cells. *Nat Methods*. 7:387-390.

Godinho, S.A., R. Picone, M. Burute, R. Dagher, Y. Su, C.T. Leung, K. Polyak, J.S. Brugge, M. Thery, and D. Pellman. 2014. Oncogene-like induction of cellular invasion from centrosome amplification. *Nature*. 510:167-171.

Gonzalez, S., and C. Rallis. 2017. The TOR Signaling Pathway in Spatial and Temporal Control of Cell Size and Growth. *Front Cell Dev Biol*. 5:61.

Goranov, A.I., M. Cook, M. Ricicova, G. Ben-Ari, C. Gonzalez, C. Hansen, M. Tyers, and A. Amon. 2009. The rate of cell growth is governed by cell cycle stage. *Genes Dev.* 23:1408-1422.

Goto, J., D.M. Talos, P. Klein, W. Qin, Y.I. Chekaluk, S. Anderl, I.A. Malinowska, A. Di Nardo, R.T. Bronson, J.A. Chan, H.V. Vinters, S.G. Kernie, F.E. Jensen, M. Sahin, and D.J. Kwiatkowski. 2011. Regulable neural progenitor-specific Tsc1 loss yields giant cells with organellar dysfunction in a model of tuberous sclerosis complex. *Proc. Natl. Acad. Sci. U. S. A.* 108:E1070-1079.

Gratz, S.J., A.M. Cummings, J.N. Nguyen, D.C. Hamm, L.K. Donohue, M.M. Harrison, J. Wildonger, and K.M. O'Connor-Giles. 2013. Genome engineering of Drosophila with the CRISPR RNA-guided Cas9 nuclease. *Genetics*. 194:1029-1035.

Green, R.A., E. Paluch, and K. Oegema. 2012. Cytokinesis in animal cells. *Annu. Rev. Cell Dev. Biol.* 28:29-58.

Greenwald, I. 1997. Development of the Vulva. *In* C. elegans II. D.L. Riddle, T. Blumenthal, B.J. Meyer, and J.R. Priess, editors, Cold Spring Harbor (NY).

Grewal, S.S., L. Li, A. Orian, R.N. Eisenman, and B.A. Edgar. 2005. Myc-dependent regulation of ribosomal RNA synthesis during Drosophila development. *Nat Cell Biol*. 7:295-302.

Gruneberg, U., M. Glotzer, A. Gartner, and E.A. Nigg. 2002. The CeCDC-14 phosphatase is required for cytokinesis in the Caenorhabditis elegans embryo. *J. Cell Biol.* 158:901-914.

Gruneberg, U., R. Neef, R. Honda, E.A. Nigg, and F.A. Barr. 2004. Relocation of Aurora B from centromeres to the central spindle at the metaphase to anaphase transition requires MKlp2. *J. Cell Biol.* 166:167-172.

Guertin, D.A., and D.M. Sabatini. 2006. Cell Size Control. *In* Encyclopedia of Life Sciences.

Guillot, C., and T. Lecuit. 2013. Adhesion disengagement uncouples intrinsic and extrinsic forces to drive cytokinesis in epithelial tissues. *Developmental cell*. 24:227-241.

Gupta, B.P., W. Hanna-Rose, and P.W. Sternberg. 2012. Morphogenesis of the vulva and the vulval-uterine connection. *WormBook*:1-20.

Hadwiger, J.A., C. Wittenberg, M.D. Mendenhall, and S.I. Reed. 1989. The Saccharomyces cerevisiae CKS1 gene, a homolog of the Schizosaccharomyces pombe suc1+ gene, encodes a subunit of the Cdc28 protein kinase complex. *Mol. Cell. Biol.* 9:2034-2041.

Haldane, J.B.S. 1985. On being the right size and other essays. Oxford University Press.

Hara, K., Y. Maruki, X. Long, K. Yoshino, N. Oshiro, S. Hidayat, C. Tokunaga, J. Avruch, and K. Yonezawa. 2002. Raptor, a binding partner of target of rapamycin (TOR), mediates TOR action. *Cell*. 110:177-189.

Hara, K., K. Yonezawa, Q.P. Weng, M.T. Kozlowski, C. Belham, and J. Avruch. 1998. Amino acid sufficiency and mTOR regulate p70 S6 kinase and eIF-4E BP1 through a common effector mechanism. *J. Biol. Chem.* 273:14484-14494.

Hara, Y., and A. Kimura. 2009. Cell-size-dependent spindle elongation in the Caenorhabditis elegans early embryo. *Curr. Biol.* 19:1549-1554.

Hart, T., M. Chandrashekhar, M. Aregger, Z. Steinhart, K.R. Brown, G. MacLeod, M. Mis, M. Zimmermann, A. Fradet-Turcotte, S. Sun, P. Mero, P. Dirks, S. Sidhu, F.P. Roth, O.S. Rissland, D. Durocher, S. Angers, and J. Moffat. 2015. High-Resolution CRISPR

Screens Reveal Fitness Genes and Genotype-Specific Cancer Liabilities. *Cell*. 163:1515-1526.
Hartmann, V.M.B.-D. 1926. Uber experimentelle Unsterblichkeit von Protozoen-individuen.
Hartwell, L.H., J. Culotti, and B. Reid. 1970. Genetic control of the cell-division cycle in yeast. I. Detection of mutants. *Proc. Natl. Acad. Sci. U. S. A.* 66:352-359.
Hartwell, L.H., R.K. Mortimer, J. Culotti, and M. Culotti. 1973. Genetic Control of the Cell Division Cycle in Yeast: V. Genetic Analysis of cdc Mutants. *Genetics*. 74:267-286.
Heim, A., B. Rymarczyk, and T.U. Mayer. 2017. Regulation of Cell Division. *Adv. Exp. Med. Biol.* 953:83-116.
Heineke, J., and J.D. Molkentin. 2006. Regulation of cardiac hypertrophy by intracellular signalling pathways. *Nat Rev Mol Cell Biol*. 7:589-600.
Heitman, J., N.R. Movva, and M.N. Hall. 1991. Targets for cell cycle arrest by the immunosuppressant rapamycin in yeast. *Science*. 253:905-909.
Henery, C.C., J.B.L. Bard, and M.H. Kaufman. 1992. Tetraploidy in Mice, Embryonic-Cell Number, and the Grain of the Developmental Map. *Dev. Biol.* 152:233-241.
Herrera, A., I. Garcia, N. Gaytan, E. Jones, A. Maldonado, and R. Gilkerson. 2015. Endangered species: mitochondrial DNA loss as a mechanism of human disease. *Front Biosci (Schol Ed)*. 7:109-124.
Herszterg, S., A. Leibfried, F. Bosveld, C. Martin, and Y. Bellaiche. 2013a. Interplay between the dividing cell and its neighbors regulates adherens junction formation during cytokinesis in epithelial tissue. *Developmental cell*. 24:256-270.
Herszterg, S., D. Pinheiro, and Y. Bellaiche. 2013b. A multicellular view of cytokinesis in epithelial tissue. *Trends Cell Biol.*
Hickson, G.R., and P.H. O'Farrell. 2008. Rho-dependent control of anillin behavior during cytokinesis. *J. Cell Biol.* 180:285-294.
Higashi, T., T.R. Arnold, R.E. Stephenson, K.M. Dinshaw, and A.L. Miller. 2016. Maintenance of the Epithelial Barrier and Remodeling of Cell-Cell Junctions during Cytokinesis. *Curr. Biol.* 26:1829-1842.
Hirose, K., T. Kawashima, I. Iwamoto, T. Nosaka, and T. Kitamura. 2001. MgcRacGAP is involved in cytokinesis through associating with mitotic spindle and midbody. *J. Biol. Chem.* 276:5821-5828.
Horvitz, H.R., and P.W. Sternberg. 1991. Multiple intercellular signalling systems control the development of the Caenorhabditis elegans vulva. *Nature*. 351:535-541.
Hoyos, E., K. Kim, J. Milloz, M. Barkoulas, J.B. Penigault, E. Munro, and M.A. Felix. 2011. Quantitative variation in autocrine signaling and pathway crosstalk in the Caenorhabditis vulval network. *Curr. Biol.* 21:527-538.
Hu, C.K., M. Coughlin, C.M. Field, and T.J. Mitchison. 2011. KIF4 Regulates Midzone Length during Cytokinesis. *Curr. Biol.* 21:815-824.
Hwang, W.Y., Y. Fu, D. Reyon, M.L. Maeder, P. Kaini, J.D. Sander, J.K. Joung, R.T. Peterson, and J.R. Yeh. 2013a. Heritable and precise zebrafish genome editing using a CRISPR-Cas system. *PloS one*. 8:e68708.
Hwang, W.Y., Y. Fu, D. Reyon, M.L. Maeder, S.Q. Tsai, J.D. Sander, R.T. Peterson, J.R. Yeh, and J.K. Joung. 2013b. Efficient genome editing in zebrafish using a CRISPR-Cas system. *Nat. Biotechnol.* 31:227-229.
Ihara, S., E.J. Hagedorn, M.A. Morrissey, Q. Chi, F. Motegi, J.M. Kramer, and D.R. Sherwood. 2011. Basement membrane sliding and targeted adhesion remodels tissue

boundaries during uterine-vulval attachment in Caenorhabditis elegans. *Nat Cell Biol*. 13:641-651.
Inoki, K., Y. Li, T. Xu, and K.L. Guan. 2003. Rheb GTPase is a direct target of TSC2 GAP activity and regulates mTOR signaling. *Genes Dev.* 17:1829-1834.
Inoki, K., Y. Li, T. Zhu, J. Wu, and K.L. Guan. 2002. TSC2 is phosphorylated and inhibited by Akt and suppresses mTOR signalling. *Nat Cell Biol*. 4:648-657.
Iritani, B.M., and R.N. Eisenman. 1999. c-Myc enhances protein synthesis and cell size during B lymphocyte development. *Proc. Natl. Acad. Sci. U. S. A*. 96:13180-13185.
Iyer, V.R., C.E. Horak, C.S. Scafe, D. Botstein, M. Snyder, and P.O. Brown. 2001. Genomic binding sites of the yeast cell-cycle transcription factors SBF and MBF. *Nature*. 409:533-538.
Jantsch-Plunger, V., P. Gonczy, A. Romano, H. Schnabel, D. Hamill, R. Schnabel, A.A. Hyman, and M. Glotzer. 2000. CYK-4: A Rho family gtpase activating protein (GAP) required for central spindle formation and cytokinesis. *J. Cell Biol.* 149:1391-1404.
Jefferies, H.B., S. Fumagalli, P.B. Dennis, C. Reinhard, R.B. Pearson, and G. Thomas. 1997. Rapamycin suppresses 5'TOP mRNA translation through inhibition of p70s6k. *EMBO J.* 16:3693-3704.
Jennings, B.H., and D. Ish-Horowicz. 2008. The Groucho/TLE/Grg family of transcriptional co-repressors. *Genome Biol*. 9:205.
Jiang, F., and J.A. Doudna. 2017. CRISPR-Cas9 Structures and Mechanisms. *Annu Rev Biophys*. 46:505-529.
Jiang, W., G. Jimenez, N.J. Wells, T.J. Hope, G.M. Wahl, T. Hunter, and R. Fukunaga. 1998. PRC1: A human mitotic spindle-associated CDK substrate protein required for cytokinesis. *Mol. Cell*. 2:877-885.
Jinek, M., K. Chylinski, I. Fonfara, M. Hauer, J.A. Doudna, and E. Charpentier. 2012. A programmable dual-RNA-guided DNA endonuclease in adaptive bacterial immunity. *Science*. 337:816-821.
Johnston, G.C., J.R. Pringle, and L.H. Hartwell. 1977. Coordination of growth with cell division in the yeast Saccharomyces cerevisiae. *Exp. Cell Res*. 105:79-98.
Johnston, L.A., D.A. Prober, B.A. Edgar, R.N. Eisenman, and P. Gallant. 1999. Drosophila myc regulates cellular growth during development. *Cell*. 98:779-790.
Jorgensen, P., J.L. Nishikawa, B.J. Breitkreutz, and M. Tyers. 2002. Systematic identification of pathways that couple cell growth and division in yeast. *Science*. 297:395-400.
Jorgensen, P., I. Rupes, J.R. Sharom, L. Schneper, J.R. Broach, and M. Tyers. 2004. A dynamic transcriptional network communicates growth potential to ribosome synthesis and critical cell size. *Genes Dev.* 18:2491-2505.
Jorgensen, P., and M. Tyers. 2004. How cells coordinate growth and division. *Curr. Biol.* 14:R1014-R1027.
Kafri, R., J. Levy, M.B. Ginzberg, S. Oh, G. Lahav, and M.W. Kirschner. 2013. Dynamics extracted from fixed cells reveal feedback linking cell growth to cell cycle. *Nature*. 494:480-483.
Kaitna, S., M. Mendoza, V. Jantsch-Plunger, and M. Glotzer. 2000. Incenp and an aurora-like kinase form a complex essential for chromosome segregation and efficient completion of cytokinesis. *Curr. Biol.* 10:1172-1181.
Kamasaki, T., M. Osumi, and I. Mabuchi. 2007. Three-dimensional arrangement of F-actin in the contractile ring of fission yeast. *J. Cell Biol.* 178:765-771.

Kamath, R.S., and J. Ahringer. 2003. Genome-wide RNAi screening in Caenorhabditis elegans. *Methods*. 30:313-321.

Kamath, R.S., A.G. Fraser, Y. Dong, G. Poulin, R. Durbin, M. Gotta, A. Kanapin, N. Le Bot, S. Moreno, M. Sohrmann, D.P. Welchman, P. Zipperlen, and J. Ahringer. 2003. Systematic functional analysis of the Caenorhabditis elegans genome using RNAi. *Nature*. 421:231-237.

Kechad, A., S. Jananji, Y. Ruella, and G.R. Hickson. 2012. Anillin acts as a bifunctional linker coordinating midbody ring biogenesis during cytokinesis. *Curr. Biol.* 22:197-203.

Killander, D., and A. Zetterberg. 1965. A quantitative cytochemical investigation of the relationship between cell mass and initiation of DNA synthesis in mouse fibroblasts in vitro. *Exp. Cell Res.* 40:12-20.

Kim, H., F. Guo, S. Brahma, Y.N. Xing, and M.E. Burkard. 2014. Centralspindlin assembly and 2 phosphorylations on MgcRacGAP by Polo-like kinase 1 initiate Ect2 binding in early cytokinesis. *Cell Cycle*. 13:2952-2961.

Kim, S., Q. Li, C.V. Dang, and L.A. Lee. 2000. Induction of ribosomal genes and hepatocyte hypertrophy by adenovirus-mediated expression of c-Myc in vivo. *Proc. Natl. Acad. Sci. U. S. A*. 97:11198-11202.

Kimball, R.F., S.W. Perdue, E.H. Chu, and J.R. Ortiz. 1971. Microphotometric and autoradiographic studies on the cell cycle and cell size during growth and decline of Chinese hamster cell cultures. *Exp. Cell Res.* 66:17-32.

Kimble, J., and D. Hirsh. 1979. The postembryonic cell lineages of the hermaphrodite and male gonads in Caenorhabditis elegans. *Dev. Biol.* 70:396-417.

Kinoshita, M., C.M. Field, M.L. Coughlin, A.F. Straight, and T.J. Mitchison. 2002. Self- and actin-templated assembly of Mammalian septins. *Developmental cell*. 3:791-802.

Kishi, K., T. Sasaki, S. Kuroda, T. Itoh, and Y. Takai. 1993. Regulation of cytoplasmic division of Xenopus embryo by rho p21 and its inhibitory GDP/GTP exchange protein (rho GDI). *J. Cell Biol.* 120:1187-1195.

Knust, E., and O. Bossinger. 2002. Composition and formation of intercellular junctions in epithelial cells. *Science*. 298:1955-1959.

Koch, C., T. Moll, M. Neuberg, H. Ahorn, and K. Nasmyth. 1993. A role for the transcription factors Mbp1 and Swi4 in progression from G1 to S phase. *Science*. 261:1551-1557.

Konermann, S., M.D. Brigham, A.E. Trevino, J. Joung, O.O. Abudayyeh, C. Barcena, P.D. Hsu, N. Habib, J.S. Gootenberg, H. Nishimasu, O. Nureki, and F. Zhang. 2015. Genome-scale transcriptional activation by an engineered CRISPR-Cas9 complex. *Nature*. 517:583-588.

Koppen, M., J.S. Simske, P.A. Sims, B.L. Firestein, D.H. Hall, A.D. Radice, C. Rongo, and J.D. Hardin. 2001. Cooperative regulation of AJM-1 controls junctional integrity in Caenorhabditis elegans epithelia. *Nat Cell Biol*. 3:983-991.

Kornfeld, K. 1997. Vulval development in Caenorhabditis elegans. *Trends Genet.* 13:55-61.

Kosako, H., T. Yoshida, F. Matsumura, T. Ishizaki, S. Narumiya, and M. Inagaki. 2000. Rho-kinase/ROCK is involved in cytokinesis through the phosphorylation of myosin light chain and not ezrin/radixin/moesin proteins at the cleavage furrow. *Oncogene*. 19:6059-6064.

Lacroix, B., K.G. Bourdages, J.F. Dorn, S. Ihara, D.R. Sherwood, P.S. Maddox, and A.S. Maddox. 2014. In situ imaging in C. elegans reveals developmental regulation of microtubule dynamics. *Developmental cell*. 29:203-216.

Lacroix, B., and A.S. Maddox. 2012. Cytokinesis, ploidy and aneuploidy. *J. Pathol.* 226:338-351.

Ladouceur, A.M., J.F. Dorn, and P.S. Maddox. 2015. Mitotic chromosome length scales in response to both cell and nuclear size. *J. Cell Biol.* 209:645-651.

Laplante, M., and D.M. Sabatini. 2013. Regulation of mTORC1 and its impact on gene expression at a glance. *J. Cell Sci.* 126:1713-1719.

Larson, M.H., L.A. Gilbert, X. Wang, W.A. Lim, J.S. Weissman, and L.S. Qi. 2013. CRISPR interference (CRISPRi) for sequence-specific control of gene expression. *Nat Protoc*. 8:2180-2196.

Leevers, S.J., D. Weinkove, L.K. MacDougall, E. Hafen, and M.D. Waterfield. 1996. The Drosophila phosphoinositide 3-kinase Dp110 promotes cell growth. *EMBO J.* 15:6584-6594.

Lempiainen, H., A. Uotila, J. Urban, I. Dohnal, G. Ammerer, R. Loewith, and D. Shore. 2009. Sfp1 interaction with TORC1 and Mrs6 reveals feedback regulation on TOR signaling. *Mol. Cell*. 33:704-716.

Levy, D.L., and R. Heald. 2012. Mechanisms of intracellular scaling. *Annu. Rev. Cell Dev. Biol.* 28:113-135.

Lewellyn, L., A. Carvalho, A. Desai, A.S. Maddox, and K. Oegema. 2011. The chromosomal passenger complex and centralspindlin independently contribute to contractile ring assembly. *J. Cell Biol.* 193:155-169.

Lewellyn, L., J. Dumont, A. Desai, and K. Oegema. 2010. Analyzing the Effects of Delaying Aster Separation on Furrow Formation during Cytokinesis in the Caenorhabditis elegans Embryo. *Mol. Biol. Cell*. 21:50-62.

Liang, F., M. Han, P.J. Romanienko, and M. Jasin. 1998. Homology-directed repair is a major double-strand break repair pathway in mammalian cells. *Proc. Natl. Acad. Sci. U. S. A.* 95:5172-5177.

Linderson, Y., D. Eberhard, S. Malin, A. Johansson, M. Busslinger, and S. Pettersson. 2004. Corecruitment of the Grg4 repressor by PU.1 is critical for Pax5-mediated repression of B-cell-specific genes. *EMBO Rep*. 5:291-296.

Liu, G.J., L. Cimmino, J.G. Jude, Y. Hu, M.T. Witkowski, M.D. McKenzie, M. Kartal-Kaess, S.A. Best, L. Tuohey, Y. Liao, W. Shi, C.G. Mullighan, M.A. Farrar, S.L. Nutt, G.K. Smyth, J. Zuber, and R.A. Dickins. 2014. Pax5 loss imposes a reversible differentiation block in B-progenitor acute lymphoblastic leukemia. *Genes Dev.* 28:1337-1350.

Liu, J., G.D. Fairn, D.F. Ceccarelli, F. Sicheri, and A. Wilde. 2012. Cleavage furrow organization requires PIP(2)-mediated recruitment of anillin. *Curr. Biol.* 22:64-69.

Lloyd, A.C. 2013. The regulation of cell size. *Cell*. 154:1194-1205.

Loewith, R., and M.N. Hall. 2011. Target of rapamycin (TOR) in nutrient signaling and growth control. *Genetics*. 189:1177-1201.

Loewith, R., E. Jacinto, S. Wullschleger, A. Lorberg, J.L. Crespo, D. Bonenfant, W. Oppliger, P. Jenoe, and M.N. Hall. 2002. Two TOR complexes, only one of which is rapamycin sensitive, have distinct roles in cell growth control. *Mol. Cell*. 10:457-468.

Long, X., C. Spycher, Z.S. Han, A.M. Rose, F. Muller, and J. Avruch. 2002. TOR deficiency in C. elegans causes developmental arrest and intestinal atrophy by inhibition of mRNA translation. *Curr. Biol.* 12:1448-1461.

Loughlin, R., J.D. Wilbur, F.J. McNally, F.J. Nedelec, and R. Heald. 2011. Katanin Contributes to Interspecies Spindle Length Scaling in Xenopus. *Cell*. 147:1397-1407.

Lozano, E., A.G. Saez, A.J. Flemming, A. Cunha, and A.M. Leroi. 2006. Regulation of growth by ploidy in Caenorhabditis elegans. *Curr. Biol.* 16:493-498.

Lynch, A.M., and J. Hardin. 2009. The assembly and maintenance of epithelial junctions in C. elegans. *Front Biosci (Landmark Ed)*. 14:1414-1432.

Ma, H., L.C. Tu, A. Naseri, M. Huisman, S. Zhang, D. Grunwald, and T. Pederson. 2016. Multiplexed labeling of genomic loci with dCas9 and engineered sgRNAs using CRISPRainbow. *Nat. Biotechnol.* 34:528-530.

Ma, X., M. Kovacs, M.A. Conti, A. Wang, Y. Zhang, J.R. Sellers, and R.S. Adelstein. 2012. Nonmuscle myosin II exerts tension but does not translocate actin in vertebrate cytokinesis. *Proc. Natl. Acad. Sci. U. S. A.* 109:4509-4514.

Ma, X.M., and J. Blenis. 2009. Molecular mechanisms of mTOR-mediated translational control. *Nat Rev Mol Cell Biol*. 10:307-318.

Mabuchi, I. 1990. Cleavage furrow formation and actin-modulating proteins. *Ann. N. Y. Acad. Sci.* 582:131-146.

Mabuchi, I., S. Tsukita, S. Tsukita, and T. Sawai. 1988. Cleavage furrow isolated from newt eggs: contraction, organization of the actin filaments, and protein components of the furrow. *Proc. Natl. Acad. Sci. U. S. A.* 85:5966-5970.

Maciak, S., E. Bonda-Ostaszewska, M. Czarnoleski, M. Konarzewski, and J. Kozlowski. 2014. Mice divergently selected for high and low basal metabolic rates evolved different cell size and organ mass. *J Evol Biol*. 27:478-487.

Maddox, A.S., L. Lewellyn, A. Desai, and K. Oegema. 2007. Anillin and the septins promote asymmetric ingression of the cytokinetic furrow. *Developmental cell*. 12:827-835.

Mali, P., L. Yang, K.M. Esvelt, J. Aach, M. Guell, J.E. DiCarlo, J.E. Norville, and G.M. Church. 2013. RNA-guided human genome engineering via Cas9. *Science*. 339:823-826.

Malumbres, M. 2014. Cyclin-dependent kinases. *Genome Biol*. 15:122.

Mancuso, V.P., J.M. Parry, L. Storer, C. Poggioli, K.C. Nguyen, D.H. Hall, and M.V. Sundaram. 2012. Extracellular leucine-rich repeat proteins are required to organize the apical extracellular matrix and maintain epithelial junction integrity in C. elegans. *Development*. 139:979-990.

Manguso, R.T., H.W. Pope, M.D. Zimmer, F.D. Brown, K.B. Yates, B.C. Miller, N.B. Collins, K. Bi, M.W. LaFleur, V.R. Juneja, S.A. Weiss, J. Lo, D.E. Fisher, D. Miao, E. Van Allen, D.E. Root, A.H. Sharpe, J.G. Doench, and W.N. Haining. 2017. In vivo CRISPR screening identifies Ptpn2 as a cancer immunotherapy target. *Nature*. 547:413-418.

Maniloff, J., and H.J. Morowitz. 1972. Cell biology of the mycoplasmas. *Bacteriol. Rev.* 36:263-290.

Marshall, W.F., K.D. Young, M. Swaffer, E. Wood, P. Nurse, A. Kimura, J. Frankel, J. Wallingford, V. Walbot, X. Qu, and A.H.K. Roeder. 2012. What determines cell size? *Bmc Biology*. 10.

Mastronarde, D.N., K.L. Mcdonald, R. Ding, and J.R. Mcintosh. 1993. Interpolar Spindle Microtubules in Ptk Cells. *J. Cell Biol.* 123:1475-1489.

Matus, D.Q., E. Chang, S.C. Makohon-Moore, M.A. Hagedorn, Q. Chi, and D.R. Sherwood. 2014. Cell division and targeted cell cycle arrest opens and stabilizes basement membrane gaps. *Nature communications*. 5:4184.

Mavrakis, M., Y. Azou-Gros, F.C. Tsai, J. Alvarado, A. Bertin, F. Iv, A. Kress, S. Brasselet, G.H. Koenderink, and T. Lecuit. 2014. Septins promote F-actin ring formation by crosslinking actin filaments into curved bundles. *Nat Cell Biol*. 16:322-334.

Melmed, S. 2009. Acromegaly pathogenesis and treatment. *J. Clin. Invest.* 119:3189-3202.

Mendes Pinto, I., B. Rubinstein, A. Kucharavy, J.R. Unruh, and R. Li. 2012. Actin depolymerization drives actomyosin ring contraction during budding yeast cytokinesis. *Developmental cell*. 22:1247-1260.

Miller, A.L., and W.M. Bement. 2009. Regulation of cytokinesis by Rho GTPase flux. *Nat Cell Biol*. 11:71-77.

Minoshima, Y., T. Kawashima, K. Hirose, Y. Tonozuka, A. Kawajiri, Y.C. Bao, X. Deng, M. Tatsuka, S. Narumiya, W.S. May, Jr., T. Nosaka, K. Semba, T. Inoue, T. Satoh, M. Inagaki, and T. Kitamura. 2003. Phosphorylation by aurora B converts MgcRacGAP to a RhoGAP during cytokinesis. *Developmental cell*. 4:549-560.

Mishima, M., S. Kaitna, and M. Glotzer. 2002. Central spindle assembly and cytokinesis require a kinesin-like protein/RhoGAP complex with microtubule bundling activity. *Developmental cell*. 2:41-54.

Mishima, M., V. Pavicic, N. Gruneberg, E.A. Nigg, and M. Glotzer. 2004. Cell cycle regulation of central spindle assembly. *Nature*. 430:908-913.

Mollinari, C., J.P. Kleman, W. Jiang, G. Schoehn, T. Hunter, and R.L. Margolis. 2002. PRC1 is a microtubule binding and bundling protein essential to maintain the mitotic spindle midzone. *J. Cell Biol.* 157:1175-1186.

Montagne, J., M.J. Stewart, H. Stocker, E. Hafen, S.C. Kozma, and G. Thomas. 1999. Drosophila S6 kinase: a regulator of cell size. *Science*. 285:2126-2129.

Montgomery, M.K., and A. Fire. 1998. Double-stranded RNA as a mediator in sequence-specific genetic silencing and co-suppression. *Trends Genet.* 14:255-258.

Montgomery, M.K., S. Xu, and A. Fire. 1998. RNA as a target of double-stranded RNA-mediated genetic interference in Caenorhabditis elegans. *Proc. Natl. Acad. Sci. U. S. A.* 95:15502-15507.

Morais-de-Sa, E., and C. Sunkel. 2013a. Adherens junctions determine the apical position of the midbody during follicular epithelial cell division. *EMBO Rep*. 14:696-703.

Morais-de-Sa, E., and C.E. Sunkel. 2013b. Connecting polarized cytokinesis to epithelial architecture. *Cell Cycle*. 12:3583-3584.

Mortimer, R.K. 1958. Radiobiological and Genetic Studies on a Polyploid Series (Haploid to Hexaploid) of Saccharomyces-Cerevisiae. *Radiat. Res.* 9:312-326.

Mundkur, B.D. 1953. Interphase nuclei and cell sizes in a polyploid series of Saccharomyces. *Experientia*. 9:373-374.

Munoz, D.M., P.J. Cassiani, L. Li, E. Billy, J.M. Korn, M.D. Jones, J. Golji, D.A. Ruddy, K. Yu, G. McAllister, A. DeWeck, D. Abramowski, J. Wan, M.D. Shirley, S.Y. Neshat, D. Rakiec, R. de Beaumont, O. Weber, A. Kauffmann, E.R. McDonald, 3rd, N. Keen, F. Hofmann, W.R. Sellers, T. Schmelzle, F. Stegmeier, and M.R. Schlabach. 2016. CRISPR Screens Provide a Comprehensive Assessment of Cancer Vulnerabilities but Generate False-Positive Hits for Highly Amplified Genomic Regions. *Cancer Discov*. 6:900-913.

Munro, E., J. Nance, and J.R. Priess. 2004. Cortical flows powered by asymmetrical contraction transport PAR proteins to establish and maintain anterior-posterior polarity in the early C. elegans embryo. *Developmental cell*. 7:413-424.

Muschen, M. 2015. Rationale for targeting the pre-B-cell receptor signaling pathway in acute lymphoblastic leukemia. *Blood*. 125:3688-3693.

Nash, R., G. Tokiwa, S. Anand, K. Erickson, and A.B. Futcher. 1988. The WHI1+ gene of Saccharomyces cerevisiae tethers cell division to cell size and is a cyclin homolog. *EMBO J.* 7:4335-4346.

Neef, R., C. Preisinger, J. Sutcliffe, R. Kopajtich, E.A. Nigg, T.U. Mayer, and F.A. Barr. 2003. Phosphorylation of mitotic kinesin-like protein 2 by polo-like kinase 1 is required for cytokinesis. *J. Cell Biol.* 162:863-875.

Neufeld, T.P., A.F. de la Cruz, L.A. Johnston, and B.A. Edgar. 1998. Coordination of growth and cell division in the Drosophila wing. *Cell*. 93:1183-1193.

Neufeld, T.P., and B.A. Edgar. 1998. Connections between growth and the cell cycle. *Curr. Opin. Cell Biol.* 10:784-790.

Newman, A.P., J.G. White, and P.W. Sternberg. 1996. Morphogenesis of the C. elegans hermaphrodite uterus. *Development*. 122:3617-3626.

Nishimura, Y., and S. Yonemura. 2006. Centralspindlin regulates ECT2 and RhoA accumulation at the equatorial cortex during cytokinesis. *J. Cell Sci.* 119:104-114.

Nurse, P. 1975. Genetic control of cell size at cell division in yeast. *Nature*. 256:547-551.

Nutt, S.L., D. Eberhard, M. Horcher, A.G. Rolink, and M. Busslinger. 2001. Pax5 determines the identity of B cells from the beginning to the end of B-lymphopoiesis. *Int. Rev. Immunol.* 20:65-82.

O'Connell, C.B., S.P. Wheatley, S. Ahmed, and Y.L. Wang. 1999. The small GTP-binding protein rho regulates cortical activities in cultured cells during division. *J. Cell Biol.* 144:305-313.

Odell, G.M., and V.E. Foe. 2008. An agent-based model contrasts opposite effects of dynamic and stable microtubules on cleavage furrow positioning. *J. Cell Biol.* 183:471-483.

Oegema, K., M.S. Savoian, T.J. Mitchison, and C.M. Field. 2000. Functional analysis of a human homologue of the Drosophila actin binding protein anillin suggests a role in cytokinesis. *J. Cell Biol.* 150:539-552.

Oldham, S., R. Bohni, H. Stocker, W. Brogiolo, and E. Hafen. 2000. Genetic control of size in Drosophila. *Philos. Trans. R. Soc. Lond. B. Biol. Sci.* 355:945-952.

Otto, J.J., and T.E. Schroeder. 1990. Association of actin and myosin in the contractile ring. *Ann. N. Y. Acad. Sci.* 582:179-184.

Pardee, A.B. 1974. A restriction point for control of normal animal cell proliferation. *Proc. Natl. Acad. Sci. U. S. A.* 71:1286-1290.

Park, K., L.J. Millet, N. Kim, H. Li, X. Jin, G. Popescu, N.R. Aluru, K.J. Hsia, and R. Bashir. 2010. Measurement of adherent cell mass and growth. *Proc. Natl. Acad. Sci. U. S. A.* 107:20691-20696.

Patel, S.J., N.E. Sanjana, R.J. Kishton, A. Eidizadeh, S.K. Vodnala, M. Cam, J.J. Gartner, L. Jia, S.M. Steinberg, T.N. Yamamoto, A.S. Merchant, G.U. Mehta, A. Chichura, O. Shalem, E. Tran, R. Eil, M. Sukumar, E.P. Guijarro, C.P. Day, P. Robbins, S. Feldman, G. Merlino, F. Zhang, and N.P. Restifo. 2017. Identification of essential genes for cancer immunotherapy. *Nature*. 548:537-542.

Pavicic-Kaltenbrunner, V., M. Mishima, and M. Glotzer. 2007. Cooperative assembly of CYK-4/MgcRacGAP and ZEN-4/MKLP1 to form the centralspindlin complex. *Mol. Biol. Cell*. 18:4992-5003.

Pende, M., S.H. Um, V. Mieulet, M. Sticker, V.L. Goss, J. Mestan, M. Mueller, S. Fumagalli, S.C. Kozma, and G. Thomas. 2004. S6K1(-/-)/S6K2(-/-) mice exhibit perinatal lethality and rapamycin-sensitive 5'-terminal oligopyrimidine mRNA translation and reveal a mitogen-activated protein kinase-dependent S6 kinase pathway. *Mol. Cell. Biol.* 24:3112-3124.

Piekny, A., M. Werner, and M. Glotzer. 2005. Cytokinesis: welcome to the Rho zone. *Trends Cell Biol.* 15:651-658.

Piekny, A.J., and M. Glotzer. 2008. Anillin is a scaffold protein that links RhoA, actin, and myosin during cytokinesis. *Curr. Biol.* 18:30-36.

Piekny, A.J., and A.S. Maddox. 2010. The myriad roles of Anillin during cytokinesis. *Semin. Cell Dev. Biol.* 21:881-891.

Potter, C.J., L.G. Pedraza, and T. Xu. 2002. Akt regulates growth by directly phosphorylating Tsc2. *Nat Cell Biol*. 4:658-665.

Powers, J., O. Bossinger, D. Rose, S. Strome, and W. Saxton. 1998. A nematode kinesin required for cleavage furrow advancement. *Curr. Biol.* 8:1133-1136.

Prescott, D.M. 1956a. Relation between Cell Growth and Cell Division .2. The Effect of Cell Size on Cell Growth Rate and Generation Time in Amoeba Proteus. *Exp. Cell Res.* 11:86-98.

Prescott, D.M. 1956b. Relation between cell growth and cell division. III. Changes in nuclear volume and growth rate and prevention of cell division in Amoeba proteus resulting from cytoplasmic amputations. *Exp. Cell Res.* 11:94-98.

Prokopenko, S.N., A. Brumby, L. O'Keefe, L. Prior, Y. He, R. Saint, and H.J. Bellen. 1999. A putative exchange factor for Rho1 GTPase is required for initiation of cytokinesis in Drosophila. *Genes Dev.* 13:2301-2314.

Purves, D., W.D. Snider, and J.T. Voyvodic. 1988. Trophic regulation of nerve cell morphology and innervation in the autonomic nervous system. *Nature*. 336:123-128.

Raich, W.B., A.N. Moran, J.H. Rothman, and J. Hardin. 1998. Cytokinesis and midzone microtubule organization in Caenorhabditis elegans require the kinesin-like protein ZEN-4. *Mol. Biol. Cell*. 9:2037-2049.

Ran, F.A., P.D. Hsu, J. Wright, V. Agarwala, D.A. Scott, and F. Zhang. 2013. Genome engineering using the CRISPR-Cas9 system. *Nat Protoc*. 8:2281-2308.

Ranjan, A., B.T. Townsley, Y. Ichihashi, N.R. Sinha, and D.H. Chitwood. 2015. An intracellular transcriptomic atlas of the giant coenocyte Caulerpa taxifolia. *PLoS Genet*. 11:e1004900.

Rappaport, R. 1961. Experiments Concerning Cleavage Stimulus in Sand Dollar Eggs. *J. Exp. Zool.* 148:81-&.

Rappaport, R. 1985. Repeated Furrow Formation from a Single Mitotic Apparatus in Cylindrical Sand Dollar Eggs. *J. Exp. Zool.* 234:167-171.

Rappe, M.S., S.A. Connon, K.L. Vergin, and S.J. Giovannoni. 2002. Cultivation of the ubiquitous SAR11 marine bacterioplankton clade. *Nature*. 418:630-633.

Rathmell, J.C., M.G. Vander Heiden, M.H. Harris, K.A. Frauwirth, and C.B. Thompson. 2000. In the absence of extrinsic signals, nutrient utilization by lymphocytes is insufficient to maintain either cell size or viability. *Mol. Cell*. 6:683-692.

Reber, S., and N.W. Goehring. 2015. Intracellular Scaling Mechanisms. *Cold Spring Harb Perspect Biol*. 7.

Reinsch, S., and E. Karsenti. 1994. Orientation of spindle axis and distribution of plasma membrane proteins during cell division in polarized MDCKII cells. *J. Cell Biol.* 126:1509-1526.

Richardson, H.E., C. Wittenberg, F. Cross, and S.I. Reed. 1989. An essential G1 function for cyclin-like proteins in yeast. *Cell*. 59:1127-1133.

Rickert, R.C. 2013. New insights into pre-BCR and BCR signalling with relevance to B cell malignancies. *Nat Rev Immunol*. 13:578-591.

Ririe, T.O., J.S. Fernandes, and P.W. Sternberg. 2008. The Caenorhabditis elegans vulva: a post-embryonic gene regulatory network controlling organogenesis. *Proc. Natl. Acad. Sci. U. S. A.* 105:20095-20099.

Roh-Johnson, M., and B. Goldstein. 2009. In vivo roles for Arp2/3 in cortical actin organization during C. elegans gastrulation. *J. Cell Sci.* 122:3983-3993.

Saffer, A.M., D.H. Kim, A. van Oudenaarden, and H.R. Horvitz. 2011. The Caenorhabditis elegans synthetic multivulva genes prevent ras pathway activation by tightly repressing global ectopic expression of lin-3 EGF. *PLoS Genet*. 7:e1002418.

Saleh-Gohari, N., and T. Helleday. 2004. Conservative homologous recombination preferentially repairs DNA double-strand breaks in the S phase of the cell cycle in human cells. *Nucleic Acids Res*. 32:3683-3688.

Salmon, E.D., and S.M. Wolniak. 1990. Role of Microtubules in Stimulating Cytokinesis in Animal-Cells. *Ann. N. Y. Acad. Sci.* 582:88-98.

Sancak, Y., L. Bar-Peled, R. Zoncu, A.L. Markhard, S. Nada, and D.M. Sabatini. 2010. Ragulator-Rag complex targets mTORC1 to the lysosomal surface and is necessary for its activation by amino acids. *Cell*. 141:290-303.

Sancak, Y., T.R. Peterson, Y.D. Shaul, R.A. Lindquist, C.C. Thoreen, L. Bar-Peled, and D.M. Sabatini. 2008. The Rag GTPases bind raptor and mediate amino acid signaling to mTORC1. *Science*. 320:1496-1501.

Sanger, J.M., and J.W. Sanger. 1980. Banding and polarity of actin filaments in interphase and cleaving cells. *J. Cell Biol.* 86:568-575.

Santamaria, D., C. Barriere, A. Cerqueira, S. Hunt, C. Tardy, K. Newton, J.F. Caceres, P. Dubus, M. Malumbres, and M. Barbacid. 2007. Cdk1 is sufficient to drive the mammalian cell cycle. *Nature*. 448:811-815.

Saucedo, L.J., X. Gao, D.A. Chiarelli, L. Li, D. Pan, and B.A. Edgar. 2003. Rheb promotes cell growth as a component of the insulin/TOR signalling network. *Nat Cell Biol*. 5:566-571.

Schindler, A.J., and D.R. Sherwood. 2013. Morphogenesis of the caenorhabditis elegans vulva. *Wiley Interdiscip Rev Dev Biol*. 2:75-95.

Schroeder, T.E. 1970. The contractile ring. I. Fine structure of dividing mammalian (HeLa) cells and the effects of cytochalasin B. *Z. Zellforsch. Mikrosk. Anat.* 109:431-449.

Schroeder, T.E. 1972. Contractile Ring .2. Determining Its Brief Existence, Volumetric Changes, and Vital Role in Cleaving Arbacia Eggs. *J. Cell Biol.* 53:419-+.

Segbert, C., K. Johnson, C. Theres, D. van Fürden, and O. Bossinger. 2004. Molecular and functional analysis of apical junction formation in the gut epithelium of Caenorhabditis elegans. *Dev. Biol.* 266:17-26.

Sengupta, S., T.R. Peterson, and D.M. Sabatini. 2010. Regulation of the mTOR complex 1 pathway by nutrients, growth factors, and stress. *Mol. Cell*. 40:310-322.

Severson, A.F., D.R. Hamill, J.C. Carter, J. Schumacher, and B. Bowerman. 2000. The Aurora-related kinase AIR-2 recruits ZEN-4/CeMKLP1 to the mitotic spindle at metaphase and is required for cytokinesis. *Curr. Biol.* 10:1162-1171.

Shalem, O., N.E. Sanjana, E. Hartenian, X. Shi, D.A. Scott, T. Mikkelson, D. Heckl, B.L. Ebert, D.E. Root, J.G. Doench, and F. Zhang. 2014. Genome-scale CRISPR-Cas9 knockout screening in human cells. *Science*. 343:84-87.

Sharma-Kishore, R., J.G. White, E. Southgate, and B. Podbilewicz. 1999. Formation of the vulva in Caenorhabditis elegans: a paradigm for organogenesis. *Development*. 126:691-699.

Shields, R., R.F. Brooks, P.N. Riddle, D.F. Capellaro, and D. Delia. 1978. Cell size, cell cycle and transition probability in mouse fibroblasts. *Cell*. 15:469-474.

Shima, H., M. Pende, Y. Chen, S. Fumagalli, G. Thomas, and S.C. Kozma. 1998. Disruption of the p70(s6k)/p85(s6k) gene reveals a small mouse phenotype and a new functional S6 kinase. *EMBO J.* 17:6649-6659.

Shioi, T., J.R. McMullen, P.M. Kang, P.S. Douglas, T. Obata, T.F. Franke, L.C. Cantley, and S. Izumo. 2002. Akt/protein kinase B promotes organ growth in transgenic mice. *Mol. Cell. Biol.* 22:2799-2809.

Sidorova, J., and L. Breeden. 1993. Analysis of the SWI4/SWI6 protein complex, which directs G1/S-specific transcription in Saccharomyces cerevisiae. *Mol. Cell. Biol.* 13:1069-1077.

Silkworth, W.T., I.K. Nardi, L.M. Scholl, and D. Cimini. 2009. Multipolar spindle pole coalescence is a major source of kinetochore mis-attachment and chromosome mis-segregation in cancer cells. *PloS one*. 4:e6564.

Simmer, F., M. Tijsterman, S. Parrish, S.P. Koushika, M.L. Nonet, A. Fire, J. Ahringer, and R.H. Plasterk. 2002. Loss of the putative RNA-directed RNA polymerase RRF-3 makes C. elegans hypersensitive to RNAi. *Curr. Biol.* 12:1317-1319.

Simon, I., J. Barnett, N. Hannett, C.T. Harbison, N.J. Rinaldi, T.L. Volkert, J.J. Wyrick, J. Zeitlinger, D.K. Gifford, T.S. Jaakkola, and R.A. Young. 2001. Serial regulation of transcriptional regulators in the yeast cell cycle. *Cell*. 106:697-708.

Singh, J., and M. Tyers. 2009. A Rab escort protein integrates the secretion system with TOR signaling and ribosome biogenesis. *Genes Dev.* 23:1944-1958.

Skorobogata, O., J.M. Escobar-Restrepo, and C.E. Rocheleau. 2014. An AGEF-1/Arf GTPase/AP-1 ensemble antagonizes LET-23 EGFR basolateral localization and signaling during C. elegans vulva induction. *PLoS Genet*. 10:e1004728.

Skotheim, J.M., S. Di Talia, E.D. Siggia, and F.R. Cross. 2008. Positive feedback of G1 cyclins ensures coherent cell cycle entry. *Nature*. 454:291-296.

Smith, A.V., and T.L. Orr-Weaver. 1991. The regulation of the cell cycle during Drosophila embryogenesis: the transition to polyteny. *Development*. 112:997-1008.

Smith, M.L., J.N. Bruhn, and J.B. Anderson. 1992. The Fungus Armillaria-Bulbosa Is among the Largest and Oldest Living Organisms. *Nature*. 356:428-431.

Somers, W.G., and R. Saint. 2003. A RhoGEF and Rho family GTPase-activating protein complex links the contractile ring to cortical microtubles at the onset of cytokinesis. *Developmental cell*. 4:29-39.

Son, S., A. Tzur, Y. Weng, P. Jorgensen, J. Kim, M.W. Kirschner, and S.R. Manalis. 2012. Direct observation of mammalian cell growth and size regulation. *Nat Methods*. 9:910-912.

Sonnichsen, B., L.B. Koski, A. Walsh, P. Marschall, B. Neumann, M. Brehm, A.M. Alleaume, J. Artelt, P. Bettencourt, E. Cassin, M. Hewitson, C. Holz, M. Khan, S. Lazik, C. Martin, B. Nitzsche, M. Ruer, J. Stamford, M. Winzi, R. Heinkel, M. Roder, J. Finell, H. Hantsch, S.J. Jones, M. Jones, F. Piano, K.C. Gunsalus, K. Oegema, P. Gonczy, A. Coulson, A.A. Hyman, and C.J. Echeverri. 2005. Full-genome RNAi profiling of early embryogenesis in Caenorhabditis elegans. *Nature*. 434:462-469.

Soto, X., J. Li, R. Lea, E. Dubaissi, N. Papalopulu, and E. Amaya. 2013. Inositol kinase and its product accelerate wound healing by modulating calcium levels, Rho GTPases, and F-actin assembly. *Proc. Natl. Acad. Sci. U. S. A.* 110:11029-11034.

Sternberg, P.W. 1988. Lateral inhibition during vulval induction in Caenorhabditis elegans. *Nature*. 335:551-554.

Sternberg, P.W. 2005. Vulval development. *WormBook*:1-28.

Sternberg, P.W., and H.R. Horvitz. 1986. Pattern formation during vulval development in C. elegans. *Cell*. 44:761-772.

Sternberg, P.W., and H.R. Horvitz. 1989. The combined action of two intercellular signaling pathways specifies three cell fates during vulval induction in C. elegans. *Cell*. 58:679-693.

Stiernagle, T. 2006. Maintenance of C. elegans. *WormBook*:1-11.

Straight, A.F., C.M. Field, and T.J. Mitchison. 2005. Anillin binds nonmuscle myosin II and regulates the contractile ring. *Mol. Biol. Cell*. 16:193-201.

Su, K.C., T. Takaki, and M. Petronczki. 2011. Targeting of the RhoGEF Ect2 to the equatorial membrane controls cleavage furrow formation during cytokinesis. *Developmental cell*. 21:1104-1115.

Sudbery, P. 2002. Cell biology. When wee meets whi. *Science*. 297:351-352.

Sudbery, P.E., A.R. Goodey, and B.L. Carter. 1980. Genes which control cell proliferation in the yeast Saccharomyces cerevisiae. *Nature*. 288:401-404.

Sulston, J.E., and H.R. Horvitz. 1977. Post-embryonic cell lineages of the nematode, Caenorhabditis elegans. *Dev. Biol.* 56:110-156.

Sulston, J.E., E. Schierenberg, J.G. White, and J.N. Thomson. 1983. The embryonic cell lineage of the nematode Caenorhabditis elegans. *Dev. Biol.* 100:64-119.

Sulston, J.E., and J.G. White. 1980. Regulation and cell autonomy during postembryonic development of Caenorhabditis elegans. *Dev. Biol.* 78:577-597.

Sun, L., R. Guan, I.J. Lee, Y. Liu, M. Chen, J. Wang, J.Q. Wu, and Z. Chen. 2015. Mechanistic insights into the anchorage of the contractile ring by anillin and Mid1. *Developmental cell*. 33:413-426.

Takeichi, M. 2011. Self-organization of animal tissues: cadherin-mediated processes. *Developmental cell*. 21:24-26.

Tanaka-Takiguchi, Y., M. Kinoshita, and K. Takiguchi. 2009. Septin-mediated uniform bracing of phospholipid membranes. *Curr. Biol.* 19:140-145.

Tatsumoto, T., X. Xie, R. Blumenthal, I. Okamoto, and T. Miki. 1999. Human ECT2 is an exchange factor for Rho GTPases, phosphorylated in G2/M phases, and involved in cytokinesis. *J. Cell Biol.* 147:921-928.

Terada, Y., M. Tatsuka, F. Suzuki, Y. Yasuda, S. Fujita, and M. Otsu. 1998. AIM-1: a mammalian midbody-associated protein required for cytokinesis. *EMBO J.* 17:667-676.

Toledo, C.M., Y. Ding, P. Hoellerbauer, R.J. Davis, R. Basom, E.J. Girard, E. Lee, P. Corrin, T. Hart, H. Bolouri, J. Davison, Q. Zhang, J. Hardcastle, B.J. Aronow, C.L. Plaisier, N.S. Baliga, J. Moffat, Q. Lin, X.N. Li, D.H. Nam, J. Lee, S.M. Pollard, J. Zhu, J.J. Delrow, B.E. Clurman, J.M. Olson, and P.J. Paddison. 2015. Genome-wide CRISPR-Cas9 Screens Reveal Loss of Redundancy between PKMYT1 and WEE1 in Glioblastoma Stem-like Cells. *Cell Rep*. 13:2425-2439.

Turlier, H., B. Audoly, J. Prost, and J.F. Joanny. 2014. Furrow constriction in animal cell cytokinesis. *Biophys. J.* 106:114-123.

Turner, J.J., J.C. Ewald, and J.M. Skotheim. 2012. Cell Size Control in Yeast. *Curr. Biol.* 22:R350-R359.

Tyers, M., G. Tokiwa, and B. Futcher. 1993. Comparison of the Saccharomyces cerevisiae G1 cyclins: Cln3 may be an upstream activator of Cln1, Cln2 and other cyclins. *EMBO J.* 12:1955-1968.

Tzur, A., R. Kafri, V.S. LeBleu, G. Lahav, and M.W. Kirschner. 2009. Cell growth and size homeostasis in proliferating animal cells. *Science*. 325:167-171.

Uetake, Y., and G. Sluder. 2004. Cell cycle progression after cleavage failure: mammalian somatic cells do not possess a "tetraploidy checkpoint". *J. Cell Biol.* 165:609-615.

Urban, J., A. Soulard, A. Huber, S. Lippman, D. Mukhopadhyay, O. Deloche, V. Wanke, D. Anrather, G. Ammerer, H. Riezman, J.R. Broach, C. De Virgilio, M.N. Hall, and R. Loewith. 2007. Sch9 is a major target of TORC1 in Saccharomyces cerevisiae. *Mol. Cell*. 26:663-674.

Uwins, P.J.R., R.I. Webb, and A.P. Taylor. 1998. Novel nano-organisms from Australian sandstones. *Am Mineral*. 83:1541-1550.

van Zelm, M.C., M. van der Burg, D. de Ridder, B.H. Barendregt, E.F. de Haas, M.J. Reinders, A.C. Lankester, T. Revesz, F.J. Staal, and J.J. van Dongen. 2005. Ig gene rearrangement steps are initiated in early human precursor B cell subsets and correlate with specific transcription factor expression. *J. Immunol.* 175:5912-5922.

Verbrugghe, K.J., and J.G. White. 2007. Cortical centralspindlin and G alpha have parallel roles in furrow initiation in early C. elegans embryos. *J. Cell Sci.* 120:1772-1778.

Verbrugghe, K.J.C., and J.G. White. 2004. SPD-1 is required for the formation of the spindle midzone but is not essential for the completion of cytokinesis in C. elegans embryos (vol 14, pg 1755, 2004). *Curr. Biol.* 14:2311-2311.

Verdu, J., M.A. Buratovich, E.L. Wilder, and M.J. Birnbaum. 1999. Cell-autonomous regulation of cell and organ growth in Drosophila by Akt/PKB. *Nat Cell Biol*. 1:500-506.

Wang, H., H. Yang, C.S. Shivalila, M.M. Dawlaty, A.W. Cheng, F. Zhang, and R. Jaenisch. 2013. One-step generation of mice carrying mutations in multiple genes by CRISPR/Cas-mediated genome engineering. *Cell*. 153:910-918.

Wang, K., G. Wei, and D. Liu. 2012. CD19: a biomarker for B cell development, lymphoma diagnosis and therapy. *Exp Hematol Oncol*. 1:36.

Wang, T., K. Birsoy, N.W. Hughes, K.M. Krupczak, Y. Post, J.J. Wei, E.S. Lander, and D.M. Sabatini. 2015. Identification and characterization of essential genes in the human genome. *Science*. 350:1096-1101.

Wang, T., J.J. Wei, D.M. Sabatini, and E.S. Lander. 2014. Genetic screens in human cells using the CRISPR-Cas9 system. *Science*. 343:80-84.

Watanabe, S., K. Okawa, T. Miki, S. Sakamoto, T. Morinaga, K. Segawa, T. Arakawa, M. Kinoshita, T. Ishizaki, and S. Narumiya. 2010. Rho and anillin-dependent control of mDia2 localization and function in cytokinesis. *Mol. Biol. Cell*. 21:3193-3204.

Weigmann, K., S.M. Cohen, and C.F. Lehner. 1997. Cell cycle progression, growth and patterning in imaginal discs despite inhibition of cell division after inactivation of Drosophila Cdc2 kinase. *Development*. 124:3555-3563.

Weinkove, D., T.P. Neufeld, T. Twardzik, M.D. Waterfield, and S.J. Leevers. 1999. Regulation of imaginal disc cell size, cell number and organ size by Drosophila class I(A) phosphoinositide 3-kinase and its adaptor. *Curr. Biol.* 9:1019-1029.

Wheat, J.C., D.S. Krause, T.H. Shin, X. Chen, J. Wang, D. Ding, R. Yamin, and D.A. Sweetser. 2014. The corepressor Tle4 is a novel regulator of murine hematopoiesis and bone development. *PloS one*. 9:e105557.

Williams, B.R., and A. Amon. 2009. Aneuploidy: cancer's fatal flaw? *Cancer Res.* 69:5289-5291.

Winzeler, E.A., D.D. Shoemaker, A. Astromoff, H. Liang, K. Anderson, B. Andre, R. Bangham, R. Benito, J.D. Boeke, H. Bussey, A.M. Chu, C. Connelly, K. Davis, F. Dietrich, S.W. Dow, M. El Bakkoury, F. Foury, S.H. Friend, E. Gentalen, G. Giaever, J.H. Hegemann, T. Jones, M. Laub, H. Liao, N. Liebundguth, D.J. Lockhart, A. Lucau-Danila, M. Lussier, N. M'Rabet, P. Menard, M. Mittmann, C. Pai, C. Rebischung, J.L. Revuelta, L. Riles, C.J. Roberts, P. Ross-MacDonald, B. Scherens, M. Snyder, S. Sookhai-Mahadeo, R.K. Storms, S. Veronneau, M. Voet, G. Volckaert, T.R. Ward, R. Wysocki, G.S. Yen, K. Yu, K. Zimmermann, P. Philippsen, M. Johnston, and R.W. Davis. 1999. Functional characterization of the S. cerevisiae genome by gene deletion and parallel analysis. *Science*. 285:901-906.

Wolfson, R.L., L. Chantranupong, G.A. Wyant, X. Gu, J.M. Orozco, K. Shen, K.J. Condon, S. Petri, J. Kedir, S.M. Scaria, M. Abu-Remaileh, W.N. Frankel, and D.M. Sabatini. 2017. KICSTOR recruits GATOR1 to the lysosome and is necessary for nutrients to regulate mTORC1. *Nature*. 543:438-442.

Wuhr, M., Y. Chen, S. Dumont, A.C. Groen, D.J. Needleman, A. Salic, and T.J. Mitchison. 2008. Evidence for an upper limit to mitotic spindle length. *Curr. Biol.* 18:1256-1261.

Wullschleger, S., R. Loewith, and M.N. Hall. 2006. TOR signaling in growth and metabolism. *Cell*. 124:471-484.

Yamashiro, S., G. Totsukawa, Y. Yamakita, Y. Sasaki, P. Madaule, T. Ishizaki, S. Narumiya, and F. Matsumura. 2003. Citron kinase, a Rho-dependent kinase, induces di-phosphorylation of regulatory light chain of myosin II. *Mol. Biol. Cell*. 14:1745-1756.

Ycas, M., M. Sugita, and A. Bensam. 1965. A model of cell size regulation. *J. Theor. Biol.* 9:444-470.

Yoneda, M., and K. Dan. 1972. Tension at the surface of the dividing sea-urchin egg. *J. Exp. Biol.* 57:575-587.

Yuce, O., A. Piekny, and M. Glotzer. 2005. An ECT2-centralspindlin complex regulates the localization and function of RhoA. *J. Cell Biol.* 170:571-582.

Zanin, E., A. Desai, I. Poser, Y. Toyoda, C. Andree, C. Moebius, M. Bickle, B. Conradt, A. Piekny, and K. Oegema. 2013. A conserved RhoGAP limits M phase contractility and

coordinates with microtubule asters to confine RhoA during cytokinesis. *Developmental cell*. 26:496-510.

Zaragoza, O., and K. Nielsen. 2013. Titan cells in Cryptococcus neoformans: cells with a giant impact. *Curr. Opin. Microbiol.* 16:409-413.

Zhang, J., C. Schneider, L. Ottmers, R. Rodriguez, A. Day, J. Markwardt, and B.L. Schneider. 2002. Genomic scale mutant hunt identifies cell size homeostasis genes in S. cerevisiae. *Curr. Biol.* 12:1992-2001.

Zhang, L., and A.S. Maddox. 2010. Anillin. *Curr. Biol.* 20:R135-136.

Zhang, Y., X. Gao, L.J. Saucedo, B. Ru, B.A. Edgar, and D. Pan. 2003. Rheb is a direct target of the tuberous sclerosis tumour suppressor proteins. *Nat Cell Biol*. 5:578-581.

Zhou, M., and Y.L. Wang. 2008. Distinct pathways for the early recruitment of myosin II and actin to the cytokinetic furrow. *Mol. Biol. Cell*. 19:318-326.

Zhou, Y., S. Zhu, C. Cai, P. Yuan, C. Li, Y. Huang, and W. Wei. 2014. High-throughput screening of a CRISPR/Cas9 library for functional genomics in human cells. *Nature*. 509:487-491.

Zoncu, R., A. Efeyan, and D.M. Sabatini. 2011. mTOR: from growth signal integration to cancer, diabetes and ageing. *Nat Rev Mol Cell Biol*. 12:21-35.